Institut für Wasserbau · Universität Stuttgart

Mitteilungen

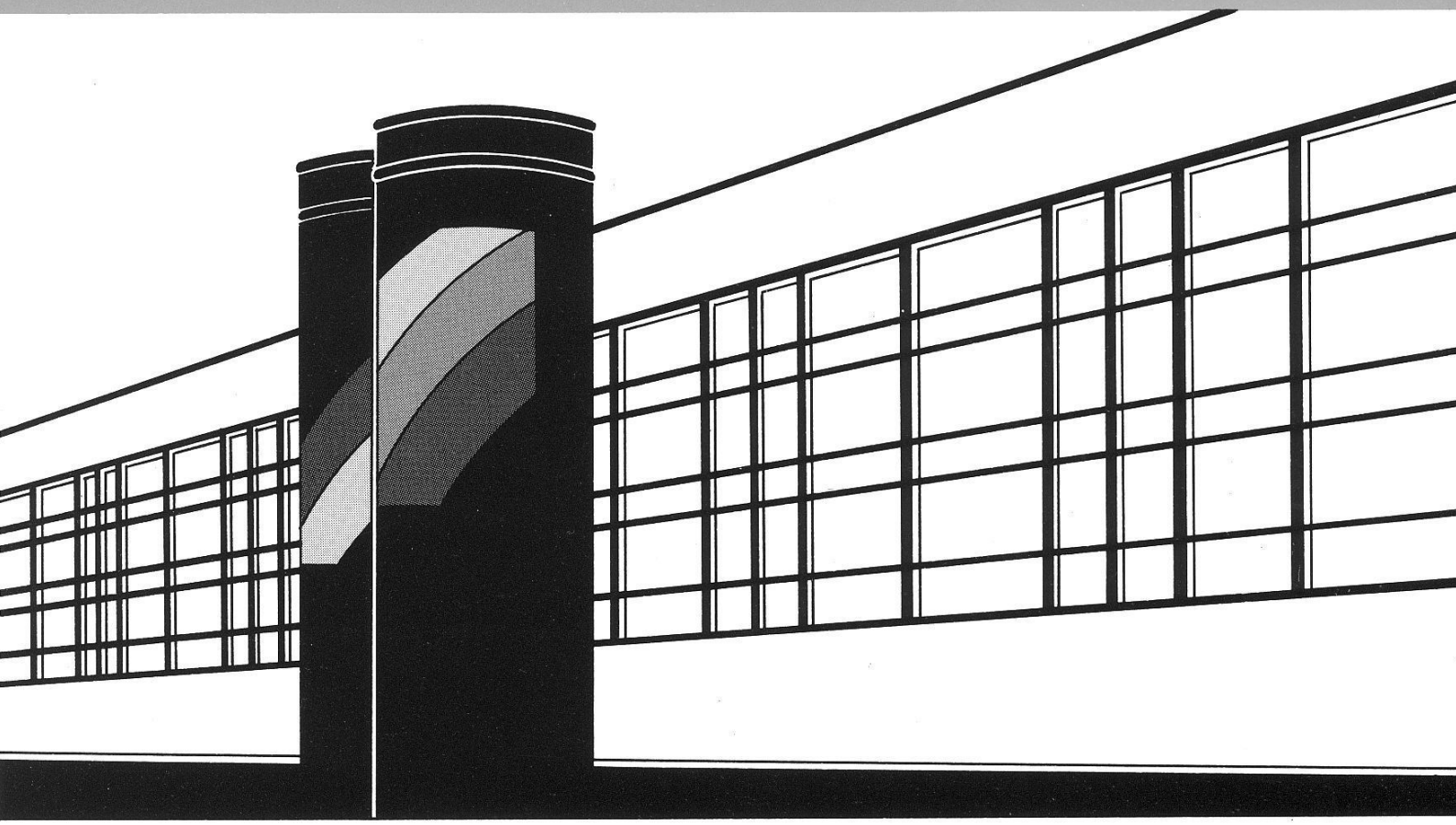

Heft 199

Mehmet Onur Doğan

Coupling of porous media flow with pipe flow

Coupling of porous media flow with pipe flow

Von der Fakultät Bau- und Umweltingenieurwissenschaften der
Universität Stuttgart zur Erlangung der Würde eines
Doktor-Ingenieurs (Dr.-Ing.) genehmigte Abhandlung

Vorgelegt von
Mehmet Onur Doğan
aus Amasya / Türkei

Hauptberichter:	Prof. Dr.-Ing. Rainer Helmig
Mitberichter:	Prof. Dr.-Ing. Reinhard Hinkelmann
	PD Dr.-Ing. Holger Class
Tag der mündlichen Prüfung:	19. November 2010

Institut für Wasserbau der Universität Stuttgart
2011

Heft 199 Coupling of porous media flow with pipe flow

von
Dr.-Ing.
Mehmet Onur Doğan

Eigenverlag des Instituts für Wasserbau der Universität Stuttgart

D93 Coupling of porous media flow with pipe flow

Bibliografische Information der Deutschen Nationalbibliothek
Die Deutsche Nationalbibliothek verzeichnet diese Publikation in der Deutschen Nationalbibliografie; detaillierte bibliografische Daten sind im Internet über http://www.d-nb.de abrufbar

Doğan, Mehmet Onur:
Coupling of porous media flow with pipe flow / von Mehmet Onur Doğan. Institut für Wasserbau, Universität Stuttgart. - Stuttgart: Inst. für Wasserbau, 2011

(Mitteilungen / Institut für Wasserbau, Universität Stuttgart: H. 199)
Zugl.: Stuttgart, Univ., Diss., 2011
ISBN 978-3-942036-03-0
NE: Institut für Wasserbau <Stuttgart>: Mitteilungen

Gegen Vervielfältigung und Übersetzung bestehen keine Einwände, es wird lediglich um Quellenangabe gebeten.

Herausgegeben 2011 vom Eigenverlag des Instituts für Wasserbau
Druck: Document Center S. Kästl, Ostfildern

"Every great advance in science has issued from a new audacity of imagination."

John Dewey

Acknowledgement

I would like to thank all of those who encouraged me to establish this work.

In particular, Rainer Helmig who gave me the opportunity to be a member of his working group, for his constant motivation and for his creative new ideas.

I would also like to thank Reinhard Hinkelmann for co-supervising the thesis.

Especially, I am grateful to Holger Class for his guidance this work, his sound scientific knowledge, his fast problem solving abilities and for his fairness during my time in the department.

I am grateful to the German Research Foundation (DFG) for funding the project.

I am thankful to my colleges at the department not only for their technical support but also for creating a comfortable working environment.

Finally, I would like to thank my family for their emotional support and being always beside me when I needed them.

Contents

List of Figures

List of Tables

Notation

The following table shows the significant symbols used in this work. Local notations are explained in the text.

Symbol	Meaning	Dimension
Greek Letters:		
ϕ	porosity	[-]
ϱ	density	[kg/m^3]
$\bar{\bar{\sigma}}$	total internal stress tensor	[Pa]
$\bar{\bar{\tau}}$	shear stress tensor	[Pa]
$\bar{\bar{\varphi}}$	deformation rate tensor	[1/s]
θ	angle in cylindrical coordinate system	[radian]
β	correction factor for 1D-averaged momentum convection term	[-]
τ_w	wall shear stress	[Pa]
λ	mobility	[(m·s)/kg]
ζ	Darcy-Weisbach friction factor	[-]
ϵ	equivalent sand grain roughness	[m]
α_{EX}	lumped exchange coefficient	[m·s]
α_{ex}	exchange coefficient	[m^2]
μ	dynamic viscosity	[kg/(m·s)]
ν	kinematic viscosity	[m^2/s]
$\tilde{\mu}$	effective viscosity	[m^2/s]
$\int_\Omega$	volume integral	[-]
$\int_\Gamma$	surface integral	[-]
Ψ	total potential	[N/m^2]
ξ	very small number	[-]
φ	deformation rate tensor	[1/s]
$\int$	integration operator	[-]
$\sum$	summation operator	[-]
∇	gradient operator	[-]
$\vec{\nabla}$	divergence operator	[-]

Latin Letters:

A	cross-sectional area of pipe	[m^2]
$A_{outerface}$	circumference area of a pipe element	[m^2]
B_i	control volume at node i	[-]
$\bar{\bar{D}}$	diffusion coefficient tensor	[m^2/s]
d	pipe diameter	[m]
e	element	[-]
$\vec{f_{ext}}$	external volume force tensor per unit mass	[m/s^2]
$\vec{g}$	gravitational acceleration	[m/s^2]
$\bar{\bar{I}}$	unit tensor	[-]
J	jacobian matrix	[-]
k_r	relative permeability	[-]
$\bar{\bar{K}}$	permeability tensor	[m^2]
N	ansatz function	[-]
$\vec{n}$	unit normal vector	[-]
p	pressure	[N/m^2]
p_n	non-wetting phase pressure	[N/m^2]
p_{nref}	reference non-wetting phase pressure	[N/m^2]
p_w	wetting phase pressure	[N/m^2]
p_c	capillary pressure	[N/m^2]
q	source/sink term	[$kg/(m^3 \cdot s)$]
q_{ex}	mass exchange term	[$kg/(m^3 \cdot s)$]
r	pipe radius variable	[m]
R	pipe radius	[m]
R_{ind}	individual gas constant	[$J/(kg \cdot K)$]
R_e	Reynolds number	[-]
S	saturation	[-]
S_w	wetting phase saturation	[-]
S_n	non-wetting phase saturation	[-]
$\vec{s}$	unit positive direction vector of the pipe	[-]
t	time	[s]
T	temperature	[K]
$\vec{u}$	velocity vector	[m/s]
u_s	velocity along the positive pipe direction	[m/s]
$\bar{u}_s$	cross-sectionally averaged velocity along the positive pipe direction	[m/s]
V	volume	[m^3]
W	weighting function	[-]
x_α^k	mass fraction of a component k in phase α	[-]

Subscripts:

b	at the boundary
ex	exchange
EX	lumped exchange
ff	free flow variable
g	gas phase
i	node index
j	neighboring nodes of node i
n	non-wetting phase
o	characteristic quantity
pm	porous media variable
r	radial direction
ref	reference
s	along the axial pipe direction
t	tangential component
v	vertical component
w	water phase
α	phase
$*$	non-dimensional variable

Superscripts:

k	component
r	Newton-Raphson iteration index
t	time

Abstract

Many flow problems in environmental, technical and biological systems are characterized by a distinct interaction between a flow region in porous medium and a free flow region in quasi-one-dimensional hollow structures. Examples for such systems are:

- Mines: Methane released from unmined coal seams migrates through the porous rocks, but also through tunnels and shafts in the mine.
- Landslides: A sudden water infiltration through macropores may trigger landslides.
- Polymer electrolyte membrane fuel cells: The supply of reactive gases through free-flow channels into the porous diffusion layers interacts strongly with the evacuation process of the water, which is formed at the cathode reaction layer and flows from the porous diffusion layers into the free-flow channels .
- Cancer therapy: Therapeutic agents are delivered via the blood vessels into the tissue, targeting the tumor cells.

The goal of this study is to introduce new coupling strategies and to develop coupled numerical models which can form a basis for further studies modeling the complex systems mentioned above.

In this study, different model concepts based on a dual-continuum strategy for the simulation of coupled porous media flow with lower-dimensional pipe flow are further developed and tested. For the numerical implementation a special grid called 1D pipe network grid in a 3D porous grid is developed.

The dual-continuum concept is extended for coupling multi-phase porous media flow with lower-dimensional single-phase pipe flow. The complexity of the considered flow regimes is increased gradually. Examples are given for a coupled single-phase incompressible and compressible flow in both porous media and pipe flow domains. The single-phase coupling strategy is tested by comparing the results with results of the experiment done in controlled laboratory conditions. Furthermore, the coupling of single-phase pipe flow with a multi-phase flow based on Richards equation for the unsaturated soil zone is modeled, where the important role of capillary effects for the mass exchange rate between the two continua can be illustrated. The next model introduces a concept for a two-phase porous media flow coupled with a single-phase (gas) pipe flow problem, which reveals that the mobility exchange term can be decisive for the mass exchange rate. The final model presents a concept for

coupling two-phase two-component porous media flow with single-phase two-component pipe flow. This model is able to simulate more complicated transport systems by accounting not only for the mobility exchange term but also for the concentrations of the exchanged components between the continua. It is shown that the concentration of the components in each continua play a significant role for the compositional ratio of the exchanged mass.

Zusammenfassung

Die numerische Simulation von Strömung und Transport von Mehrphasen-Systemen in porösen Medien ist für viele umweltrelevante, technische und biologische Anwendungsbereiche von Bedeutung. Oft erschwert aber die Struktur der porösen Matrix die konzeptionelle Modellbildung. Dies gilt besonders dann, wenn ausgeprägte Hohlstrukturen das poröse Medium durchziehen beziehungsweise die jeweiligen Strömungen gekoppelt sind.

Beispiele hierfür findet man in folgenden Bereichen:

- Kohlebergwerke: Die Migration von Methan aus Kohlebergwerken durch Gebirge und Schacht-/Strecken-Systeme.
- Erdrutsche: Ein plötzliches Eindringen von Wasser durch Makroporen kann Erdrutsche auslösen.
- Niedertemperatur-Brennstoffzellen (PEMFC): Die Strömung von Gas (Luft, Sauerstoff) durch Gasverteilerplatten von Brennstoffzellen mit Kontakt zur porösen Diffusionsschicht interagiert mit der Drainage des in der Kathode entstehenden Wassers, das von der Diffusionsschicht in die Gasverteilerplatten strömt.
- Krebstherapie: Therapeutika, die auf die Krebszellen abzielen, werden durch Blutgefäße in das Gewebe transportiert.

Zielstellung der Arbeit

Die primären Ziele der durchgeführten Arbeit sind zum einen, neue Kopplungstrategien einzubringen, und zum anderen, neue gekoppelte numerische Modelle zu entwickeln, die eine Grundlage für weitere Forschungsarbeiten bieten könnten. Die Schwerpunkte liegen in der Entwicklung unterschiedlicher neuer Konzepte für die Modellierung von gekoppelter 3D-Strömung in porösen Medien mit 1D-Rohrströmung, sowie auf der Untersuchung des charakteristischen Verhaltens von derartigen Systemen mit numerischen Testbeispielen.

Erhaltungsgleichungen auf unterschiedlichen Skalen

In der Natur sind die Systeme in der Regel sehr komplex, nicht nur aufgrund der Komplexität der Strukturen, sondern auch aufgrund der Komplexität der physikalischen Prozesse. Die Wahrnehmung eines physikalischen Prozesses kann sich je nach Auflösung der Beobachtung ändern. Daher muss der Modellierer die geeignete Skala des Modells für das untersuchte Problemgebiet bestimmen. Im Allgemeinen werden die Erhaltungsgleichungen

der Strömung im porösen Medium und der freien Strömung auf verschiedenen Skalen definiert. Die Erhaltungsgleichungen von Mehrphasen-Strömungen in porösen Medien sind auf der makroskopischen Betrachtungsebene formuliert, wo die Geschwindigkeiten durch das Darcy-Gesetz gegeben sind, die freie Strömung wird jedoch durch die Navier-Stokes-Gleichungen beschrieben, die auf der Mikroskala definiert sind.

Kopplungsstrategien

Die allgemeinen Ansätze zur Kopplung von Strömungsmodellen für poröse Medien mit Strömungsmodellen für freie Strömungen können in zwei Hauptgruppen nach der jeweiligen Dimension der gekoppelten Modelle untergliedert werden.

- Äquidimensionale Kopplungsansätze
- Niederdimensionale Kopplungsansätze

„Äquidimensionale Kopplung“ bedeutet, dass beide Systeme die gleiche Dimension haben. „Niederdimensionale Kopplung“ bedeutet in diesem Zusammenhang, dass ein gekoppeltes System eine niedrigere Dimension als das andere System hat. Unabhängig von der äquidimensionalen beziehungsweise niederdimensionalen Klassifizierung können die Kopplungsstrategien nach der Kopplungstechnik in zwei Hauptgruppen unterteilt werden:

- Diskrete Modelle
- Doppelkontinuumsmodelle

In diskreten Modellen werden die Rohre mit ihren tatsächlichen geometrischen Standorten in das poröse Medienmodell eingebettet, und die Interaktion der Strömung im porösen Medium mit der freien Strömung ist mit klar definierten Übergangsbedingungen modelliert. Bei Doppelkontinuumsmodellen liegen zwei Kontinua übereinander und der Austausch zwischen den beiden Modellen erfolgt über einen Quell-/Senkterm, der mit gegensätzlichem Vorzeichen zu der jeweiligen Massenerhaltungsgleichung addiert wird. Eine Kombination der oben genannten Klassifikationen ist möglich; Beispielsweise existieren diskrete äquidimensionale Modelle aber auch niederdimensionale Doppelkontinuumsmodelle.

Diskrete, äquidimensionale Kopplungsansätze

Äquidimensionale Kopplung bedeutet, dass für die mathematische Beschreibung aller Teilsysteme die selbe räumliche Dimension verwendet wird. Das Darcy-Gesetz – die gebräuchlichste Vereinfachung der Impulserhaltungsgleichung im Kontext von porösen Medien – ist eine Differentialgleichung erster Ordnung, während die Navier-Stokes-Gleichungen – als Impulserhaltungsgleichungen für freie Strömungen – eine Differentialgleichung zweiter Ordnung darstellen. Aus diesem Grund sind die Erhaltungsgleichungen für poröse Medien und für freie Strömungen mathematisch nicht direkt kombinierbar. Das Darcy-Gesetz beinhaltet, im Gegensatz zu den Navier-Stokes-Gleichungen, nur Terme mit Ableitungen erster Ordnung. Dies impliziert, dass eine exakte Beschreibung des Verhaltens der Strömungsgeschwindigkeiten an der Grenzschicht zwischen porösem Medium und freier Strömung nicht

möglich ist. Daher wird das Strömungsfeld in den Übergangsbereichen von den Grundgleichungen nicht mit hinreichender Genauigkeit definiert. In der Literatur gibt es zwei Ansätze, um dieses Problem zu lösen:

- Den Einbereichsansatz mittels der Brinkmangleichung und
- Den Zweibereichsansatz via der Beavers-Joseph-Kopplungsbedingung.

Brinkmangleichung (Einbereichsansatz):

Brinkman (1949) schlägt eine Impulserhaltungsgleichung vor, die sowohl für poröse Medien als auch bei freien Strömungen gilt. Mathematisch ist die Brinkmangleichung eine Überlagerung der Stokesgleichung mit dem Darcy-Gesetz. Da die Brinkmangleichung im gesamten Definitionsbereich gilt, besteht keine Notwendigkeit, Übergangsbedingungen zwischen der Strömung im porösen Medium und der freien Strömung zu definieren. Der Ansatz benötigt jedoch einen empirischen Parameter, der als effektive Viskosität bezeichnet wird. Zum gegenwärtigen Zeitpunkt wurde noch keine verlässliche Methode zur Ermittlung dieser effektiven Viskosität publiziert, weshalb die meisten Autoren sie nahe der dynamischer Viskosität der Fluide wählen. Des Weiteren muss die Übergangszone vom porösen Medium auf die freie Strömung beim Brinkmanansatz räumlich diskretisiert werden, da diese Übergangszone durch räumliche Variation von Parametern, beispielsweise der Durchlässigkeit (K), Porosität (ϕ) und der effektiven Viskosität ($\tilde{\mu}$), modelliert wird. Die Wahl dieser Parameter in der Übergangszone ist noch nicht hinreichend verstanden, hat aber entscheidenden Einfluss auf die Vorhersagegenauigkeit des Modells. Folglich existiert zum gegenwärtigen Zeitpunkt keine rigorose Methode zur Festlegung dieser Parameter; ein gebräuchlicher empirischer Ansatz ist jedoch der Folgende:

- In der *freien Strömung* wird für die Porosität $\phi = 1$ und $K \gg 1$ für die Durchlässigkeit gewählt, sowie die effektive Viskosität identisch zur realen Viskosität des Fluids gesetzt ($\tilde{\mu} = \mu$).
- Im *porösen Medium* gilt für die Porosität $\phi < 1$ und in der Regel $K \ll 1$ für die Durchlässigkeit. Außerdem gilt für die effektive Viskosität $\tilde{\mu} = \mu/\phi$.
- In der *Übergangszone* werden Porosität, Durchlässigkeit und effektive Viskosität linear interpoliert werden indem die Entfernung eines Punktes von den beiden Teilgebieten betrachtet wird.

Beavers und Joseph Kopplungsbedingung (Zweibereichsansatz):

Beim Zweibereichsansatz werden die Unterdomänen mittels auf die jeweiligen Gegebenheiten angepassten Gleichungssystemen modelliert, beispielsweise können die Stokesgleichungen in der freien Strömung und das Darcygesetz für das poröse Medium verwendet werden. Da sich die beiden Gleichungen an der Grenzfläche der Definitionsbereiche widersprechen können, sind Kopplungsbedingungen notwendig. Diese stellen sicher, dass die Massenbilanz und das vertikale sowie das tangentiale Kräftegleichgewicht an der Grenzfläche

erfüllt werden. Die Formulierung der Massenbilanz und des vertikalen Kräftegleichgewichts ist bei diesem Ansatz in der Regel relativ leicht zu bewerkstelligen. Anders verhält es sich beim tangentialen Kräftegleichgewicht am Übergang: Für dieses schlugen Beavers und Joseph (1967) erstmals eine Beziehung zwischen der Darcygeschwindigkeit und der freien Strömungsgeschwindigkeit (und deren Gradienten) an der Grenzfläche vor. Für die Beavers-Joseph-Bedingung wird aber, wie bei die Brinkmangleichung, ein problemspezifischer, dimensionsloser, empirischer Parameter (α_{BJ}) für die Grenzfläche benötigt. Die derzeit meistverwendete Kopplungsbedingung wurde von Saffman (1971) durch Vernachlässigung der (relativ kleinen) Darcygeschwindigkeit aus der Beavers-Joseph-Bedingung abgeleitet. Diese Kopplungsbedingung wird in der Literatur deshalb häufig als Beavers-Joseph-Saffman-Bedingung bezeichnet.

Niederdimensionaler Doppelkontinuumsansatz

Der Fokus der vorliegenden Arbeit liegt auf der Kopplung von dreidimensionalen Strömungen in porösen Medien mit Strömungen durch im porösen Medium eingebettete quasi-eindimensionale Hohlkörper (im Folgenden als "Rohrströmungen" bezeichnet). Eine wichtige Voraussetzung für die eindimensionale Betrachtung der Rohrströmung ist, dass die Geschwindigkeit für jeden Querschnitt des Hohlkörpers gemittelt werden kann, die gemittelte Geschwindigkeit also in jedem Querschnitt konstant ist. Die Annahme einer eindimensionalen Beschreibung der Rohrströmung schließt die direkte Anwendung bereits publizierter Kopplungsansätze aus. So beschreibt beispielsweise die Beavers-Joseph-Kopplungsbedingung eine Beziehung zwischen der Geschwindigkeit der freien Strömung (und deren Gradienten) an der Grenzfläche mit der Darcygeschwindigkeit. Bei eindimensionalen Rohrströmungsmodellen werden die Geschwindigkeit senkrecht zur Rohrrichtung jedoch nicht modelliert. Deshalb wird der Impulsaustausch zwischen Hohlkörper und porösem Medium im Kontext dieser Arbeit vernachlässigt, und nur der Massenaustausch zwischen beiden Systemen wird berücksichtigt. Die Rohrströmung wird als Graph[1] modelliert. Die reale Hohlkörpergeometrie bleibt dabei erhalten. Damit besteht bei diesem Ansatz auch keine Notwendigkeit der Homogenisierung der Rohrparameter auf dem gesamten Definitionsbereich. In diesem Punkt unterscheidet sich der hier vorgestellte Ansatz von den konventionellen Doppelkontinuumsmodellen für geklüftete, poröse Medien. Wie bei konventionellen Doppelkontinuumsmodellen überlappen sich jedoch die Definitionsbereiche der beiden Modellgebiete (hier: poröses Medium und Hohlkörpernetzwerk), und der Massenaustausch zwischen den Kontinua wird durch Quellterme in den Massenerhaltungsgleichungen mit gegensätzlichem Vorzeichen beschrieben. Im einfachsten Fall wird der Quellterm durch die Multiplikation eines Koeffizienten (α_{EX}) mit der Druckdifferenz zwischen den beiden Kontinua berechnet:

$$\int q_{ex}\, dV \; = \alpha_{EX} \cdot (p_{pipe} - p_{pm}),$$

wobei α_{EX} eine Funktion der Drücke in beiden Modellgebieten, der Fluideigenschaften, der Geometrie des Rohres und der Eigenschaften des porösen Mediums ist. Statt der Verwendung eines einzelnen Austauschkoeffizienten (α_{EX}), kann der Massenaustausch auch

[1] Ein Graph $G = (K, V)$ ist definiert als Zweitupel einer endliche Menge K und einer binären Relation $V \subseteq K \times K$. In konkreten Fall ist K die Menge der Hohlkörperverbindungstellen und V die Menge der Hohlkörper.

expliziter durch getrennte Betrachtung der Fluideigenschaften (Dichte ϱ und Viskosität μ), der Hohlkörpergeometrie (Rohrdurchmesser d und Rohraußenfläche $A_{outerface}$) und der Eigenschaften des porösen Mediums (Austauschkoeffizient α_{ex}) beschrieben werden. Im einfachsten Fall (einphasig) wird dies durch:

$$\alpha_{EX} = \varrho \frac{\alpha_{ex}}{\mu} \frac{A_{outerface}}{d}$$

ausgedrückt. Auf die Berechnung der Massenaustauschterme wird in dieser Arbeit in den Kapiteln über die jeweiligen Modelle detailliert eingegangen. Die Kopplungsstrategie kann bezüglich der Massenaustauschterme als explizit bezeichnet werden. Um eine gute Konvergenz des Gesamtmodells zu erreichen, werden die Kopplungsterme nach jeder Newtoniteration des dreidimensionalen Teilmodells neu berechnet.

Querschnittsgemittelte eindimensionale Rohrströmungen

Man kann Rohrströmungen mittels der dreidimensionalen Navier-Stokes-Gleichungen modellieren, jedoch ist der hierfür erforderliche Rechenaufwand sehr hoch. Statt die dreidimensionalen Navier-Stokes-Gleichungen zu lösen, kann die Strömung im Rohr auch eindimensional beschrieben werden, sofern die Länge des Hohlkörpers mehrere Ordnungen größer ist als sein Durchmesser. Die gemittelten Navier-Stokes-Gleichungen für quasieindimensionale axialsymmetrische Rohrströmungssysteme ergeben sich – mit Ausnahme der gemittelten viskosen Reibungskräfte – direkt aus den Navier-Stokes-Gleichungen. Folglich ähnelt diese Gleichung den Navier-Stokes-Gleichungen stark, verwendet jedoch eine gemittelte Reibungskraft (Schubspannungterm) und enthält zusätzlich einen Korrekturfaktor (β) im konvektiven Impulsterm. Die Bestimmung der gemittelten viskosen Reibungskräfte kann mit Hilfe der dimensionslosen Navier-Stokes-Gleichungen im zylindrischen Koordinatensystem erfolgen. Ein ähnlicher Ansatz wird auch von Barnard *et al.* (1966) und Canic und Kim (2003) verwendet. Die gemittelten viskosen Reibungskräfte können auch vom Darcy-Weisbach Reibungsfaktor (ζ) abgeleitet werden, welcher eine Funktion der Reynoldszahl (Re), der Rohrrauhigkeit (ϵ) und dem Rohrdurchmesser (d) ist. Die genaue Formulierung des Darcy-Weisbach Reibungsfaktors ist abhängig vom Abflussregime.

Modellkonzepte und Diskretisierungsverfahren

In dieser Arbeit werden zwei Arten von Rohrströmungsgleichungen abhängig von der Komplexität der Systeme verwendet. Das Hagen-Poiseuille-Modell wird für inkompressible, stationäre und laminare Strömungen eingesetzt, andernfalls wird ein Modell für kompressible, instationäre Rohrströmung verwendet. Für die räumliche Diskretisierung der Gleichungen im porösen Medium wird die Box-Methode verwendet. Die Hagen-Poiseuille-Gleichung wird mittels einer knotenzentrierten Finite-Volumen Methode diskretisiert, die kompressiblen Rohrströmungsgleichungen werden mit einer „Staggered Grid“ (versetztem Gitter) Finite-Volumen-Methode diskretisiert, d.h. die Kontrollvolumina für die Massenbilanz und die Impulsbilanz sind jeweils um eine halbe Zelldistanz zueinander versetzt. Die Zeitdiskretisierung erfolgt immer voll implizit; als nichtlineares Lösungsverfahren kommt ein gedämpftes Newton-Raphson Verfahren zum Einsatz.

Diskrete Einbettung des verzweigten Hohlkörpernetzwerks in das poröse Medium

Für die numerische Modellierung von gekoppelten Systemen wird eine Gitterimplementierung benötigt, welche in der Lage ist, Graphen in dreidimensionale Gebiete einzubetten. Aus diesem Grund wurde im Rahmen dieser Arbeit ein entsprechendes Gitter entwickelt. Die Grundidee der Einbettung besteht darin, das 1D-Hohlkörpernetzwerk durch Kanten des dreidimensionalen Gitters zu repräsentieren, so dass jedem Knoten des Hohlkörpernetzwerks ein Knoten im porösen Medium eindeutig zugeordnet werden kann. Die Erzeugung des oben genannten Gitters erfolgt mittels folgender Prozedur:

- Zunächst wird ein vollständiges dreidimensionales Gitter mit Hilfe der Netzgenerierungssoftware Ansys-Icem erzeugt.
- Anschließend wird dieses Gitter im CSP Datenformat gespeichert.
- Danach wird manuell eine PPS-Datei (*p*ipe *p*osition) erstellt, welche die Geometrie, die Topologie sowie die Randbedinungen des Hohlkörpernetzwerks definiert. Die Geometrie wird hierbei durch die dreidimensionale Position der Hohlkörperverbindungstellen festgelegt, die Topologie als paarweise Vernetzung der Verbindungsstellen.
- Das dreidimensionale Gitter der CSP-Datei und das Hohlkörpernetzwerk der PPS-Datei werden miteinander verknüpft und in einer DGF-Datei abgespeichert.
- Obwohl die DGF-Datei jedem Knoten im Hohlkörpernetzwerk eindeutig einen Knoten im dreidimensionalen Gitter zuordnet, enthält die DGF-Datei nicht die vollständige Topologieinformation des Rohrnetzwerks. Diese wird in einem weiteren Vorverarbeitungsschritt berechnet.

Numerische Modelle

In dieser Arbeit wird der einphasige Doppelkontinuumskopplungsansatz auf die Kopplung von Mehrphasenströmungen in porösen Medien mit niederdimensionaler einphasiger freier Strömung untersucht, wobei die physikalischen Prozesse in jedem Teilgebiet mittels angepasster Modelle beschrieben werden. Es wird eine Reihe numerischer Modelle entwickelt, wobei die Komplexität der einzelnen Modelle und die der Kopplungsansätze schrittweise erhöht wird. Diese Vorgehensweise soll zum Verständnis der neu eingeführten Kopplungsansätze und deren Motivation beitragen.

Numerische Modelle für gekoppelte einphasige Strömungssysteme

Zunächst werden gekoppelte Einphasensysteme untersucht. Hierzu wird zunächst ein einfaches Modell vorgestellt, das in der Lage ist, stationäre Einphasenströmungen in porösen Medien mit (ebenfalls einphasigen) Hagen-Poiseuille-Strömungen zu koppeln. Der Massenaustauschterm berücksichtigt die Fluideigenschaften Dichte und dynamische Viskosität, die Eigenschaften des porösen Mediums (über den Austauschkoeffizienten α_{ex}), die Rohrgeometrie (mittels der äußeren Oberfläche des Rohrelementes) und den Durchmesser des

Rohres, sowie die Druckdifferenz zwischen den beiden Kontinua:

$$\int q_{ex}\, dV \;=\; \varrho\, \frac{\alpha_{ex}}{\mu}\, \frac{A_{outerface}}{d}\, (p_{pipe} - p_{pm})$$

Mit diesem Modell kann gezeigt werden, dass die gegenseitige Beeinflussung der Druckverteilung beider Systeme durch die Doppelkontinuums-Kopplungstrategie wiedergegeben werden kann. Bevor komplexere Modelle untersucht werden, wird die Gitterkonvergenz untersucht, um die Gitterabhängigkeit der Lösung abzuschätzen. Im Gegensatz zu diskreten Kluftmodellen, wo der Druckgradient rund um die Klüfte stark von der Gitterverfeinerung abhängt, konnten für die untersuchten Modelle nur minimale Auswirkungen auf den stationären Druckgradienten zwischen den beiden Kontinua festgestellt werden. Dies kann dadurch erklärt werden, dass der (virtuelle) Austauschabstand (d) ausschließlich durch den Durchmesser des Rohres festgelegt wird. Anschließend wird die Komplexität durch Einführung kompressibler Strömung und zeitabhängiger Speicherterme in beiden Kontinua erhöht. Dieses Modell ist in der Lage, gekoppelte Gasströmungen in beiden Teilgebieten zu modellieren, wobei der Kopplungsansatz – mit Ausnahme der Berechnung des ϱ_{ex} Terms – identisch zum vorherigen Modell bleibt. Da sich in kompressiblen Strömungen die Dichte als Funktion des Drucks ändert, wird für den ϱ_{ex} Term upwinding verwendet, d.h.

wenn $p_{pipe} < p_{pm}$, dann $\varrho_{ex} = \varrho_{pm}$; sonst $\varrho_{ex} = \varrho_{pipe}$.

Ein Validierungversuch des gekoppelten Einphasenmodells

Mit Hilfe eines Vergleichs zwischen einem Laborexperiment und dem Ergebnis einer numerischer Simulation wird anschließend versucht, das im Rahmen dieser Arbeit entwickelte und implementierte einphasige Modellkonzept zu validieren. Dazu wurde zunächst ein einfaches Strömungsexperiment mit Luft durchgeführt, bei dem die anteiligen Massenflüsse durch ein poröses Medium und ein darin eingebettetes Rohr bestimmt wurden. Das Experiment besteht aus einem luftdichten Behälter, der mit Sand gefüllt und in dem ein perforiertes L-förmiges Rohr vergraben ist. Ein kontrollierter, gleichmäßiger Luftstrom wird dann über den Boden des annähernd würfelförmigen Behälters injiziert. Das L-förmige Rohr nimmt dabei einen Teil des nach oben gerichteten Luftstroms auf, während der Rest durch das poröse Medium abfließt. Das Experiment wurde zweimal mit unterschiedlichen Sandfüllungen und mit sieben unterschiedlichen Luftquellen durchgeführt und mit dem kompressiblen gekoppelten Einphasenmodell simuliert. Der vom Modell benötigte α_{ex} Parameter, welcher nicht direkt gemessen werden kann, hängt hauptsächlich von den Eigenschaften des porösen Mediums, wie Porenstruktur und Korngröße an der Übergangszone ab. Der Ansatz zur Bestimmung von α_{ex} ist wie folgt:

- α_{ex} einer Sandfüllung wird für die mittlere Luftquelle gemessen.
- Dann wird der gleiche α_{ex} Parameter zur Vorhersage der Ergebnisse der restlichen sechs Luftquellen verwendet.
- Da Porenstruktur und Korngrößen abhängig von der Sandart sind, muss α_{ex} für jeden Sand neu bestimmt werden.

Die Validierung des Modells durch den Vergleich der numerischen Simulation mit den Ergebnissen des durchgeführten Experiments kann als zufriedenstellend bezeichnet werden, da das Modell die Auswirkungen von Änderungen der Permeabilitäten des Sandes und die Veränderung des Quellflusses erfolgreich vorhersagen konnte. Dieses Experiment zeigt, dass der Doppelkontinuumsansatz für gekoppelte poröse Medien-Rohrströmungssysteme anwendbar ist. Die Schwierigkeit liegt in der Parameterbestimmung.

Kopplung der Richardsgleichung mit Hagen-Poiseuille

Danach wird ein Modell für die Kopplung der Richardsgleichung für das poröse Medium mit der Hagen-Poiseuille-Gleichung für das Hohlkörpersystem untersucht. Dies stellt einen Zwischenschritt hin zur Kopplung von Mehrphasensystemen dar. Ein solches System ist beispielsweise für Probleme aus der Bodenphysik relevant, bei denen Wasser in sogenannten Makroporenstrukturen wie Wurzelkanälen oder Wurmlöchern relativ schnell fließt und ein Austausch von Wasser zwischen den Makroporen und der ungesättigten Zone (dem porösen Medium) stattfindet. Der Massenaustausch wird hier modifiziert durch die Einführung des Mobilitätaustauschterms (λ_{ex}):

$$\int q_{ex}\, dV \;=\; \varrho\, \lambda_{ex}\, \alpha_{ex} \frac{A_{outerface}}{d}\, (p_{pipe} - p_{w_{pm}})$$

Für den Mobilitätaustauschterm wird upwinding verwendet, d.h.

wenn $p_{pipe} < p_{pm}$, dann $\lambda_{ex} = \dfrac{k_{rw}}{\mu}$; sonst $\lambda_{ex} = \dfrac{1}{\mu}$.

Die numerischen Ergebnisse deuten darauf hin, dass Kapillarkräften in der ungesättigten Zone eine entscheidende Rolle beim Massenaustausch zukommt.

Kopplung eines Zweiphasenmodells in der Matrix mit einem Einphasenmodell im Hohlkörper

Im nächsten Schritt wird die Modellkomplexität durch die Einführung der Kopplung eines zweiphasigen Strömungsmodells für das poröse Medium mit einer Einphasenströmung im Hohlkörper erhöht. Solche Problemstellungen treten beispielsweise in stillgelegten Bergwerken auf, in denen aus Kohleflözen desorbiertes Methangas durch Schächte und das Streckensystem an die Oberfläche gelangt. Wenn die Zeche nicht mit Grundwasser geflutet wird, bleibt die Umgebung der Tunnel und Schächte relativ trocken. In diesen Fällen kann das Methanmigrationsproblem als Zweiphasenströmung im porösen Medium, die mit einer Einphasenströmung im Rohr gekoppelt ist, modelliert werden. Der Massenaustausch findet hierbei jedoch nur zwischen den Gasphasen der beiden Systeme statt. In diesem Fall wird der Massenaustausch durch Einführung eines Mobilitätaustauschterms (λ_{ex}) und eines Dichteaustauschterms ϱ_{ex} modifiziert:

$$\int q_{ex}\, dV \;=\; \varrho_{ex}\, \lambda_{ex}\, \alpha_{ex} \frac{A_{outerface}}{d}\, (p_{pipe} - p_{g_{pm}}) \tag{1}$$

Für die Mobilitäts- und Dichteaustauschterme wird wie schon in den beiden vorherigen Modellen upwinding verwendet, d.h.

wenn $p_{pipe} < p_{pm}$, dann $\varrho_{ex} = \varrho_{pm}$, $\lambda_{ex} = \dfrac{k_{rg}}{\mu}$; sonst $\varrho_{ex} = \varrho_{pipe}$, $\lambda_{ex} = \dfrac{1}{\mu}$.

Das Modell wird anhand von zwei Testproblemen (Setup A und Setup B) untersucht. In Setup A bleibt der Definitionsbereich trocken und in Setup B ist er mit Wasser gesättigt, um die Wirkung des λ_{ex} Terms abzuschätzen. Es zeigt sich, dass im Mehrphasensystem dem Austauschterm eine noch wichtigere Bedeutung zukommt als im Einphasensystem. Dies kann dadurch erklärt werden, dass die Mobilität der Phase, über die der Massenaustausch stattfindet (in diesem Fall die Gasphase), von der Phasensättigung abhängt. Für das Testbeispiel wird anhand von zwei Szenarien mit unterschiedlicher Wassersättigung im porösen Medium gezeigt, dass die Abnahme des in die Rohrströmung induzierten Gasflusses vom Modell wiedergegeben werden kann, sofern die Fluidmobilität bei der Berechnung des Massenaustausches einbezogen wird.

Kopplung eines Zweiphasen-, Zweikomponentenmodells in der Matrix mit einem Einphasen-, Zweikomponentenmodell im Hohlkörper

Das komplexeste Modell, das im Rahmen der vorliegenden Arbeit entwickelt wurde, betrachtet die gekoppelte Simulation von Zweiphasen-, Zweikomponentenströmungen im porösen Medium und Einphasen-, Zweikomponentenströmungen im Rohr. Als Anwendung eines solchen Modells kommen beispielsweise Transportprozesse in Brennstoffzellen in Betracht. Hierbei müssen in der freien Strömung des Gaskanals die Komponente Sauerstoff aus dem Zustrom sowie zusätzlich die Komponente Wasserdampf im Abstrom bilanziert werden, wobei entlang des Kanals ein Austausch mit der porösen Gasdiffusionsschicht stattfindet. Ebenso anwendbar ist dieses Modell für Szenarien in stillgelegten Kohlebergwerken, in denen vor der vollständigen Flutung des Bergwerks in den Strecken und Schächten noch vorwiegend „trockene“ Bedingungen vorherrschen. Der Massenaustausch wird durch die Einführung der Konzentration der jeweiligen Komponenten in den Phasen modifiziert. Für jede ausgetauschte Komponente muss ein Massenaustauschterm formuliert werden:

$$\int q^a_{ex}\, dV \;=\; \varrho_{g_{ex}}\, x^a_{g_{ex}} \lambda_{ex}\, \alpha_{ex} \frac{A_{outerface}}{d}\, (p_{g_{pipe}} - p_{g_{pm}}) \tag{2}$$

$$\int q^w_{ex}\, dV \;=\; \varrho_{g_{ex}}\, x^w_{g\ ex} \lambda_{ex}\, \alpha_{ex} \frac{A_{outerface}}{d}\, (p_{g_{pipe}} - p_{g_{pm}}) \tag{3}$$

Für die Mobilitäts-, Dichte- und Konzentrationsaustauschterme wird, wie schon in den vorigen Modellen, upwinding verwendet, d.h.

wenn $p_{g_{pipe}} < p_{g_{pm}}$, dann $\varrho_{g_{ex}} = \varrho_{g_{pm}}$, $x_g^{a,w}{}_{ex} = x_g^{a,w}{}_{pm}$, $\lambda_{ex} = \frac{kr_g}{\mu}$;

sonst $\varrho_{g_{ex}} = \varrho_{g_{pipe}}$, $x_g^{a,w}{}_{ex} = x_g^{a,w}{}_{pipe}$, $\lambda_{ex} = \frac{1}{\mu}$.

Die Ergebnisse der Modellrechnungen zeigen, dass die Richtung des Masseaustausches einer Komponente von der Differenz des Gesamtdrucks des Fluids bestimmt wird und dass Partialdruckdifferenzen der Komponente eine untergeordnete Rolle spielen. Das Verhältnis der ausgetauschten Komponentenmassen wird jedoch von der Zusammensetzung des Fluids im Kontinuum mit dem höheren Druck vorgegeben.

Die implementierten numerischen Modelle und die präsentierten Beispiele sind möglichst einfach gewählt, um die grundlegenden Merkmale der Modellkonzepte aufzuzeigen, welche Prozesse unterschiedlicher Komplexität beschreiben.

Ausblick

Diese Arbeit leistet einen wichtigen Beitrag zur gekoppelten Modellierung von Strömungen in porösen Medien mit freien Strömungen, im vorliegenden Fall beschränkt auf freie Strömungen in quasi-eindimensionalen Hohlräumen, die mit Hilfe von Gleichungen aus der Rohrhydraulik approximiert werden können. Die Interaktion zwischen freier Strömung und porösem Medium wurde in verschiedenen Vorhaben und für sehr unterschiedliche Anwendungen als Forschungsthema aufgegriffen. Im Mittelpunkt steht dabei vor allem die Gültigkeit der Kopplungsansätze für Mehrphasenströmungen in porösen Medien, was die Entwicklung spezieller Kopplungsbedingungen notwendig macht. Die hier entwickelten Ansätze können dabei zum einen weiterentwickelt werden, zum anderen können für manche der vorgeschlagenen Anwendungsbereiche spezifischere Konzepte entwickelt werden. Aus dem weiten Feld möglicher weiterer Forschungsarbeiten in diesem Bereich sollen die Folgenden hervorgehoben werden:

- Das Makroporenmodell kann für die Modellierung von oberflächennahen Rutschungen durch Einbeziehung eines Bodenmechanikmodells weiterentwickelt werden. Das sich daraus ergebende Modell kann möglicherweise dabei helfen, den Einfluss von Makroporen beim Auslösen von Erdrutschen aufzuklären.
- Der Kopplungsansatz des Zweiphasenmodells im porösen Medium mit dem Einphasenrohrströmungsmodell kann im Kontext der Methanmigrationsproblematik in Bergwerken durch die Einführung von Isothermen, beispielsweise der Langmuir-Isotherme, für die Beschreibung von Adsorption und Desorption von Methan aus Kohleflözen weiterentwickelt werden. Hierfür ist zudem die Implementierung der Fluideigenschaften von Methan – insbesondere von Viskosität, Dichte und Diffusionskoeffizient – erforderlich.
- Das gekoppelte Modell für Zweiphasen-, Zweikomponentenströmungen im porösen Medium und Einphasen-, Zweikomponentenrohrströmungen kann für Brennstoffzellen weiterentwickelt werden, indem die Fluideigenschaften von Wasserstoff und Sauerstoff implementiert und in ein Reaktionskinetikmodell integriert werden.
- Um komplexe großskalige Probleme in angemessener Zeit lösen zu können, sollte die implementierten Modelle parallelisiert werden. Dabei ist zu beachten, dass die Parallelisierung der Flussberechnung des Hohlkörpernetzwerks verträglich sein muss mit der Parallelisierung des dreidimensionalen Kontinuums für die poröse Medien.
- In dieser Studie wird die Rohrströmung als eine einzelne Phase berücksichtigt. Zur besseren Beschreibung des gekoppelten Mehrphasengesamtsystems kann die Überführung der Einzelphase in ein Mehrphasenströmungsmodell hilfreich sein. Dafür müssen neue Konzepte entwickelt werden. Möglicherweise kann ein Kopplungskonzept auf Basis der modifizierten Freispiegelströmungsgleichungen dazu beitragen.

- Der mit Abstand wichtigste Parameter der untersuchten niederdimensionalen Doppelkontinuummodelle ist der Austauschkoeffizient (α_{EX}), welcher im Allgemeinen problemspezifisch ermittelt werden muss. α_{EX} wird durch eine getrennte Betrachtung des Einflusses der Fluideigenschaften, der Rohrgeometrie und der Eigenschaften des porösen Mediums (α_{ex}) beschrieben. Folglich könnte α_{ex} in einer weiteren Arbeit für verschiedene poröse Medien und Hohlkörperwände systematisch untersucht werden. Für die numerischen Simulationen würde dies zum einen den Aufwand der Parameterbestimmung reduzieren, zum anderen würde sich dies positiv auf die Parameterunsicherheiten auswirken.

- Die untersuchten niederdimensionalen Doppelkontinuumskopplungansätze berücksichtigen nur den Massenaustausch zwischen den beiden Kontinua. Als Erweiterung kann ein Impulsaustauschterm eingeführt werden, welcher die Unstetigkeit der Geschwindigkeit am Übergangsbereich beschreibt. Allerdings sind zur Bestimmung des Impulsaustausches für eindimensionale Rohrströmungmodelle neue Mittelungsmethoden erforderlich, welche die Einführung neuer Konzepte in das Rohrströmungsmodell erforderlich machen. Wenn diese theoretischen Grundlagen hinreichend verstanden sind, kann die von der Beavers-Joseph-Saffman-Bedingung beschriebene Unstetigkeit der Geschwindigkeit an der Grenzfläche in das eindimensionale Rohrströmungsmodell integriert werden.

1 Introduction

1.1 Motivation

Numerical models for simulating flow and transport in porous media are applicable in many environmental, technical and biological problems. Distinct structures embedded in the porous media often make conceptual modeling difficult. In particular, if the porous medium is intersected with distinct quasi-one-dimensional hollow structures, porous media flow and free flow in the hollow structures can interact strongly. Different governing equations are commonly used to model the flow in porous media and free flow regions. In porous media, the velocities are calculated by using Darcy's law (Darcy (1856)), where the Reynolds number is typically less than unity. However, in free flow regions Darcy's law is not applicable. There is a need to develop concepts for the modeling of coupled systems where porous media flow and free flow strongly interact.

Examples for such systems are:

- Mines: Methane released from unmined coal seams migrates through the porous rocks, but also through tunnels and shafts in the mine.
- Landslides: A sudden water infiltration through macropores may trigger landslides.
- Polymer electrolyte membrane fuel cells: The supply of reactive gases through free-flow channels into the porous diffusion layers interacts strongly with the evacuation process of the water, which is formed at the cathode reaction layer and flows from the porous diffusion layers into the free-flow channels.
- Cancer therapy: Therapeutic agents are delivered via the blood vessels into the tissue, targeting the tumor cells.

In the following, more insight is given into each of the above mentioned systems.

Methane migration problem:

Over millions of years coal seams have been formed by the so called coalification process by biochemical decay and metamorphic transformation of vegetable matter under high pressure. During the coalification process a large amount of different gases has been produced. Most of these gases escape to the atmosphere and some of them retain in the coal. Coalbed methane is the name given to methane found in coal seams (IEA Coal Industry Advisory Board (1994)). In its natural state, coal seams are under pressure deep in the subsurface. The mining of coal dramatically reduces the pressure of the coal seams, which eventually

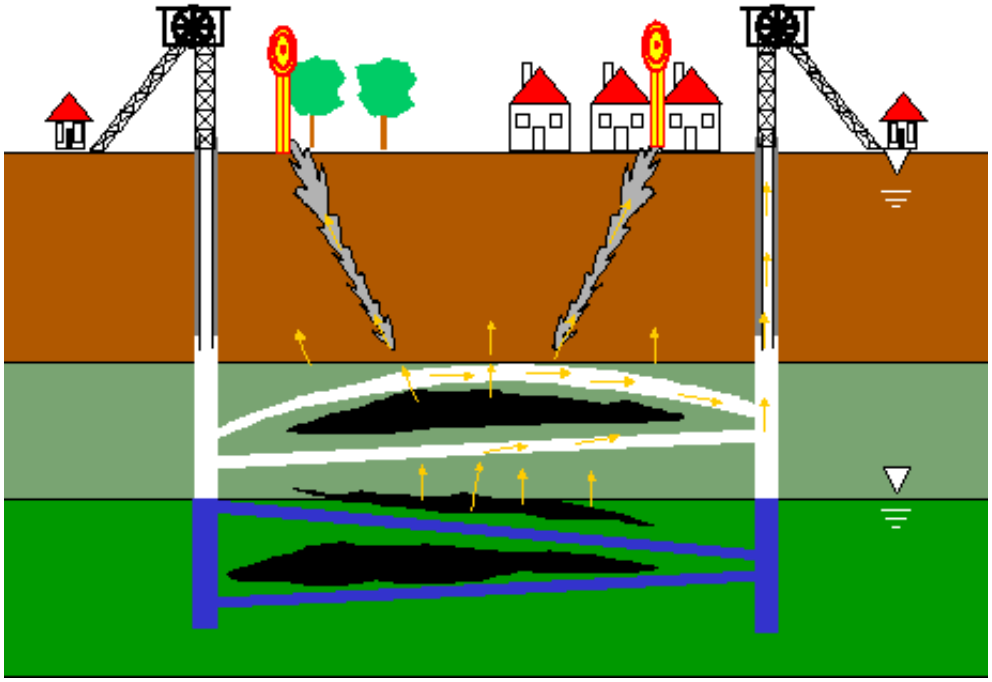

Figure 1: Coal-bed methane migration problem (Breiting *et al.* (2000))

results in the release of the coalbed methane via desorption. Fig. 1 shows a cross-section of an abandoned coal-mine. The desorption of the coalbed methane can take years to decades. Methane is less dense than air. The density difference between air and methane causes buoyancy forces which eventually result in the upward movement of methane. The desorbed methane finds its way to the surface either through tunnels or so called mine shafts or through the overlaying fractured porous media (Sheta *et al.* (2004)).

Methane, which is an odorless gas, may cause serious harm to people and the environment:

- It is explosive if the concentration in air is in the range of 5 to 15 vol.-%.
- There is a risk of suffocation where methane is leaking near residential areas.
- It can be harmful to the vegetation growth.
- Methane is a greenhouse gas.

Since the governing equations describing the flow and transport of methane in porous coal seams and in the tunnels of the mine are different, the numerical modeling of the methane migration problem requires coupling of pipe flow with porous media flow.

Landslide problem:

Parallel to the soil surface in hillslopes a chain of interconnected macropores can be naturally found. These macropores are called as "soil pipes" (Uchida and Mizuyama (2002)). Flow in soil pipes is one of the important storm runoff mechanisms on hillslopes (Uchida *et al.* (2001)). In studies of shallow land slides often scars of soil pipes are found, which might play a significant role in triggering shallow landslides (Pierson (1983)).

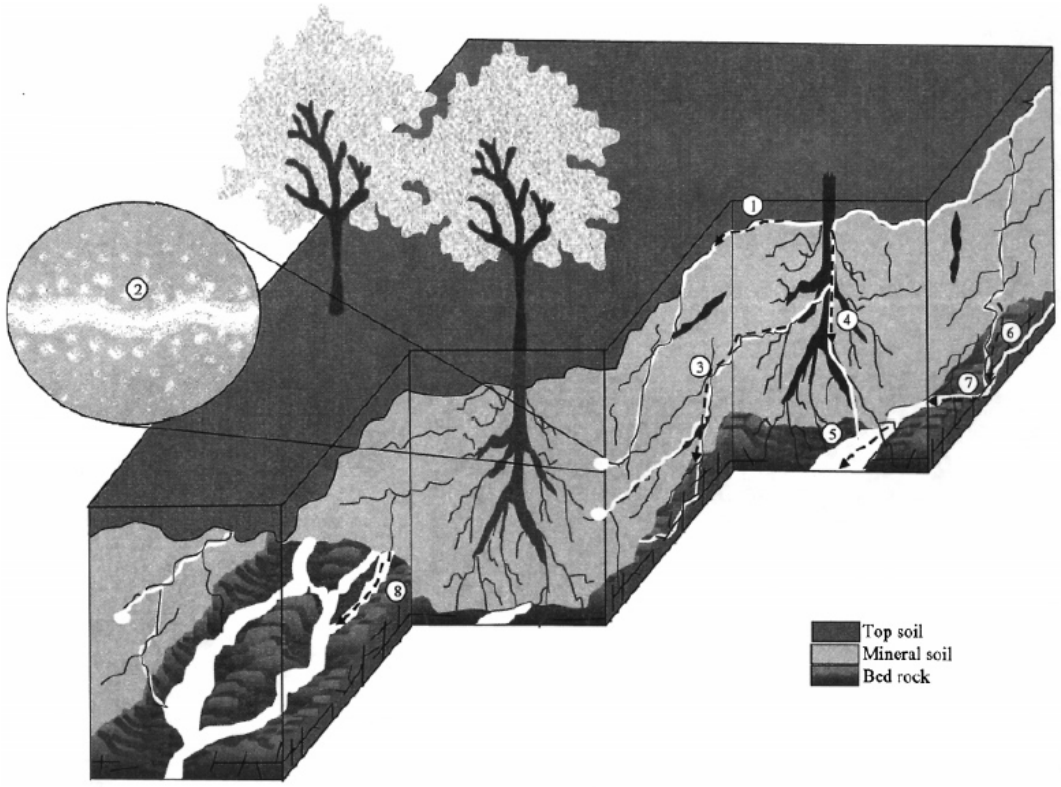

Figure 2: A conceptual model of preferential flow pathways in a hillslope segment based on staining, tracer, and hydrometric tests conducted at Hitachi Ohta experimental watershed in Japan (Sidle *et al.* (2000))

Preferential flow pathways in a hillslope segment can be separated into the following sections (see Fig. 2):

1) Preferential flow occurring between the organic rich top soil and the mineral soil
2) Macropores interacting with the surrounding mesopores (pores $< 1\ mm$)
3) Chain of interconnected macropores
4) Macropores interacting with the root channels
5) Contact of macropores with the bedrock

6) Preferential flow into the bedrock fractures

7) Exfiltration of water from the bedrock fractures

8) Flow over microchannels on the surface of bedrock

The flow of water from the soil into the macropores and vice versa is a typical example of a coupled pipe flow with porous media flow system.

Efficiency problem of PEM fuel cell:

A Polymer electrolyte membrane (PEM) fuel cell can convert chemical energy into electrical energy. Fig. 3 shows a schematic sketch of a PEM fuel cell. The operating principle of a fuel

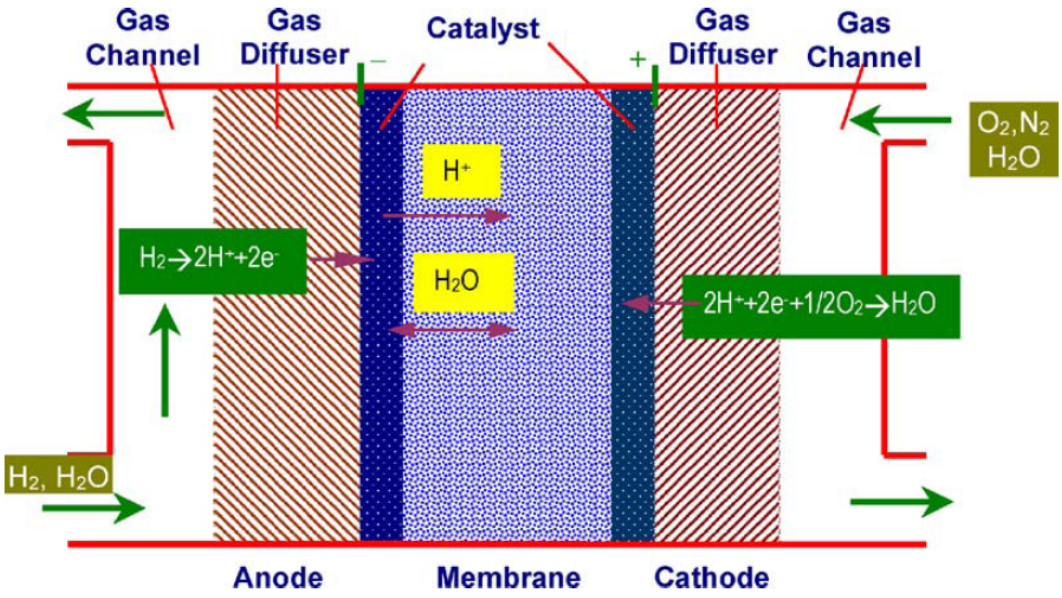

Figure 3: A schematic illustration of a PEM fuel cell (You and Liu (2006))

cell can be described as follows:

- H_2 and O_2 gases are supplied from two different sides of a fuel cell through gas channels.
- H_2 reaches the anode through a porous gas diffusion layer which is responsible for an efficient distribution of the gases and the evacuation of resulting water between the reaction layer (catalyst) and the gas channels.
- At the anode H_2 separates into its positive H^+ ions, which can pass through the PEM membrane (Tab. 1). However, the PEM membrane forces the electrons to reach the cathode through an external circuit.
- At the cathode O_2 reacts with positive H^+ ions and electrons to create water and energy (Tab. 1).

- The resulting water has to be evacuated from the system through the gas channels.

Anode:	H_2	$\rightarrow$	$2H^+ + 2e^-$
Cathode:	$\frac{1}{2}O_2 + 2H^+ + 2e^-$	$\rightarrow$	H_2O
Total reaction	$H_2 + \frac{1}{2}O_2$	$\rightarrow$	H_2O

Table 1: Chemical reactions in polymer electrolyte membrane fuel cell

The evacuation of resulting water at the cathode is problematic, since it blocks the transport of the reaction gases through the diffusion layer to the reaction layer (Acosta *et al.* (2006)). To facilitate the water evacuation process, the gas diffusion layer is made out of a hydrophobic material. The hydrophobic property has to be adjusted in such a way that on the one hand the blocking of the diffusion layer is prevented and on the other hand the PEM membrane doesn't dry out in order that the PEM fuel cell still produces electricity (Thoben (2006)). The transport of the reactive gases between gas channels and gas diffusion layers is a typical example of a coupled pipe flow with porous media flow system.

Cancer therapy:

Cancer is one of the most frequent causes of death. There are many medical researches carried out to cure cancer. One of the therapies to kill the tumor cells is to use a therapeutic

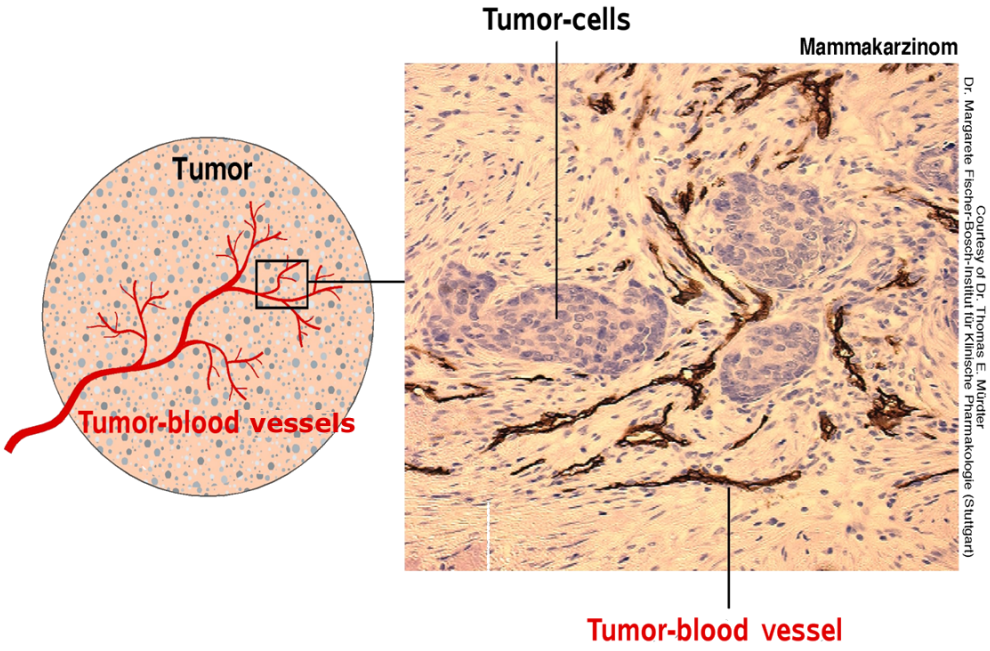

Figure 4: Tumor cells of a breast cancer and tumor-blood vessels

agent. Fig. 4 shows tumor cells of a breast cancer. The tumor cells are surrounded by healthy tissue and blood vessels, which can be considered as compliant tubes, i.e. the cross-section of blood vessels is changing as a function of pressure (Canic and Kim (2003)). Blood is a highly concentrated suspension which is strongly influenced by red blood cells and exhibits non-newtonian fluid behavior (Gijsen *et al.* (1999)). The therapeutic agent is injected into the blood vessel targeting the tumor cells and with the help of the cardiovascular system it is transported through the body. The dosage of the therapeutic agent is more or less a trial and error process, which is mostly due to nonuniform distribution of the therapeutic agent in the tumor (Jain (1989)). The estimation of dosage and distribution of the therapeutic agent is crucial for the therapy. The transport of the therapeutic agent from blood vessels into the surrounding tumor cells designates another pipe flow with porous media flow coupling problem.

1.2 Introduction to coupled models

The general approaches to coupling porous media flow with free flow models may be divided into two main groups according to the dimensions of the coupled models: (i) equi-dimensional coupling and (ii) lower-dimensional coupling. Independent from the equi-dimensional and lower-dimensional classification, the coupling strategies can be divided into two main groups according to the coupling technique applied: (i) discrete coupling and (ii) dual-continuum (multi-continuum) coupling. In discrete models, pipes are embedded in their actual geometrical locations into the porous media model and the interaction with porous media and free flow are modeled with clearly defined interface conditions. Whereas in dual-continuum models two continua lie on top of each other, and the interaction between the continua is modeled by adding an exchange source/sink term to the equations of both systems with different signs. The combination of the above mentioned classifications is possible, e.g. a model can be classified as equi-dimensional discrete or lower-dimensional dual-continuum model, etc.

In equi-dimensional coupling approaches, the term “equi-dimensional” means that both continua have the same dimensions, such as two-dimensional porous - two-dimensional free flow systems or three-dimensional porous - three-dimensional free flow systems. Darcy’s law, which commonly substitutes the momentum equation in the porous media region, is a first-order differential equation, whereas the momentum equation in the free flow region is in general a second-order differential equation. Thus, porous media flow equations and free flow equations are mathematically incompatible at the interface between the domains. In the literature, there are different approaches to overcome this problem. Brinkman suggests to use the same momentum equation for both flow regions (Brinkman (1949)). Another approach, proposed by Beavers and Joseph, applies an interface condition between the two flow regions which simply relates the free flow velocity and its gradient at the interface to the Darcy velocity in the porous medium (Beavers and Joseph (1967)).

In a lower-dimensional coupling approach, one system - in the present study this is always the free-flow system - has a lower dimension than the other one. If, for example, the free-flow region has a pipe-shaped form, i.e. the length of the pipe is much greater than its

diameter, one may reasonably use one-dimensional pipe flow equations where the velocity along the pipe network is cross-sectionally averaged. In this case, frictional forces can be calculated, for example, by using the Darcy-Weisbach friction factor (Darcy (1857), Weisbach (1855)).

Lower-dimensional modeling is not new but has also been widely used for the simulation of flow in fractured porous media. The fractures are then implemented as being one dimension lower than the dimensions of the porous medium. Reichenberger *et al.* (2006), for example, developed a discrete lower-dimensional fracture model, in which the flow in the fracture system is described by the parallel plate concept. Bauer (2003) used a lower-dimensional dual-continuum coupling technique for single-phase flow to model the karstification of a conduit in a fissured porous medium.

Coupling strategies of porous media flow with pipe flow are more extensively discussed in Chapter 2.2.

1.3 Objectives of the thesis

The goal of this study is to introduce new coupling strategies and to develop coupled numerical models which can form a basis for further studies modeling the complex systems mentioned in the motivation. In this study the dual-continuum concept is extended in order to couple multi-phase porous media flow with lower-dimensional single-phase free flow, where different physical processes in each continua are described by different equations. The focus is to present different new concepts for modeling three-dimensional flow in porous media coupled with one-dimensional pipe flow and to illustrate the characteristic behavior of such systems by numerical test examples. Since there is no need for homogenization of the pipe parameters for the whole porous media domain, this approach differs from commonly used dual-continuum models in fractured porous media.

1.4 Structure

The thesis is organized as follows:

After this introduction, the basic concepts and methods used in this study are explained. These include the consideration of scales, a broad overview on the coupling strategies of porous media flow with free flow, the explanation of the lower-dimensional dual-continuum coupling strategy, the introduction of fundamental governing equations as well as the numerical methods with detailed discretization techniques. For the numerical modeling of coupled systems a special grid implementation is necessary. For this purpose the construction of the 1D pipe network grid in a 3D porous grid is developed, which makes the lower-dimensional dual-continuum description of the two domains of different dimensions possible. After that, the coupled numerical models are introduced and the simulation results of each coupled model are presented. The complexity of the considered systems is gradually

increased. In the beginning, coupled single-phase systems are treated, where two models are introduced, which consist of the coupling of single-phase porous media flow with Hagen-Poiseuille flow and the coupling of single-phase porous media flow with compressible pipe flow. Then, the single-phase coupling strategy is tested by comparing the results with results of the experiment conducted under controlled laboratory conditions. Furthermore, the dual-continuum concept is extended for coupling multi-phase porous media flow with lower-dimensional single-phase pipe flow, where three new models are introduced, which include the coupling of Richards equation with Hagen-Poiseuille flow, the coupling of two-phase porous media flow with single-phase pipe flow and the coupling of two-phase two-component porous media flow with single-phase two-component pipe flow. With the introduction of each new model the conceptual and related numerical models for each specific problem case are described and then numerical results showing the characteristic behavior of these systems are presented and discussed in detail. Finally, the work is summarized and an outlook is given for further studies in the field of coupled porous media - pipe flow systems.

2 Basic Model Concept

Natural systems are generally highly complex not only due to the complexity of the structures but also due to the complexity of the physical processes. A model can not represent all natural processes at each scale in every detail. In the end, a model is merely a simplification of the natural processes under certain assumptions. First of all, the processes of interest in a natural system for a chosen scale are conceptually determined. This includes the determination of physical parameters for material properties and relevant physical processes, such as advection and diffusion. Then, the conceptual model should be replaced with an equivalent mathematical equation system. If the mathematical model is too complex to be solved analytically, which is usually the case for the coupled complex flow and transport systems, a numerical model is necessary to solve the equation system.

The perception of a physical phenomenon might change depending on the resolution of the observation. Therefore, the modeler should always determine the appropriate scale of the model for the problem that is about to be studied.

2.1 Consideration of spatial scales

If one looks at the same physical phenomena at different scales, one might see different processes depending on the scale of the observation. The definition of the physical fluid properties, e.g. viscosity and density, and the description of physical processes of interest also depend on the spatial scales. The fluid properties and physical processes should be related to an appropriate scale. Therefore, there is a need for a classification of the spatial scales. The spatial scales can be classified as done in Helmig (1997):

- **Molecular scale:** At this scale, the motion of individual molecules and their interaction with other molecules are observed. The computational costs of the models in this scale are typically very high even for small systems due to very high numbers of molecules.
- **Microscale:** One could assign averaged properties for a very big group of molecules, e.g. viscosity and density. At that level, the individual molecules and their interaction with the neighboring molecules are blended to the observer, and the properties of the matter are assumed to be continuous. This concept is denoted as continuum approach. At the microscale, the interfaces between the fluids and solids are clearly defined. The Navier-Stokes equations (Eq. 5 and Eq. 4) are microscale continuum equations, which describe the motion of the fluids. One can use the Navier-Stokes equations to model porous-media flow. However, it requires the geometric description of individual grains and the pore geometries, which are rarely available and even if it can be

obtained for small lab scale experiments, the computational costs of the models are very high compared to the macroscale models.

- **Macroscale:** At the macroscale range, the microscale conservation equations are averaged in a defined region. As a result of the averaging process, new properties appear in the macroscale conservation equations. In this work the conservation equations of one-dimensional pipe flow systems (Eq. 6 and Eq. 7) and multi-phase flow in porous media (Eq. 8 and Eq. 9) are both defined in macroscale range:
  - One can model pipe flow with full 3D Navier-Stokes equations. However, the computational costs are high. Since the pipe length is typically much bigger than the pipe diameter, instead of solving 3D Navier-Stokes equations, one could average Navier-Stokes equations along the pipe cross-section to get simplified 1D-averaged pipe flow equations, which look similar to the Navier-Stokes equation with the exception that the latter equation includes a correction coefficient (β) in the momentum convection term, a friction factor (ζ) in the cross-sectionally averaged viscous term and cross-sectionally averaged velocity ($\bar{u}_s$) (see Fig. 5). The derivation of the 1D-averaged pipe flow equations is discussed in Sections 2.3.1.3 and 2.3.1.4.
  - Multi-phase flow in porous media is generally modeled at the macroscale range, where microscale equations are averaged in a defined volume, denoted as representative elementary volume (REV). In porous media, one of these properties is the porosity, which is the ratio of the pore space to the total volume. The size of the REV should be chosen in such a way that small deviations in size should not have an effect on the averaged properties. Fig. 6 shows porosity depending on the averaging volume size. If the averaging volume size is too small, one observes strong fluctuations in the porosity value, which means that the chosen volume is too small and it falls into microscale range. If the averaging volume size reaches V_o, the fluctuations in the porosity disappear and stay constant until it is distorted again by the heterogeneities where the maximum size of the REV is reached. Therefore, REV should be chosen in the spatial range where the averaged macroscale property stays constant.

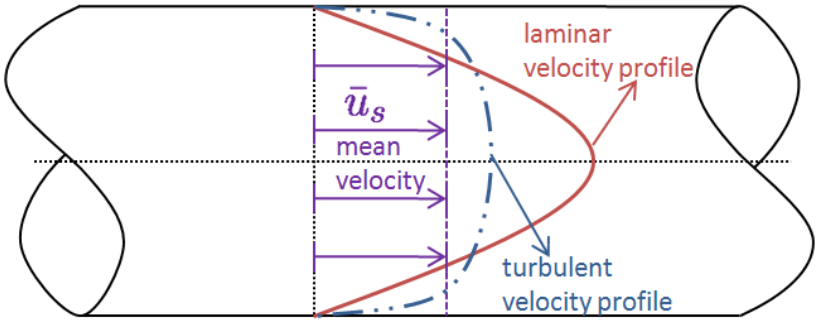

Figure 5: Cross-sectionally averaged 1D velocity profile

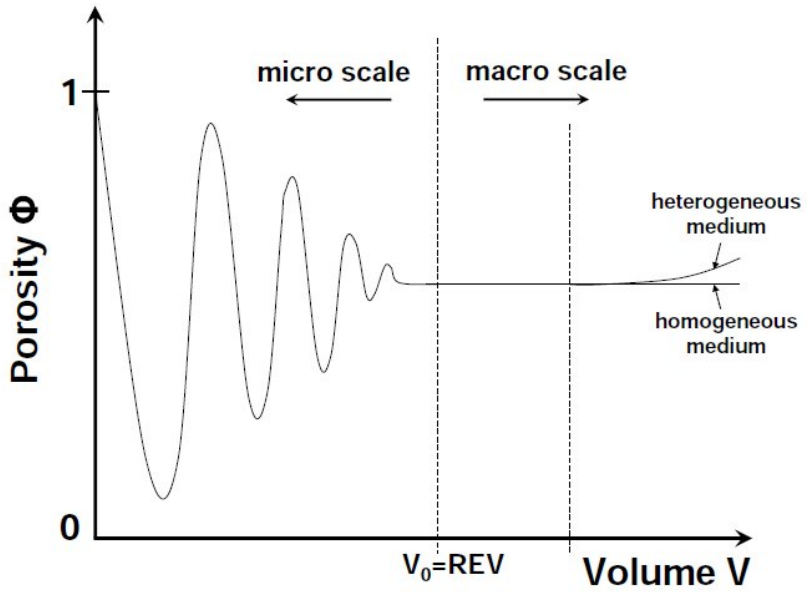

Figure 6: Representative elementary volume (REV) for a macroscale property (in this case porosity) after Bear (1988)

The conservation equations in microscale and macroscale systems are discussed in Section 2.3 in detail. However, for the completeness of the consideration of scales, the conservation equations are introduced as follows:

See the notation tables at the beginning of the thesis for an explanation of the symbols used in the equations.

Microscale conservation equations for free flow:

$$\frac{\partial \varrho}{\partial t} + \vec{\nabla} \cdot (\varrho \vec{u}) = q \tag{4}$$

$$\frac{\partial (\varrho\ \vec{u})}{\partial t} + \vec{\nabla} \cdot (\varrho\ \vec{u} \otimes \vec{u} + p\ \bar{\bar{I}} - \bar{\bar{\tau}}) = \varrho\ \vec{f_{ext}} \tag{5}$$

Macroscale conservation equations for one-dimensional pipe-flow system:

$$\frac{\partial \varrho}{\partial t} + \frac{\partial}{\partial s}(\varrho\ \bar{u}_s) = q \tag{6}$$

$$\frac{\partial (\varrho\ \bar{u_s})}{\partial t} + \frac{\partial (\beta\ \varrho\ \bar{u}_s\ \bar{u}_s)}{\partial s} + \frac{\partial p}{\partial s} + \tau_w \frac{\pi d}{A} = \varrho\ \vec{g} \cdot \vec{s} \tag{7}$$

, where $\tau_w = \frac{\zeta}{8}\ \varrho\ \bar{u}_s^2$, and $\varrho = \frac{p}{R_{ind}\ T}$.

Macroscale conservation equations for multi-phase flow in porous media:

$$\Sigma_\alpha \left[\frac{\partial (\phi\ \varrho_\alpha\ x_\alpha^k\ S_\alpha)}{\partial t} \right] + \Sigma_\alpha \left[\vec{\nabla} \cdot (\varrho_\alpha\ x_\alpha^k\ \vec{u}_\alpha) \right] - \Sigma_\alpha \left[\vec{\nabla} \cdot (\bar{\bar{D}}_\alpha^k\ \nabla (\varrho_\alpha\ x_\alpha^k)) \right] = q^k \tag{8}$$

$$\vec{u}_\alpha = -\frac{k_{r\alpha}}{\mu_\alpha} \bar{\bar{K}} (\nabla p_\alpha - \varrho_\alpha\ \vec{g}) \tag{9}$$

2.2 Coupling strategies

Before going into the details of coupling strategies, a first simplification is done by considering only single-phase flows in both porous media and free flow systems. The single-phase coupling strategy is gradually extended for the multi-phase flow coupling from Chapter 6 on.

The general approaches for coupling porous media flow with free flow models may be subdivided into two main groups according to dimensions of the coupled models:

- Equi-dimensional coupling
- Lower-dimensional coupling

Independent from the equi-dimensional and lower-dimensional classification, the coupling strategies can be subdivided into two main groups according to the coupling technique applied:

- Discrete models
- Dual-continuum (multi-continuum) models

A combination of the above mentioned classifications is possible, e.g. a model can be classified as equi-dimensional discrete or lower-dimensional dual-continuum model.

Coupling according to the dimensions of the coupled models is discussed in the following two sections in detail.

2.2.1 Coupling in equi-dimensional systems

The meaning of equi-dimensional coupling is that both systems have the same dimensions, e.g. 2D porous - 2D free flow or 3D porous - 3D free flow. Fig. 7 shows an equi-dimensional system, where the flow in porous media and the flow in free flow are coupled along an interface. One can model both systems with microscale Navier-Stokes equations, which doesn't require special interface conditions, since in both free flow and porous media domains the same set of equations is solved. However, each pore geometry in the porous medium needs to be described in detail, which increases the computational cost of the model enormously (see Fig. 7 part b). In general, the conservation equations of porous media flow are described in macroscale and the conservation equations of free flow are described in microscale. The macroscale momentum equation of porous media flow (Eq. 32) is a 1'st order differential equation, whereas the microscale momentum equation of free flow (Eq. 34) is a 2'nd order differential equation, which means porous media flow equations and free flow equations are mathematically incompatible. In contrast to the Navier-Stokes equations, Darcy's law doesn't include higher order inertial and viscous terms, i.e. it fails to relate the porous media flow velocities to the free flow velocities and vice versa. Therefore, the velocity and

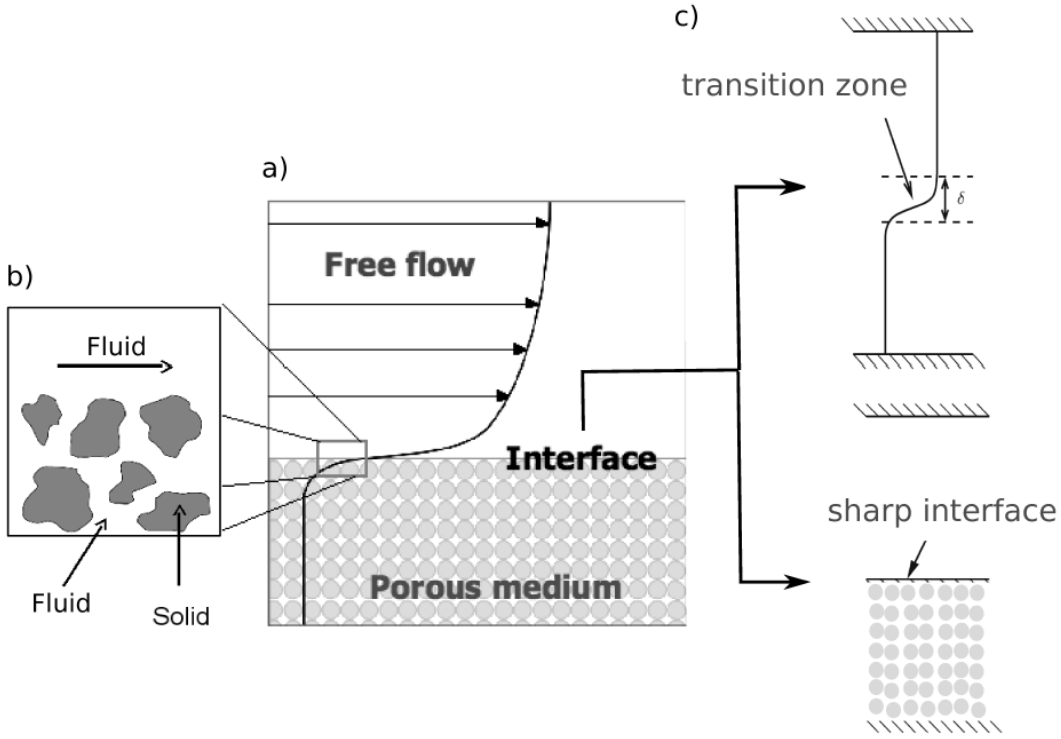

Figure 7: Interface description in equi-dimensional systems (Mosthaf *et al.* (2010))

velocity gradient at the interface remain unknown and the flow field on the free flow side of the interface remains unsolved. In the literature, there are two approaches to overcome this problem:

- Brinkman equation (single-domain approach)
- Beavers and Joseph interface condition (two-domain approach)

2.2.1.1 Brinkman equation (single-domain approach)

Brinkman (1949) proposed one momentum equation (Eq. 10) for both porous media and free flow continua, which is a superposition of the Stokes equation and Darcy's law and involves an effective viscosity ($\tilde{\mu}$) parameter. In Eq. 10 the flow is assumed to be incompressible and inertial terms are neglected. Since the Brinkman equation is valid in the whole domain, there is no need to define interface conditions between the porous media and free flow regions. However, there is a need to define the location of the interface. The interface from porous media to free flow in the Brinkmann model is generally realized by defining a spatial variation of the properties, such as the permeability, the porosity and the effective viscosity along a thickness (δ) of a transition zone between the two continua (the top figure in Fig. 7 part c)). The specified parameters in the transition zone are decisive for the results, which are eventually produced by the coupled models.

$$-\vec{\nabla} \cdot (\tilde{\mu} \nabla \vec{u}) + \mu \bar{\bar{K}}^{-1} \vec{u} + \nabla p = \vec{f}_{ext} \tag{10}$$

, where p is pressure, u is the velocity, K is the permeability and μ is dynamic fluid viscosity and $\tilde{\mu}$ is effective viscosity.

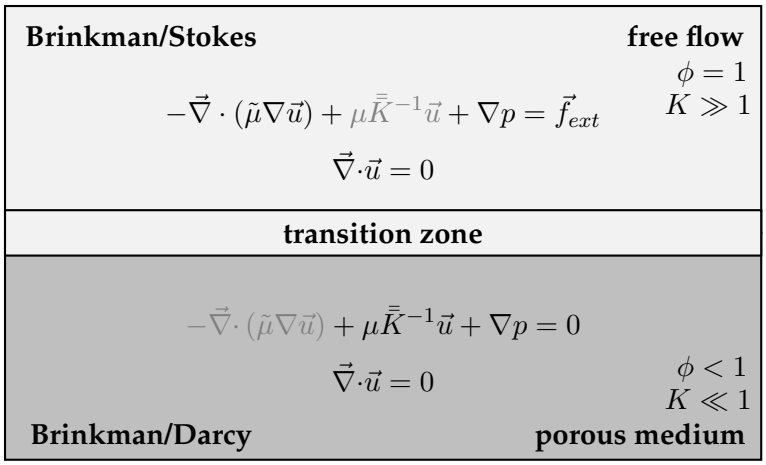

Figure 8: Single-domain coupling concept for a single-phase flow system (Mosthaf *et al.* (2010))

In the porous medium:

Since the permeability is very small, the first term of Eq. 10 is diminishing and it can be neglected. This leads to the Darcy equation (Eq. 11) and the velocity u in porous media represents a Darcy velocity (see lower part of Fig. 8):

$$-\vec{\nabla} \cdot (\tilde{\mu} \nabla \vec{u}) + \frac{\mu}{\bar{\bar{K}}} \vec{u} + \nabla p = 0 \tag{11}$$

In the free flow:

Since the permeability is very big, the second term of the Brinkman equation becomes very small and can be neglected. This leads to the Stokes equation (see upper part of Fig. 8):

$$-\vec{\nabla} \cdot (\tilde{\mu} \nabla \vec{u}) + \frac{\mu}{\bar{\bar{K}}} \vec{u} + \nabla p = \vec{f}_{ext} \tag{12}$$

The effective viscosity ($\tilde{\mu}$) is the key parameter in the Brinkman model and can be different from the dynamic viscosity of the fluid μ. In the literature, there are different opinions about the choice of the effective viscosity. Kaviany (1995) proposed that the effective viscosity should depend on the fluid and pore structure. Brinkman (1949) and Howells (1974) suggested using $\tilde{\mu} = \mu$. In the studies of Givler and Altobelli (1994), Kim and Russel (1985), Martys *et al.* (1994), Sahraoui and Kaviany (1992) and Starov (2001) it is proposed that the effective viscosity should be smaller than the fluid viscosity ($\tilde{\mu} < \mu$). On the other hand, Gupte and Advani (1997) and Koplik *et al.* (1983) suggested the opposite ($\tilde{\mu} > \mu$). Larson and Higdon (1986, 1987) found that ($\tilde{\mu}/\mu$) ratio depends on the flow orientation, i.e. $\tilde{\mu} > \mu$ for a

flow parallel and $\tilde{\mu} < \mu$ for a flow vertical to the interface. Ochoa-Tapia and Whitaker (1995) suggested that the effective viscosity can be represented by $\tilde{\mu} = \mu/\phi$, where ϕ is the porosity. Since there is no clear methodology to choose the effective viscosity, which remains an unknown empirical parameter, in most of the studies the $\tilde{\mu} = \mu$ relation is commonly used (Basu and Khalili (1999), James and Davis (2001) and Prinos *et al.* (2003)). Lately, Rosenzweig and Shavit (2007) presented a modified Brinkman equation (MBE), which doesn't need empirical adjustments, and claimed that under certain assumptions the MBE is valid within a wide range of porosities.

2.2.1.2 Beavers and Joseph interface condition (two-domain approach)

In the two-domain approach two subdomains are modeled with different equation systems, e.g. the Stokes equation in the free-flow subdomain and Darcy's law in the porous media subdomain (see Fig. 9). Appropriate interface conditions are necessary to satisfy the mass balance and the vertical and tangential force balances across the interface. The mass balance and the vertical force balances between the two subdomains are easy to formulate. However, the tangential force balance needs a special treatment.

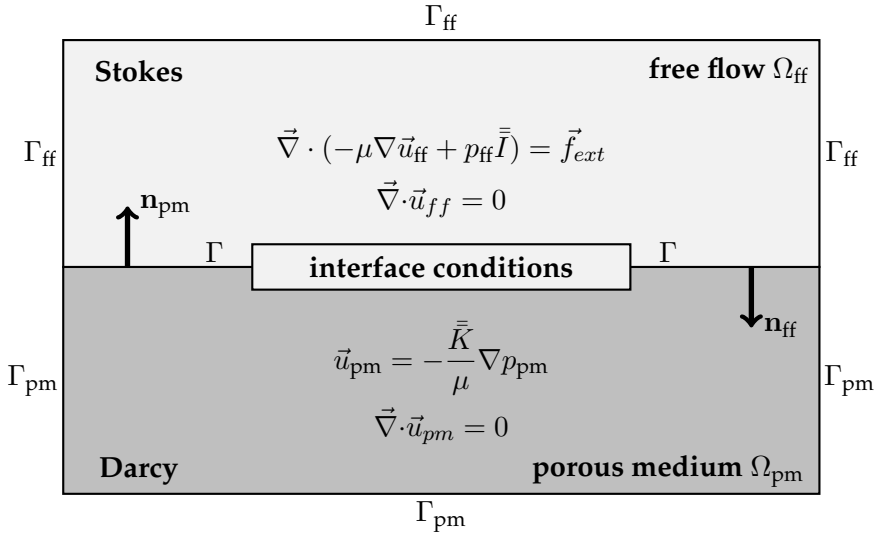

Figure 9: Two-domain coupling concept for a single-phase flow system (Mosthaf *et al.* (2010))

Beavers and Joseph (1967) carried out an experimental study, where they observed the velocity profiles at the free flow domain and the porous media domain (top and bottom layers in Fig. 10 respectively), in order to find a relation accounting for the tangential force balance along the interface. The results showed that the flux in the free flow domain is significantly increased when a porous (natural) wall is present instead of an impermeable wall. This indicated the presence of a boundary layer at the interface to the porous medium. Here, the velocity changes from the Darcy velocity (u_{pm}) to some slip value ($u_{ff_{bt}}$) immediately outside the porous medium.

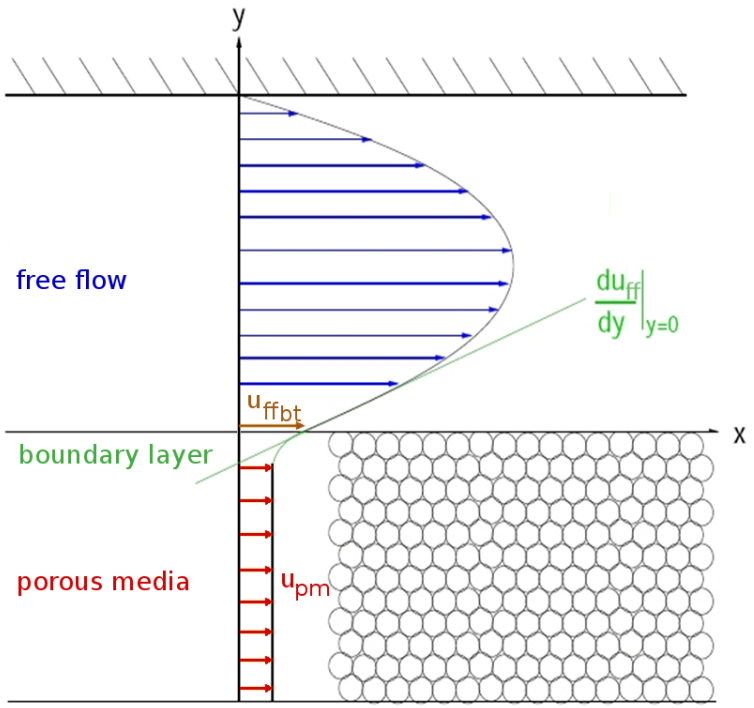

Figure 10: Velocity profile in the investigated system

For the investigated system it is necessary to define the tangential velocity of the free fluid at the interface with the porous medium. Therefore, an adequate and physically reasonable coupling strategy has to be found, that accounts for the relation between the tangential free flow velocity and the Darcy velocity. Beavers and Joseph developed a simple coupling condition for the discussed system. Basically, they used a pore-scale consideration that approximates the velocity gradient at the interface (Fig. 10) by:

$$\frac{\partial u_{ff}}{\partial y} = \frac{\alpha_{BJ}}{\sqrt{K}} \cdot (u_{ff_{bt}} - u_{pm}) \tag{13}$$

K is the permeability, $u_{ff_{bt}}$ is the tangential free flow velocity at the boundary and α_{BJ} is a dimensionless parameter known as the Beavers and Joseph slip coefficient, which presumably depends on the porous media properties in the boundary layer region (Beavers and Joseph (1967)). The Beavers and Joseph condition simply relates the free flow velocity and its gradient at the interface to Darcy velocity. Beavers *et al.* (1970) and Taylor (2006) tried to verify the existence of the Beavers and Joseph condition experimentally, and Murdoch and Soliman (1999), Zhou and Mendoza (1993) tried to verify it theoretically. James and Davis (2001) and Sahraoui and Kaviany (1992) showed that the Beavers and Joseph slip coefficient changes as a function of flow condition. Additionally, Sahraoui and Kaviany (1992) showed that it not only depends on the porous media properties but also on the interface geometry. Eventually, the Beavers and Joseph slip coefficient is an empirical parameter which needs to be adapted to each problem.

For a better understanding of the Beavers and Joseph interface condition, a simple coupled model is introduced in the following section, which is based on the work of Layton *et al.* (2003).

Model description

The model consists of Stokes flow in the free flow region Ω_{ff} and Darcy's law in the porous media region Ω_{pm}, which are separated by an interface Γ. Figure 11 gives a schematic representation of both flow regions. In the figure the outward unit normal vectors are described by n_j, $\{j = ff,\ pm\}$, each having tangential and vertical components. Steady state incompressible flow conditions are considered and inertial terms are neglected.

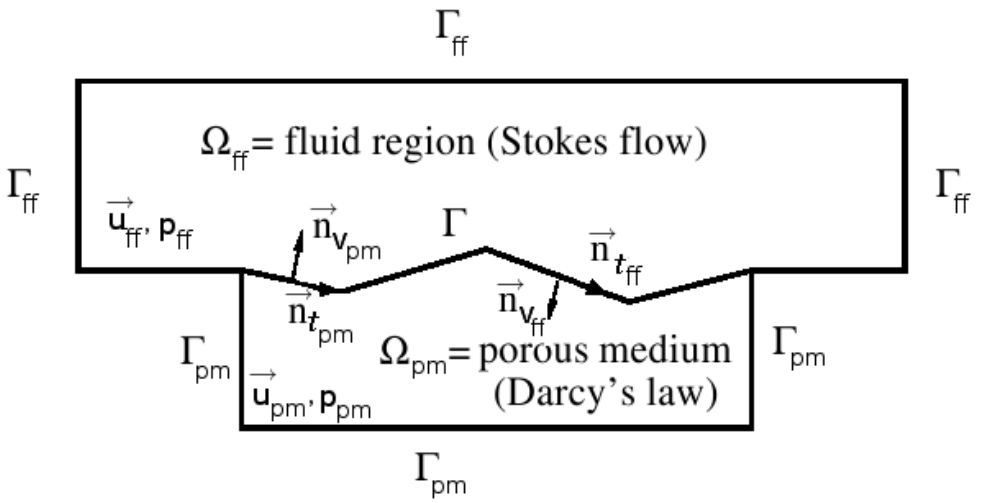

Figure 11: Interface between porous media and free flow domains Layton *et al.* (2003)

Flow equations

Free flow - Stokes equation:

$$-\nabla \cdot \bar{\bar{\sigma}}(\vec{u}_{ff}, p_{ff}) = \vec{f}_{ext} \qquad in \quad \Omega_{ff} \tag{14}$$

$$-\nabla \cdot \vec{u}_{ff} = 0 \qquad in \quad \Omega_{ff} \tag{15}$$

The total internal stress tensor ($\bar{\bar{\sigma}}$) can be associated with the pressure and the shear stress tensors as in Eq. 16:

$$\bar{\bar{\sigma}} = -p_{ff}\,\bar{\bar{I}} + \bar{\bar{\tau}} \tag{16}$$

The shear stress tensor ($\bar{\bar{\tau}}$) is related to the deformation (strain) rate tensor ($\bar{\bar{\varphi}}$) as in Eq. 17:

$$\bar{\bar{\tau}} = 2\,\mu\,\bar{\bar{\varphi}} \tag{17}$$

The deformation rate tensor is defined as follows:

$$\bar{\bar{\varphi}}(\vec{u}_{ff}) = \frac{1}{2}(\frac{\partial u_{ff_i}}{\partial j} + \frac{\partial u_{ff_j}}{\partial i}); \quad i,j \quad \in \quad x,y,z \tag{18}$$

Porous media - Darcy flow:

$$-\nabla \cdot \vec{u}_{pm} = 0 \qquad in \quad \Omega_{pm} \tag{19}$$

$$\vec{u}_{pm} \;=\; -\frac{K}{\mu}\,\nabla p_{pm} \qquad in \quad \Omega_{pm} \tag{20}$$

Interface Conditions

The porous media flow and the free flow must be coupled across Γ by the correct interface conditions.

Mass balance:

$$\vec{u}_{ff} \cdot \vec{n}_{v_{ff}} + \vec{u}_{pm} \cdot \vec{n}_{v_{pm}} = 0 \tag{21}$$

Balance of the normal forces across interface:

$\vec{F}$ = Force acting from the boundary to the fluid.

$$\vec{F} = -A\,\vec{n}_{v_{ff}} \cdot \bar{\bar{\sigma}} \tag{22}$$

$$\vec{F}_v = -A\,\vec{n}_{v_{ff}} \cdot \bar{\bar{\sigma}} \cdot \vec{n}_{v_{ff}} \tag{23}$$

$$\vec{F}_v = A\,(\vec{n}_{v_{ff}} \cdot (p_{pm}\,\bar{\bar{I}}) \cdot \vec{n}_{v_{ff}}) \tag{24}$$

$$\vec{n}_{v_{ff}} \cdot [p_{ff}\,\bar{\bar{I}} - 2\mu\,\bar{\bar{\varphi}}(\vec{u}_{ff})] \cdot \vec{n}_{v_{ff}} = p_{pm} \tag{25}$$

Note that pressure is discontinuous at the interface.

Condition for the tangential fluid velocity:

The tangential fluid velocity on Γ is described by Beavers and Joseph interface condition:

$$(\vec{u}_{ff} \cdot \vec{n}_t - \vec{u}_{pm} \cdot \vec{n}_t) \frac{\mu \, \alpha_{BJ}}{\sqrt{K}} = \frac{\vec{F}_t}{A} \tag{26}$$

$$\vec{F}_t = -A \, \vec{n}_{v_{ff}} \cdot \bar{\bar{\sigma}} \cdot \vec{n_t} \tag{27}$$

$$\vec{u}_{ff} \cdot \vec{n}_t - \vec{u}_{pm} \cdot \vec{n}_t = \frac{\sqrt{K}}{\mu \, \alpha_{BJ}} \, \vec{n}_{v_{ff}} \cdot (p_{ff} \, \bar{\bar{I}} - 2\mu \, \bar{\bar{\varphi}}(\vec{u}_{ff})) \cdot \vec{n}_t \tag{28}$$

Note that p_{ff} drops out of the Eq. 28 after the multiplication with the normal vectors and that velocity is discontinuous at the interface.

Simplification according to Saffman:

It is questionable whether Eq. 28 leads to a well-posed problem, and it has been observed that the term on the left-hand side $\vec{u}_{pm} \cdot \vec{n}_t$ is much smaller than the other terms. Thus, its inclusion in this linear approximation is unclear (Layton *et al.* (2003)). The most accepted interface condition was derived by Saffman (1971) using a statistical approach. This condition, which drops the Darcy velocity, is today known as the Beavers-Joseph-Saffman law (Eq. 29). The Beavers-Joseph-Saffman law is mathematically justified by Mikelic and Jäger (2000).

$$\vec{u}_{ff} \cdot \vec{n}_t = -\frac{\sqrt{K}}{\alpha_{BJ}} \, \vec{n}_{v_{ff}} \cdot (2 \, \bar{\bar{\varphi}}(\vec{u}_{ff})) \cdot \vec{n}_t \tag{29}$$

2.2.2 Coupling in lower-dimensional systems

The term lower-dimensional coupling in this context means that one flow system has a lower dimension than the other system with which it is coupled. The particular focus of this study is on coupling three-dimensional porous media flow with one-dimensional pipe flow. A major assumption when considering flow in a pipe as one-dimensional is that the velocity can be averaged at each cross-section along the pipe, i.e. it is then constant for each cross-section. This assumption severely limits the applicability of coupling schemes available in the literature. For example, the Beavers and Joseph interface condition, which was developed for equi-dimensional coupling, relates the free flow velocity and its gradient at the interface to the Darcy flow velocity in the porous medium. However, one cannot speak of a velocity gradient perpendicular to the pipe direction in a one-dimensional cross-sectionally averaged pipe flow model. The use of a lower-dimensional dual-continuum coupling strategy is proposed, accounting only for the mass transfer between porous media and pipe flow continua. One could add another exchange term for the momentum transfer between both continua in a dual-continuum model. However, the determination of the momentum exchange rate would require an averaging technique in which the slip boundary condition at the interface should be averaged over the cross-section of the pipe. Eventually, this would introduce another exchange coefficient for the momentum exchange rate, which would not only make the dual-continuum model more complicated but also more uncertain or overparameterized. That kind of approach is beyond the scope of this study.

The modeling techniques applied in fractured porous-media are helpful in the development of strategies for the coupling of 1D pipe flow with 3D porous media flow. There are mainly two distinct approaches according to the geological characteristics of the investigated area, where the scale of the fractures is decisive. Therefore, discrete and dual-continuum coupling in fractured porous media are discussed in the following two sections in detail.

2.2.3 Discrete models

If flow and transport processes are dominated by fractures, and fissures and the processes in the soil matrix are not negligible, one can model the soil matrix as one continuum and fractures as embedded geometries inside the matrix continuum. In such a case, each single fracture needs to be explicitly determined, which requires the detailed fracture geometries, i.e. the size, the orientation, the density; and the interaction of fractures with porous media can be modeled with clearly defined interface conditions.

The current state of research in the field of fractured porous-media can be listed as follows: In the Kolditz's book (Kolditz (1997)) systematic methods for the determination of fracture parameters and suitable methods for modeling single-phase flow in discrete fracture-models were described in detail. In the Helmig's dissertation (Helmig (1993)) the theory and the numerical methods for modeling multi-phase flow in discrete fracture-models were described. Reichenberger (2004) and Reichenberger *et al.* (2006) implemented a lower-dimensional discrete fracture-model for the simulation of multi-phase flow in fractured porous-media into numerical simulator MUFTE-UG. Equi-dimensional discrete fracture-models are developed by Gebauer *et al.* (2002), Neunhäuserer *et al.* (2002) and Ochs *et al.* (2002). Neunhäuserer (2003) studied the discretization techniques for modeling flow and transport processes in discrete fracture-models in further detail. Jakobs (2004) developed methods for modeling non-isothermal gas-water processes in discrete fracture-models. Süß (2005) analyzed the influence of structures and boundaries on flow and transport processes in fractured porous-media. Assteerawatt (2008) developed a geostatistical fracture generation module for the modeling of discrete fractures in porous media.

2.2.4 Dual-continuum models

The dual-continuum model concept for fractured aquifer systems was introduced by Barenblatt *et al.* (1960) and Warren and Root (1963). Due to the high contrast in properties of fracture system and porous matrix, the total system is idealized as two overlapping interacting continua, which occupy the same computational domain. This kind of approach requires homogenization of discrete fracture network parameters (porosity, permeability etc.) for the equivalent representative elementary volumes in fracture continua. Each continuum is modeled by its own conservation equations, and the interactions between the continua are described by an exchange term. In the literature, dual-continuum models can be classified as dual-porosity, dual-permeability or multiple interacting continua (MINC). In dual-porosity models, the fracture continuum elements are connected to each other and to the elements of the matrix continuum, whereas the elements of the matrix continuum are not connected

to each other (e.g. Bibby (1981)). This kind of model is suitable for fractured rock systems, where the flow is mainly in the fracture continuum and the rock matrix acts as an additional storage volume. In dual-permeability models the matrix continua are also connected to each other (e.g. Gerke and van Genuchten (1993)). Such models are suitable for fractured matrix systems, where flow occurs both in fracture and in matrix continua. The MINC method is developed by Pruess and Narasimhan (1985). It is basically an extension of the dual-porosity model, in which instead of a single matrix continuum several nested matrix continua are introduced to better represent transient flow behavior.

A suitable model should be selected depending on the scale of the problem. Bear *et al.* (1993) classified four different fields of flow and transport processes in fractured porous media according to their scales as follows:

- **The very near field**: Flow and transport processes are considered in a well defined single fracture and the surrounding porous rock.
- **The near field**: The study domain at this scale is relatively small and contains a relatively small number of fractures. The geometries of the individual fractures can be explicitly determined or stochastically generated based on the deterministic or stochastic information obtained from the observations.
- **The far field**: It is assumed that flow and transport processes occur simultaneously in two overlapping continua. One continuum describes the fracture network and the other describes the porous matrix. Fluid mass and its components may be exchanged between the two continua.
- **The very far field**: The entire fractured system is described as one single continuum, possibly heterogeneous and anisotropic, if geological layers and fault zones on a large scale are taken into account.

Fig. 12 shows model concepts for the description of fractured porous media depending on the size and the density of the fractures (Dietrich *et al.* (2005)). The figure is self-explanatory; on the left side of the figure model classifications and on the right side the appropriate models are presented. Fig. 12 can be used to classify the spatial scale of this work, which falls between the model classification of III and IV, where the flow and transport in the soil matrix is not negligible and a discrete 1D pipe-network is dominating the flow.

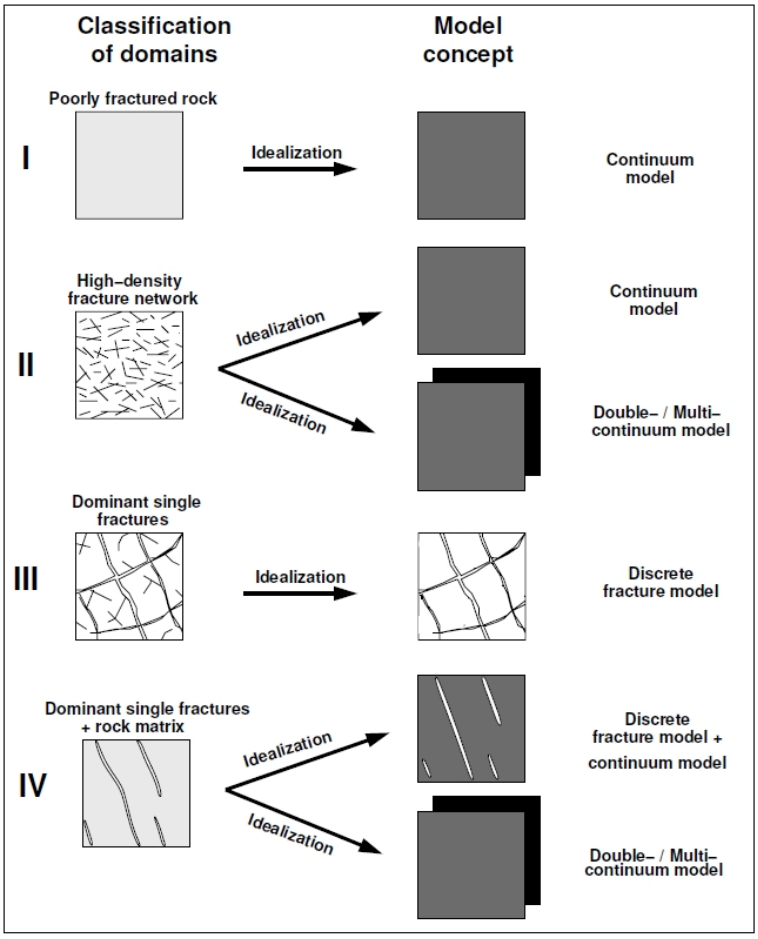

Figure 12: Dietrich *et al.* (2005) classified appropriate model concepts for the fractured porous media based on the work of Kröhn (1991) and Helmig (1993)

Beside single phase flow coupling, recent research is aimed at describing interface conditions for more complex multi-phase flow and transport systems, which is one of the main research areas in the hydromechanics and modeling of hydrosystems department of the institute of hydraulic engineering (IWS-LH2). The current research projects in this area are listed as below:

- Modeling and analysis of the movement of fluid-fluid interfaces in porous media coupled with free flow (International Research Unit MUSIS, German Research Foundation (DFG) project): The focus is on modeling and analysis of infiltration and evaporation fronts in unsaturated porous media and on the movement and the stability of liquid-gas interfaces. For this purpose, Mosthaf *et al.* (2010) developed a new concept for the coupling of two-phase compositional porous media and single-phase compositional free flow, where the Beavers-Joseph-Saffman law is utilized for the balance of the tangential forces across the interface.

- Coupling of micro and macro models for complex flow and transport processes in biological tissue (Cluster of Excellence "Simulation Technology" (SimTech), DFG project): Within the present project the flow and transport phenomena of interest are the transport processes of therapeutic agents in biological systems. Therapeutic agents spread in the circulatory system and reach the surrounding tissue by crossing the mircrovascular walls of the smallest blood vessels, which act as the main regulator of substance exchange. Hence, the flow and transport processes of the therapeutic agents in the blood vessels and especially the interaction with and transfer through the complex structure of the capillary wall are of crucial importance. This project focuses on the identification and modeling of the decisive processes for the transport of therapeutic agents between the two continua, blood vessels and tissue, by coupling microscale free flow with macroscale porous media flow. Compared to the following project it describes the processes mathematically as well as numerically at a smaller scale.

- A system biology approach towards predictive cancer therapy (Research Unit for System Biology FORSYS, BMBF project): This project focuses on the modeling of the spatial and temporal distribution of therapeutic agents in the whole organ and the tumor tissue. For this purpose, a numerical model is necessary to model the transport of the therapeutic agents between the tumor and the surrounding blood vessel-network. Two different continua can be identified, the blood vessels and the interstitial space of the surrounding tissue, which can be coupled using a double-continuum approach. While the above mentioned project focuses on the identification and modeling of the limiting processes occurring at the capillary wall, this project focuses on the modeling of the whole organ, tumor and blood vessel-network system. Therefore, the processes need to be formulated at a larger scale.

- Multi-phase multi-component processes within gas diffusion layers in fuel cells and their interactions with channel flow (International Research and Training Group NUPUS, DFG project): When optimizing the power density of the fuel-cells, it has been found that the performance is generally limited by the relatively slow kinetics of oxygen reduction at the cathode. Thus, optimal oxygen supply to the cathodic reaction

layer, which is generally constrained by liquid product water, is essential for performance. One of the difficulties in numerical models is the description of the boundary conditions at the interface between the gas channels (i.e. gas distributors) and the diffusion layer. The purpose of the gas distributors is two-fold: On the one hand the gas channels supply oxygen to the diffusion layer, on the other hand they take up the product water in the form of steam. Therefore, an important aspect of the numerical models for water management in fuel cells is the clear description of the interface conditions for the fluxes between the porous gas diffusion layer and the gas distributor. This project aims to study approaches for such interface conditions on the continuum scale and to find the required effective parameters of these continuum-scale interface conditions.

The interaction of free flow with porous media flow are studied for many different systems at different scales. In the present thesis the coupling of porous media flow with pipe flow is investigated. For this purpose, an appropriate coupling strategy needs to be developed. The new coupling concept will be adopted not only for single phase flow systems but also for multi-phase flow and transport systems and the experience gained in developing the multi-phase coupling strategies can also be utilized for the above mentioned systems. In this work a lower-dimensional dual-continuum model approach is proposed, which is explained more in detail in the following section.

2.2.5 Lower-dimensional dual-continuum coupling strategy

A major focus of this work is on the development of a lower-dimensional dual-continuum model approach, which is similar to the dual-permeability model in the sense that the elements in the porous media continuum are connected to each other. Since the pipe flow system is modeled as a discrete pipe network model with its real geometry, there is no need for homogenization of pipe parameters for the whole domain. Therefore, this approach differs from commonly used dual-continuum models in fractured porous media. Two continua (here: porous medium and pipe network) lie on top of each other and the mass exchange between the continua is calculated by adding an exchange source/sink term (Eq. 30) to the mass conservation equations of both systems with different signs. The mass exchange takes place only along the pipe network system in both continua. In the following the lower-dimensional dual-continuum coupling strategy is formulated for the single-phase flow system. However, the coupling terms will be adapted to more complex multi-phase flow and transport systems from Chapter 6 on.

$$\int q_{ex}\, dV \; = \alpha_{EX} \cdot (p_{pipe} - p_{pm}), \tag{30}$$

, where $\alpha_{EX} = f(\text{fluid properties, pipe geometry, porous media properties})$

α_{EX} is a lumped exchange coefficient which is a function of the hydraulic situation in both domains, the fluid properties, the geometry of the pipe, and the porous media properties. Each model is discretized with an implicit first order backward Euler method in time. The

coupling strategy with respect to the exchange terms can be considered as being explicit. In a kind of pseudo-algorithmic manner, the explicit coupling strategy can be described for a time step Δt at $t = t_n$ as follows (Fig. 13):

- At the beginning of time step $t = t_n$ pressures in the porous media and pipe flow models are known.
- For the calculation of the solution at $t = t_n + \Delta t$ the Newton iteration starts with a Newton step, where the defect of the total equation in the porous media flow model is calculated.
- In order to calculate the mass exchange term in the porous media flow model, one needs to determine the pressure in the pipe flow model.
- Within the Newton step of the porous media flow model, the pipe flow model is updated.
- For that purpose the current solution of the porous media flow model is passed to the pipe flow model.
- In the pipe flow model, the current solution (pressure) of the porous media flow model is set into the mass exchange term.
- The Newton iteration is started in the pipe flow model and after each Newton step the new pipe pressure is calculated.
- The new solution in the pipe flow model is checked for the convergence criteria.
- If the pipe flow model in that iteration step does not converge, a new Newton iteration is done. If the maximum number of iteration steps is exceeded, the time step is reduced and the whole procedure starts from the beginning of the current time $t = t_n$.
- If the pipe flow model converges, the solution (pipe pressure) is passed back to the Newton step of the porous media flow model.
- The updated pipe pressure is set back into the mass exchange term in the porous media flow model.
- The new solution in the porous media flow model is checked for convergence criteria.
- If the porous media flow model in that iteration step does not converge, a new Newton iteration is done. If the maximum number of iteration steps is exceeded, the time step is reduced and the whole procedure starts from the beginning of the current time $t = t_n$.
- If the porous media flow model converges, the Newton iteration ends with success and the end results of the coupled model at $t = t_n + \Delta t$ are determined.

Instead of coupling after each time step, the coupling is done at each Newton iteration step of the porous media flow model, which improves the convergence of the explicitly coupled model. As the algorithm in Fig. 13 shows, the pipe flow model is updated within the Newton iteration step of the porous media flow model. However, the porous media flow model is not updated within the Newton iteration step of the pipe flow model. This has two reasons. The first one is that the pipe flow model describes a physically much faster process than the porous media flow model, i.e. the response of the porous media flow to the changes of pipe flow will be much slower. The second one is that it is not feasible to update the porous media flow model within the Newton iteration of the pipe flow model, which leads to a chicken and egg problem.

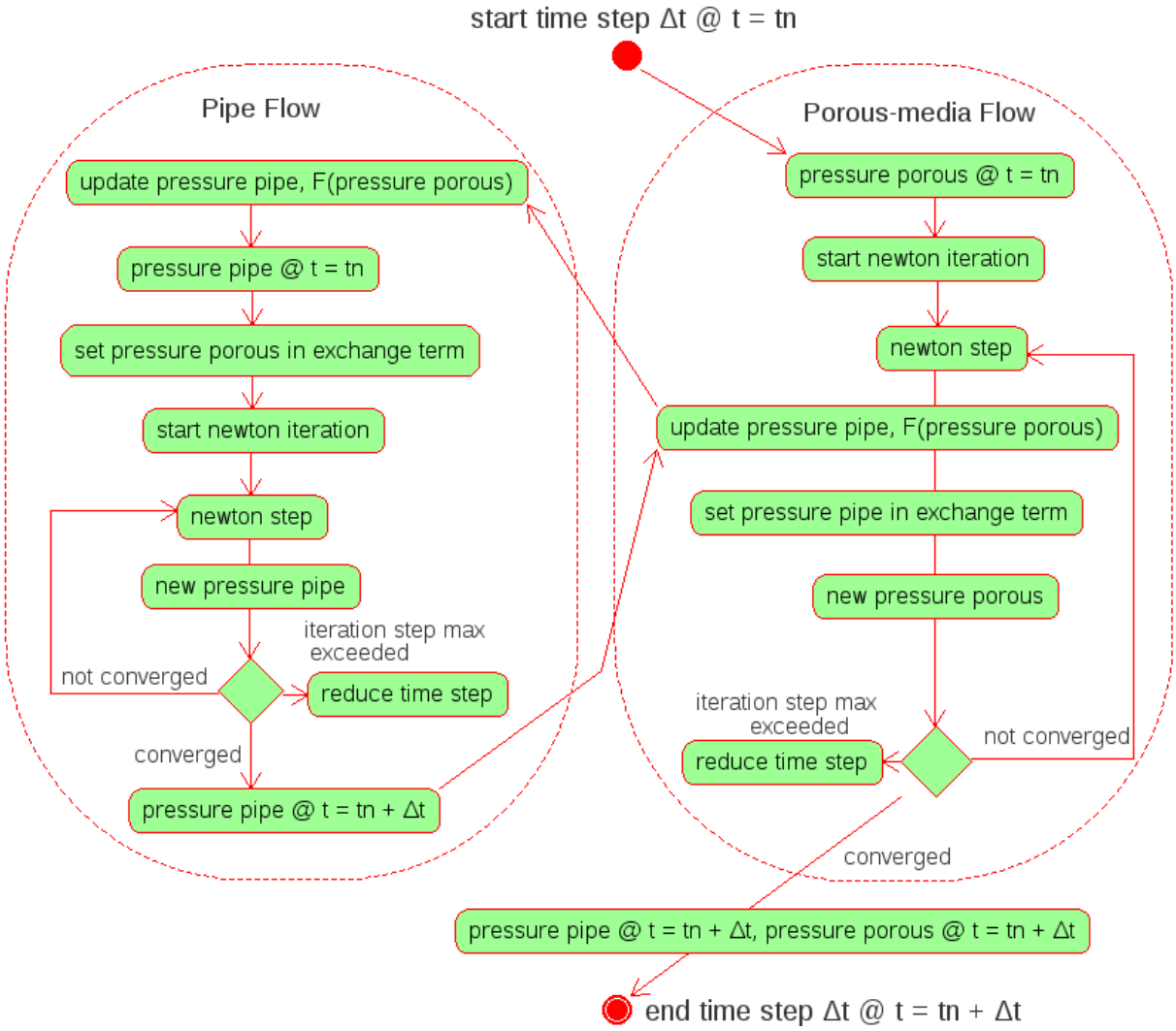

Figure 13: Flow chart explaining the explicit dual-continuum coupling between the porous media and the pipe flow models

2.3 Mathematical and numerical model

2.3.1 Conservation equations

Since the focus of this study is the development of different model concepts for the interaction of multi-phase flow processes in porous media with single-phase free flow in one-dimensional structures, it is necessary to introduce the conservation equations of each system separately.

2.3.1.1 Conservation equations for multi-phase flow in porous media

The conservation equations for multi-phase flow in porous media are the mass balance of each component k in all phases α (Eq. 31) and the momentum balance of each phase α (which is in fact an extended version of Darcy's law for multi-phase flow (Eq. 32)). The mass balance equation for each component k comprises a storage term, an advective transport term, a diffusive-dispersive transport term and a source/sink term (Class *et al.* (2002)). See the notation tables at the beginning of the thesis for the explanation of the symbols used in the equations:

$$\Sigma_\alpha \left[\frac{\partial(\phi \ \varrho_\alpha \ x_\alpha^k \ S_\alpha)}{\partial t} \right] + \Sigma_\alpha \left[\vec{\nabla} \cdot (\varrho_\alpha \ x_\alpha^k \ \vec{u}_\alpha) \right] - \Sigma_\alpha \left[\vec{\nabla} \cdot (\bar{\bar{D}}_\alpha^k \ \nabla(\varrho_\alpha \ x_\alpha^k)) \right] = q^k \tag{31}$$

$$\vec{u}_\alpha = -\frac{k_{r\alpha}}{\mu_\alpha} \bar{\bar{K}} (\nabla p_\alpha - \varrho_\alpha \ \vec{g}) \tag{32}$$

2.3.1.2 Conservation equations for free flow

The conservation equations for single-phase free flow include a mass balance equation (Eq. 33) and a momentum balance equation (Eq. 34). The momentum balance equation includes a momentum storage term, a momentum convection term, internal forces due to pressure and viscous forces, and external volume forces such as gravity (Hirsch (2007)).

$$\frac{\partial \varrho}{\partial t} + \vec{\nabla} \cdot (\varrho \vec{u}) = q \tag{33}$$

$$\frac{\partial(\varrho \ \vec{u})}{\partial t} + \vec{\nabla} \cdot (\varrho \ \vec{u} \otimes \vec{u} + p \ \bar{\bar{I}} - \bar{\bar{\tau}}) = \varrho \ \vec{f_{ext}} \tag{34}$$

The derivation of 1D-averaged Navier-Stokes equations for quasi-one-dimensional axisymmetric pipe flow systems is a straight forward process except for the derivation of the averaged shear stress term. Therefore, in the next section the averaging process of viscous forces is explained in detail.

2.3.1.3 Derivation of 1D-averaged viscous forces for the pipe flow systems

The derivation will be done for incompressible Navier-Stokes equations written in cylindrical coordinates (s, r, θ), where the s coordinate is aligned with the axis of symmetry of the channel and the r coordinate shows the radial direction of the pipe. There are different approaches in the literature. This approach is based on the non-dimensionalization of the conservation equations. A similar approach is also carried out by Barnard *et al.* (1966) and Canic and Kim (2003), who studied the blood flow through axisymmetric blood vessels, which are considered compliant tubes, i.e. the cross-section of blood vessels is changing as a function of pressure. The velocity components are $\vec{u} = (u_s, u_r, u_\theta)$. To obtain the following momentum equations, it is assumed that the angular velocity is zero:

Momentum equation in s-direction:

$$\frac{\partial u_s}{\partial t} + u_r \frac{\partial u_s}{\partial r} + u_s \frac{\partial u_s}{\partial s} + \frac{1}{\varrho}\frac{\partial p}{\partial s} = \nu \left[\frac{\partial^2 u_s}{\partial r^2} + \frac{1}{s}\frac{\partial u_s}{\partial r} + \frac{\partial^2 u_s}{\partial s^2} \right] \tag{35}$$

Momentum equation in r-direction:

$$\frac{\partial u_r}{\partial t} + u_r \frac{\partial u_r}{\partial r} + u_s \frac{\partial u_r}{\partial s} + \frac{1}{\varrho}\frac{\partial p}{\partial r} = \nu \left[\frac{\partial^2 u_r}{\partial r^2} + \frac{1}{r}\frac{\partial u_r}{\partial r} - \frac{u_r}{r^2} + \frac{\partial^2 u_r}{\partial s^2} \right] \tag{36}$$

Non-dimensional equations:

Introduction of characteristic quantities:

- r_o and s_o are characteristic inner pipe radius and characteristic pipe length.
- u_{so} and u_{ro} are characteristic axial velocity and characteristic radial velocity.

Non-dimensional variables:

$$r_* = \frac{r}{r_o},\ s_* = \frac{s}{s_o},\ u_{s*} = \frac{u_s}{u_{so}},\ u_{r*} = \frac{u_r}{u_{ro}},\ p_* = \frac{p}{\varrho u_{so}^2},\ t_* = \frac{t\ u_{so}}{s_o}$$

Note that

$$\frac{r_o}{s_o} \approx \frac{u_{ro}}{u_{so}} \approx \xi, \text{ where } \xi \text{ is a very small number}$$

Non-dimensional momentum equation in r-direction:

$$\begin{aligned} &\frac{u_{so}}{s_o}\frac{\partial(u_{ro}\,u_{r*})}{\partial t_*} + \frac{u_{ro}}{r_o}\,u_{r*}\,\frac{\partial(u_{ro}\,u_{r*})}{\partial r_*} + \frac{u_{so}}{s_o}\,u_{s*}\,\frac{\partial(u_{ro}\,u_{r*})}{\partial s_*} + \frac{1}{\varrho\,r_o}\frac{\partial(\varrho\,u_{so}^2\,p_*)}{\partial r_*} \\ &= \nu\left[\frac{1}{r_o^2}\frac{\partial^2(u_{ro}\,u_{r*})}{\partial r_*^2} + \frac{1}{r_o^2}\,\frac{1}{r_*}\,\frac{\partial(u_{ro}\,u_{r*})}{\partial r_*} - \frac{u_{ro}}{r_o^2}\frac{u_{r*}}{r_*^2} + \frac{1}{s_o^2}\frac{\partial^2(u_{ro}\,u_{r*})}{\partial s_*^2}\right] \end{aligned} \tag{37}$$

Divide Eq. 37 by u_{so}^2 and multiply by r_o to get Eq. 38:

$$\begin{aligned}&\frac{r_o\, u_{ro}}{s_o\, u_{so}}\frac{\partial u_{r*}}{\partial t_*} + \frac{u_{ro}^2}{u_{so}^2}\, u_{r*}\, \frac{\partial u_{r*}}{\partial r_*} + \frac{r_o\, u_{ro}}{s_o\, u_{so}}\, u_{s*}\, \frac{u_{r*}}{\partial s_*} + \frac{\partial p_*}{\partial r_*} \\ &= \nu \left[\frac{u_{ro}}{r_o\, u_{so}^2}\frac{\partial^2 u_{r*}}{\partial r_*^2} + \frac{u_{ro}}{r_o\, u_{so}^2}\, \frac{1}{r_*}\, \frac{\partial u_{r*}}{\partial r_*} - \frac{u_{ro}}{u_{so}^2\, r_o}\frac{u_{r*}}{r_*^2} + \frac{r_o\, u_{ro}}{s_o^2\, u_{so}}\frac{\partial^2 u_{r*}}{\partial s_*^2}\right]\end{aligned} \tag{38}$$

Since $\frac{r_o}{s_o} \approx \frac{u_{ro}}{u_{so}} \approx \xi,$ where ξ is a very small number, all the terms in the Eq. 38 are of order ξ^2 except the pressure term. After ignoring the higher order terms, the non-dimensional momentum equation in r-direction reduces to:

$$\frac{\partial p_*}{\partial r_*} = 0 \tag{39}$$

Eq. 39 implies that the pressure is constant across the pipe cross-section.

Non-dimensional momentum equation in s-direction:

The objective in this part is to derive 1D-averaged viscous forces and then relate the final state of the viscous term to the Darcy-Weisbach friction equation. For simplicity of derivation only the pressure and viscous forces are considered. Eq. 35 in non-dimensional form reads:

$$\frac{\varrho\, u_{so}^2}{s_o}\frac{\partial p_*}{\partial s_*} = \varrho\, \nu \left[\frac{u_{so}}{r_o^2}\frac{\partial^2 u_{s*}}{\partial r_*^2} + \frac{u_{so}}{r_o^2}\, \frac{1}{r_*}\, \frac{\partial u_{s*}}{\partial r_*} + \frac{u_{so}}{s_o^2}\frac{\partial^2 u_{s*}}{\partial s_*^2}\right] \tag{40}$$

Taking the right side of Eq. 40 in u_{so}/r_0^2 parenthesis leads to Eq. 41:

$$\frac{\varrho\, u_{so}^2}{s_o}\frac{\partial p_*}{\partial s_*} = \varrho\, \nu\, \frac{u_{so}}{r_o^2}\left[\frac{\partial^2 u_{s*}}{\partial r_*^2} + \frac{1}{r_*}\, \frac{\partial u_{s*}}{\partial r_*} + \frac{r_o^2}{s_o^2}\frac{\partial^2 u_{s*}}{\partial s_*^2}\right] \tag{41}$$

After neglecting higher order terms (the last term in Eq. 41 is of order $(r_o^2/s_o^2) \approx \xi^2$) and multiplying by r_*, Eq. 42 can be obtained:

$$\frac{\varrho\, u_{so}^2}{s_o}\, r_*\, \frac{\partial p_*}{\partial s_*} = \varrho\, \nu\, \frac{u_{so}}{r_o^2}\left[r_*\, \frac{\partial^2 u_{s_*}}{\partial r_*^2} + \frac{\partial u_{s*}}{\partial r_*}\right] \tag{42}$$

Making use of the product rule of derivation, the right hand side of the equation can be rearranged (Eq. 43):

$$\frac{\varrho\, u_{so}^2}{s_o}\, r_*\, \frac{\partial p_*}{\partial s_*} = \varrho\, \nu\, \frac{u_{so}}{r_o^2}\left[\frac{\partial}{\partial r_*}(r_*\, \frac{\partial u_{s*}}{\partial r_*})\right] \tag{43}$$

In order to get averaged quantities along the pipe cross-section, Eq. 43 is integrated for r_* from $[0, R_*]$ and for θ from $[0, 2\pi]$:

$$\frac{1}{\pi R_*^2}\int_0^{R_*}\int_0^{2\pi}\left(\frac{\varrho\, u_{so}^2}{s_o}\, r_*\, \frac{\partial p_*}{\partial s_*}\right)\partial r_*\, \partial\theta = \frac{1}{\pi R_*^2}\int_0^{R_*}\int_0^{2\pi}\left(\varrho\, \nu\, \frac{u_{so}}{r_o^2}\left[\frac{\partial}{\partial r_*}(r_*\, \frac{\partial u_{s*}}{\partial r_*})\right]\right)\partial r_*\, \partial\theta \tag{44}$$

After the first integration:

$$\frac{2\pi}{\pi R_*^2}\int_0^{R_*}\left(\frac{\varrho\, u_{so}^2}{s_o}\, r_*\, \frac{\partial p_*}{\partial s_*}\right)\partial r_* = \frac{2\pi}{\pi R_*^2}\int_0^{R_*}\left(\varrho\, \nu\, \frac{u_{so}}{r_o^2}\left[\frac{\partial}{\partial r_*}(r_*\, \frac{\partial u_{s*}}{\partial r_*})\right]\right)\partial r_* \tag{45}$$

Before doing the second integration, recall that p_* is constant across the pipe cross-section (see Eq. 39). After the second integration:

$$\frac{2\,\varrho\, u_{so}^2}{s_o}\,\frac{1}{R_*^2}\,\frac{\partial p_*}{\partial s_*}\left[\frac{r_*^2}{2}\right]_{r_*=R_*} = \frac{2\,\varrho\,\nu\, u_{so}}{r_o^2}\,\frac{1}{R_*^2}\,\left[r_*\,\frac{\partial u_{s*}}{\partial r_*}\right]_{r_*=R_*} \tag{46}$$

After inserting the integration boundaries Eq. 46 can be simplified to Eq. 47:

$$\frac{\varrho\, u_{so}^2}{s_o}\,\frac{\partial p_*}{\partial s_*} = \frac{2\,\varrho\,\nu\, u_{so}}{r_o^2}\,\frac{1}{R_*}\,\left[\frac{\partial u_{s*}}{\partial r_*}\right]_{r_*=R_*} \tag{47}$$

Back to the dimensional form:

1D-averaged momentum equation in r-direction:

Eq. 39 can be set back to the dimensional form by replacing the dimensionless variables with the dimensional variables:

$$\frac{r_o}{\varrho\, u_{so}^2}\frac{\partial p}{\partial r} = 0, \text{ i.e. } \frac{\partial p}{\partial r} = 0 \tag{48}$$

1D-averaged momentum equation in s-direction (only pressure and viscous terms):

Eq. 47 can be set back to the dimensional form by replacing the dimensionless variables with the dimensional variables:

$$\frac{\varrho\, u_{so}^2}{s_o}\,\frac{s_o}{\varrho\, u_{so}^2}\,\frac{\partial p}{\partial s} = \frac{2\,\varrho\,\nu\, u_{so}}{r_o^2}\,\frac{r_o^2}{u_{so}}\,\frac{1}{R}\,\left[\frac{\partial u_s}{\partial r}\right]_{r=R} \tag{49}$$

After canceling the characteristic parameters Eq. 49 simplifies to Eq. 50:

$$\frac{\partial p}{\partial s} = \frac{2\,\varrho\,\nu}{R}\,\left[\frac{\partial u_s}{\partial r}\right]_{r=R} \tag{50}$$

The right hand side of Eq. 50 implies that the 1D-averaged viscous term depends on the derivative of the velocity profile at the inner wall of the pipe. In the following part, the 1D-averaged momentum equation in s-direction will be related to the Darcy-Weisbach friction formula.

Relating the 1D-averaged momentum equation to the Darcy-Weisbach friction formula for laminar flow condition:

If laminar flow conditions exist, the velocity profile has a parabolic shape at the pipe cross-section:

$$u_s \;=\; 2\;\bar{u}_s\;(1\;-\;\frac{r^2}{R^2}) \tag{51}$$

, where $\bar{u}_s$ is the cross-sectionally averaged mean pipe velocity. The gradient of the velocity u_s in r-direction is:

$$\frac{\partial u_s}{\partial r} \;=\; -4\;\bar{u}_s\;\frac{r}{R^2} \tag{52}$$

Inserting Eq. 52 into the 1D-averaged momentum equation in s-direction (Eq. 50) leads to Eq. 53:

$$\frac{\partial p}{\partial s} \;=\; \frac{2\;\varrho\;\nu}{R}\;\left[-4\;\bar{u}_s\;\frac{r}{R^2}\right]_{\,r=R} \tag{53}$$

After rearranging the terms, Eq. 54 can be obtained:

$$\frac{\partial p}{\partial s} \;=\; -\frac{8\;\varrho\;\nu\;\bar{u}_s}{R^2} \tag{54}$$

Multiplying the right hand side of Eq. 54 by $\frac{2\bar{u}_s}{2\bar{u}_s}$ and replacing R with $\frac{d}{2}$:

$$\frac{\partial p}{\partial s} \;=\; -\frac{32\;\varrho\;\nu\;\bar{u}_s}{d^2}\;\frac{2\;\bar{u}_s}{2\;\bar{u}_s} \tag{55}$$

Rearranging the terms:

$$\frac{\partial p}{\partial s} \;=\; -\frac{64\;\varrho\;\bar{u}_s^2}{(\frac{\bar{u}_s\;d}{\nu})\;2\;d} \tag{56}$$

Introducing the Reynolds number for pipe flow ($Re \;=\; \frac{\bar{u}_s\;d}{\nu}$):

$$\frac{\partial p}{\partial s} \;=\; -\frac{64\;\varrho\;\bar{u}_s^2}{Re\;2\;d} \tag{57}$$

Multiplying the right hand side of Eq. 57 by $\frac{A}{A}$ and replacing A with $\frac{\pi\;d^2}{4}$:

$$\frac{\partial p}{\partial s} \;=\; -\frac{64\;\varrho\;\bar{u}_s^2}{Re\;2\;d}\;\frac{\pi\;d^2}{4\;A} \tag{58}$$

Introducing the Darcy-Weisbach friction factor for laminar flow condition ($\zeta = \frac{64}{Re}$):

$$\frac{\partial p}{\partial s} \;=\; -\frac{\zeta\;\varrho\;\bar{u}_s^2}{8}\;\frac{\pi\;d}{A} \tag{59}$$

Introducing the wall shear stress term ($\tau_w = \frac{\zeta\ \varrho\ \bar{u}_s^2}{8}$):

$$\frac{\partial p}{\partial s} = -\tau_w \frac{\pi\ d}{A} \tag{60}$$

Finally, Eq. 60 concludes the relation of the 1D-averaged viscous forces to the Darcy-Weisbach friction formula, where τ_w can be described by the Darcy-Weisbach friction factor ζ. Although Eq. 60 is derived for laminar flow conditions, it also holds for turbulent flow conditions, where the friction factor ζ can be described for turbulent flow conditions, too. This is explained in more detail in the following part.

The Darcy-Weisbach friction factor (ζ) :

The Darcy-Weisbach friction factor (ζ) is a function of $f(Re, \frac{\epsilon}{d})$, where Re is the Reynolds number, ϵ is the equivalent sand grain roughness and d is the pipe diameter. In the monograph by Brill and Mukherjee (1999) the frictional factor ζ is extensively discussed. Depending on the Re, the flow can be classified as laminar flow or turbulent flow. In the laminar flow regime ζ is only a function of Re (Eq. 61). The turbulent flow regime can be classified as transition zone or fully rough flow. In the transition zone ζ is a function of both Re and ϵ (Eq. 62). Whereas in the fully rough flow regime, ζ is only a function of ϵ (Eq. 63).

ζ in different flow regimes:

- If Re $\leq$ 2300: Laminar flow

$$\zeta = \frac{64}{Re} \tag{61}$$

- If Re $>$ 2300: Turbulent flow
  - transition zone: After Colebrook (1939)

$$\zeta = (1.74 - 2log(\frac{2\epsilon}{d} + \frac{18.7}{Re\sqrt{\zeta}}))^{-2} \tag{62}$$

  - fully rough flow: After Nikuradse (1933)

$$\zeta = (1.74 - 2log(\frac{2\epsilon}{d}))^{-2} \tag{63}$$

Zigrang and Sylvester (1985) proposed for the entire turbulent flow regime a simple to use formula:

$$\zeta = (-2log(\frac{2\epsilon/d}{3.7} - \frac{5.02}{Re}log(\frac{2\epsilon/d}{3.7} + \frac{13}{Re})))^{-2} \tag{64}$$

Fig. 14 shows a plot of the Darcy-Weisbach friction factor (ζ) as a function of Re and $\frac{\epsilon}{d}$. It is called Moody diagram after the American engineer, L.F. Moody, who obtained the necessary data to develop the figure (Granger (1995)).

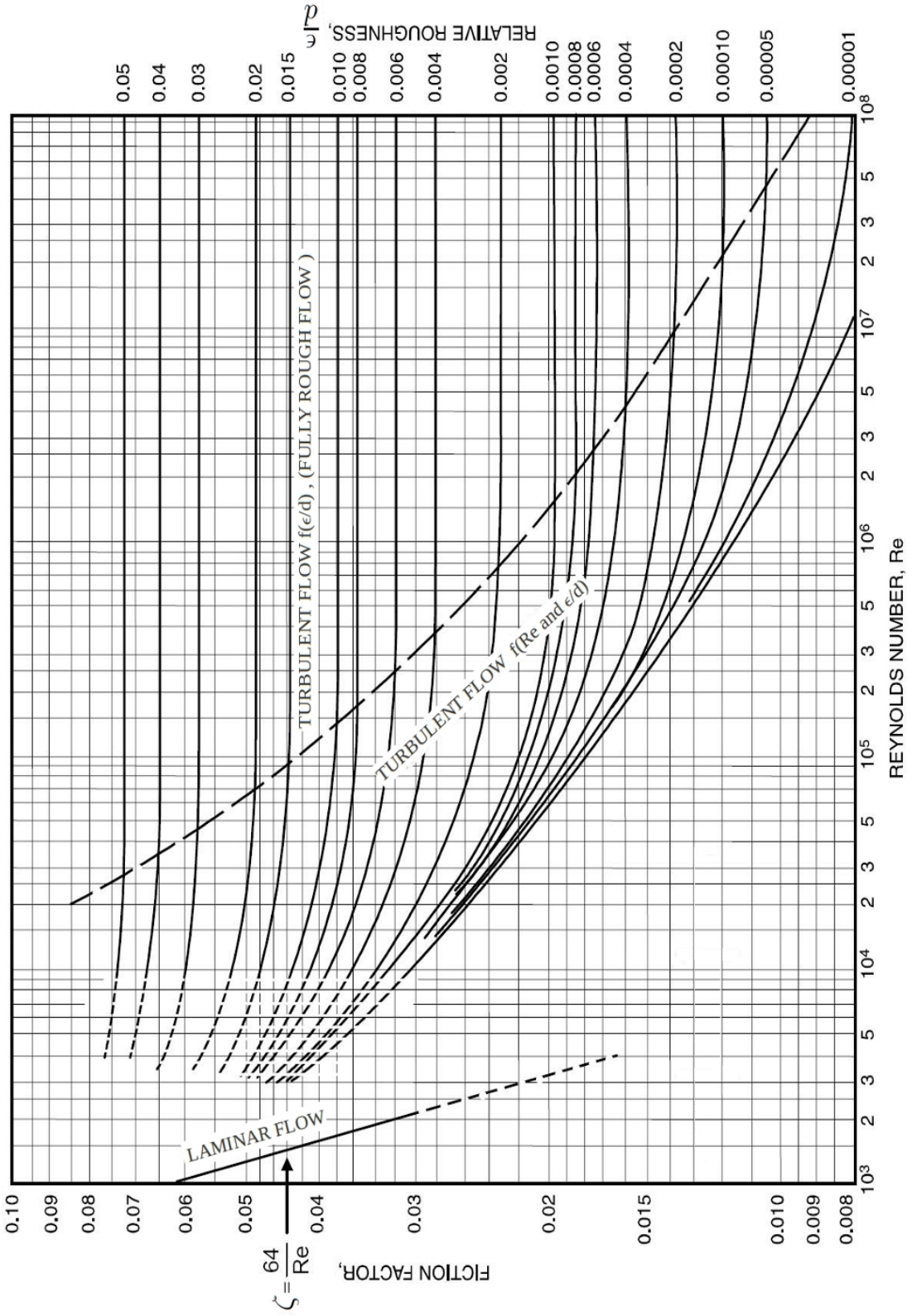

Figure 14: Moody diagram

2.3.1.4 Conservation equations for one-dimensional pipe flow system

If the free-flow equations (Eq. 33 and Eq. 34) are drived for cross-sectionally averaged velocities in 1D flow, one obtains Eq. 65 for the conservation of mass and Eq. 66 for the conservation of momentum. The vector $\vec{s}$ stands for the unit positive direction of the pipe and τ_w is the wall shear stress, which can be approximated by the Darcy-Weisbach approach.

$$\frac{\partial \varrho}{\partial t} + \frac{\partial}{\partial s}(\varrho\, \bar{u}_s) = q \tag{65}$$

$$\frac{\partial(\varrho\, \bar{u_s})}{\partial t} + \frac{\partial(\beta\, \varrho\, \bar{u}_s\, \bar{u}_s)}{\partial s} + \frac{\partial p}{\partial s} + \tau_w \frac{\pi d}{A} = \varrho\, \vec{g} \cdot \vec{s} \tag{66}$$

The velocity along the pipe can be averaged cross-sectionally according to Eq. 67. As a result of the averaging of the momentum equation, a correction factor β appears in the momentum convection term, which is defined according to Eq. 68. The correction factor β is neglected throughout this work, i.e. $\beta = 1$.

$$\bar{u}_s = \frac{1}{\pi\, R^2} \int_0^R \int_0^{2\pi} u_s\, r\, dr\, d\phi \tag{67}$$

$$\beta = \frac{1}{\bar{u}_s^2\, \pi\, R^2} \int_0^R \int_0^{2\pi} {u_s}^2\, r\, dr\, d\phi \tag{68}$$

The arising system of equations has four unknowns but only two partial differential equations. To close the system, it is assumed that the ideal gas law is valid, i.e. density and pressure are related to each other, and the wall friction is described by the Darcy-Weisbach friction factor (ζ):

$$\varrho \;=\; \frac{p}{R_{ind}\, T} \text{ (ideal gas law), and } \tau_w \;=\; \frac{\zeta}{8}\, \varrho\, \bar{u}_s^2 \text{ (wall friction via } \zeta). \tag{69}$$

2.3.2 Discretization techniques

2.3.2.1 Discretization of the multi-phase flow equations in porous media

For the spatial discretization, a subdomain-collocation finite-volume method (BOX method) is used (see Bastian and Helmig (1999)). The BOX method requires the construction of a secondary mesh. This is achieved by connecting the elements' centers of gravity with the mid-points of the element edges. Each node is assigned to a unique control volume, and each element contains a number of sub-control volumes equal to the number of nodes in that element (see Fig. 15).

The BOX scheme can be derived using the principle of weighted residuals applied to the primary finite element mesh with piece-wise constant weighting functions for the control

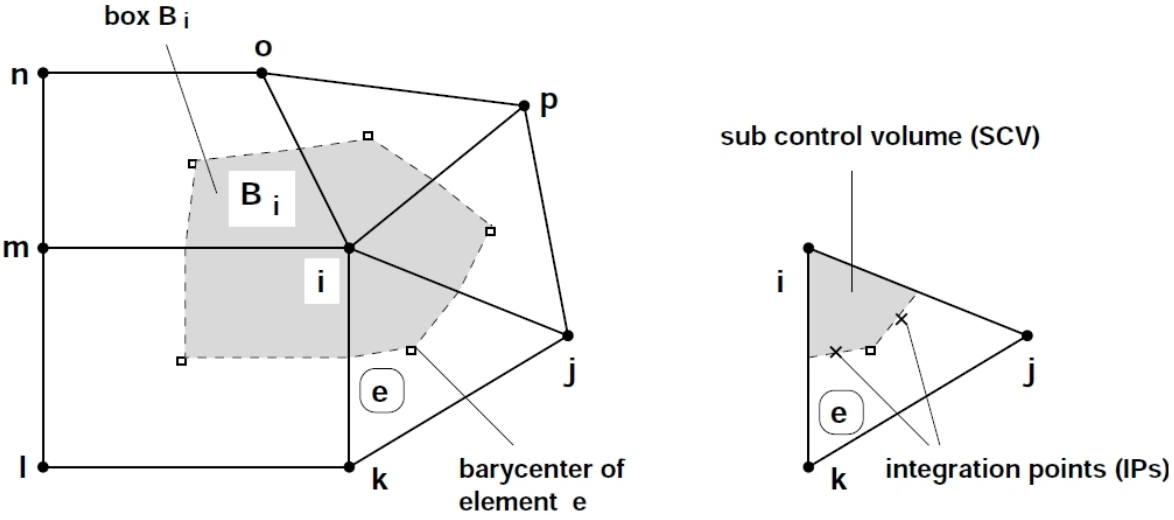

Figure 15: Dual meshes and sub-control volumes in a subdomain-collocation finite-volume method (BOX method)

volumes (boxes) on the secondary mesh. Mass lumping and full upwinding for the advective terms are applied.

If equation Eq. 32 is inserted into Eq. 31 and integrated within a volume Ω, one obtains the weak form of the equation:

$$\int_\Omega \left[\sum_\alpha \left(\frac{\partial(\phi\ \varrho_\alpha\ x_\alpha^k\ S_\alpha)}{\partial t} \right) \right] d\Omega - \int_\Omega \left[\sum_\alpha \left(\vec{\nabla} \cdot (\varrho_\alpha\ x_\alpha^k\ \frac{k_{r\alpha}}{\mu_\alpha} \bar{\bar{K}} (\nabla p_\alpha - \varrho_\alpha\ \vec{g})) \right) \right] d\Omega$$
$$- \int_\Omega \left[\sum_\alpha \left(\vec{\nabla} \cdot (\bar{\bar{D}}_\alpha^k\ \nabla(\varrho_\alpha\ x_\alpha^k)) \right) \right] d\Omega - \int_\Omega (q^k) d\Omega = 0 \tag{70}$$

The total potential of a phase can be defined as follows:

$$\Psi_\alpha = p_\alpha - \varrho_\alpha\ g\ z \tag{71}$$

In a discrete form, primary variables are defined on each node of the grid. They can be approximated with the help of ansatz functions (N) within the domain as follows:

$$\tilde{u} = \sum_{j=1}^{n_{nodes}} \hat{u}_j\ N_j \tag{72}$$

If approximated primary variables ($\tilde{u}$) are inserted into equation Eq. 70, the total sum leads to a residual ε due to approximation. The weighted residual in the entire domain should vanish:

$$\int W_i\ \varepsilon\ d\Omega\ \stackrel{!}{=}\ 0 \tag{73}$$

The weighting functions in the box method are defined as follows:

$$W_i = \begin{cases} 1 & \text{within the control volume } B_i \\ 0 & \text{outside the control volume } B_i \end{cases} \tag{74}$$

Eq. 73 can be written in a more discrete manner as follows:

$$\begin{aligned}
&\frac{1}{\Delta t}\sum_{\alpha}\sum_{j}\left[\left((\phi\ \varrho_\alpha\ \hat{x}_\alpha^k\ \hat{S}_\alpha)_j^{t+\Delta t} - (\phi\ \varrho_\alpha\ \hat{x}_\alpha^k\ \hat{S}_\alpha)_j^{t}\right)\int_\Omega W_i N_j d\Omega\right] \\
&-\sum_{\alpha}\sum_{j\in n_i}\left[\int_\Omega W_i\ \vec{\nabla}\cdot\left((\varrho_\alpha\ \frac{k_{r\alpha}}{\mu_\alpha}\bar{\bar{K}})_{ij}^{t+\Delta t}(\hat{x}_\alpha^k\ N_j)^{t+\Delta t}\ \nabla N_j\right)d\Omega\ (\hat{\Psi}_{\alpha j} - \hat{\Psi}_{\alpha i})^{t+\Delta t}\right] \\
&-\sum_{\alpha}\sum_{j\in n_i}\left[\int_\Omega W_i\ \vec{\nabla}\cdot\left((\bar{\bar{D}}_\alpha^k\ \varrho_\alpha)_{ij}^{t+\Delta t}\ \nabla N_j\right)d\Omega\ (\hat{x}_{\alpha j}^k - \hat{x}_{\alpha i}^k)^{t+\Delta t}\right] \\
&-\sum_{j}\left[(q^k)^{t+\Delta t}\int_\Omega W_i N_j d\Omega\right] = 0
\end{aligned} \tag{75}$$

, where n_i is a set of all neighboring nodes of node i.

Some terms in Eq. 75 should be simplified to make it more appropriate for numerical calculations. First, a product rule is introduced:

$$\int_\Omega \vec{\nabla}\cdot(W_i\ \mathbf{F})\ d\Omega = \int_\Omega \nabla W_i\ \cdot\mathbf{F}\ d\Omega + \int_\Omega W_i\vec{\nabla}\ \cdot\mathbf{F}\ d\Omega \tag{76}$$

Then, the Green-Gauss theorem is applied to convert volume integral into surface integral:

$$\int_\Omega \vec{\nabla}\cdot(W_i\ \mathbf{F})\ d\Omega = \int_\Gamma (W_i\ \mathbf{F})\cdot\vec{n}\ d\Gamma \tag{77}$$

If Eq. 77 is inserted into Eq. 76, one obtains:

$$\int_\Omega W_i\vec{\nabla}\ \cdot\mathbf{F}\ d\Omega = \int_\Gamma (W_i\ \mathbf{F})\cdot\vec{n}\ d\Gamma - \int_\Omega \nabla W_i\ \cdot\mathbf{F}\ d\Omega \tag{78}$$

As an example the advective part of Eq. 75 can be transformed according to Eq. 78:

$$\begin{aligned}
&\sum_{\alpha}\sum_{j\in n_i}\left[\int_\Omega W_i\ \vec{\nabla}\cdot\left((\varrho_\alpha\ \frac{k_{r\alpha}}{\mu_\alpha}\bar{\bar{K}})_{ij}^{t+\Delta t}(\hat{x}_\alpha^k\ N_j)^{t+\Delta t}\ \nabla N_j\right)d\Omega\ (\hat{\Psi}_{\alpha j} - \hat{\Psi}_{\alpha i})^{t+\Delta t}\right] \\
&=\sum_{\alpha}\sum_{j\in n_i}\left[\int_\Gamma W_i\ \left((\varrho_\alpha\ \frac{k_{r\alpha}}{\mu_\alpha}\bar{\bar{K}})_{ij}^{t+\Delta t}(\hat{x}_\alpha^k\ N_j)^{t+\Delta t}\ \nabla N_j\right)\cdot\vec{n}\ d\Gamma\ (\hat{\Psi}_{\alpha j} - \hat{\Psi}_{\alpha i})^{t+\Delta t}\right] \\
&-\sum_{\alpha}\sum_{j\in n_i}\left[\int_\Omega \nabla W_i\ \cdot\left((\varrho_\alpha\ \frac{k_{r\alpha}}{\mu_\alpha}\bar{\bar{K}})_{ij}^{t+\Delta t}(\hat{x}_\alpha^k\ N_j)^{t+\Delta t}\ \nabla N_j\right)d\Omega\ (\hat{\Psi}_{\alpha j} - \hat{\Psi}_{\alpha i})^{t+\Delta t}\right]
\end{aligned} \tag{79}$$

The last term in Eq. 79 vanishes because $\nabla W_i\ =\ 0$

For the storage and source terms, the mass lumping concept can be used (Huber and Helmig (1999)):

$$\int_{\Omega} W_i N_j d\Omega = \begin{cases} V_i & if\ i = j \\ 0 & if\ i \neq j \end{cases} \tag{80}$$

After applying mass lumping, product rule and Green-Gauss theorem, Eq. 75 can be reformulated as follows:

$$\begin{aligned} &\frac{V_i}{\Delta t} \sum_{\alpha} \sum_{j} \left[\left((\phi\ \varrho_\alpha\ \hat{x}_\alpha^k\ \hat{S}_\alpha)_j^{t+\Delta t} - (\phi\ \varrho_\alpha\ \hat{x}_\alpha^k\ \hat{S}_\alpha)_j^{t} \right) \right] \\ &= \sum_{\alpha} \sum_{j \in n_i} \left[\int_{\Gamma} W_i \left((\varrho_\alpha\ \frac{k_{r\alpha}}{\mu_\alpha} \bar{\bar{K}})_{ij}^{t+\Delta t} (\hat{x}_\alpha^k\ N_j)^{t+\Delta t}\ \nabla N_j \right) \cdot \vec{n}\ d\Gamma\ (\hat{\Psi}_{\alpha j} - \hat{\Psi}_{\alpha i})^{t+\Delta t} \right] \\ &- \sum_{\alpha} \sum_{j \in n_i} \left[\int_{\Gamma} W_i \left((\bar{\bar{D}}_\alpha^k\ \varrho_\alpha)_{ij}^{t+\Delta t}\ \nabla N_j \right) \cdot \vec{n}\ d\Gamma\ (\hat{x}_{\alpha j}^k - \hat{x}_{\alpha i}^k)^{t+\Delta t} \right] \\ &- \sum_{j} \left[(q^k)^{t+\Delta t} V_i \right] = 0 \end{aligned} \tag{81}$$

The terms appearing with subscript ij should be approximated at the integration points of the subcontrol volume faces (Fig. 15). In the diffusive flux term D and ϱ are arithmetically averaged. In the advective flux term, the permeability (K) is harmonically averaged. In order to obtain a non-oscillatory solution, the $\varrho\ k_r/\mu$ term is fully upwinded according to the following condition:

Upwinding node: If $\vec{n}$ is the normal face vector pointing from node i to node j.

$$Upwinding(i,j) = \begin{cases} upwinding\ node\ \ i & if\ ([\nabla p_\alpha - \varrho_\alpha\ \vec{g}) \cdot \vec{n}] \geq 0\ ) \\ upwinding\ node\ \ j & if\ ([\nabla p_\alpha - \varrho_\alpha\ \vec{g}) \cdot \vec{n}] < 0\ ) \end{cases}$$

2.3.2.2 Discretization of the pipe flow equations

In this study, depending on the complexity of the flow conditions in the pipe system two different models are used:

a) The Hagen-Poiseuille model is used for incompressible, steady state, laminar flow conditions.

b) The pipe flow model is used for compressible, transient flow conditions.

a) Hagen-Poiseuille flow

Derivation of Hagen-Poiseuille equation:

At steady state condition, 1D-averaged pipe flow equations (Eq. 65 and Eq. 66) simplify to Eq. 82 and Eq. 83:

$$\frac{\partial}{\partial s}(\varrho\ \bar{u}_s) = q \tag{82}$$

$$\frac{\partial(\beta\ \varrho\ \bar{u}_s\ \bar{u}_s)}{\partial s} + \frac{\partial p}{\partial s} + \tau_w \frac{\pi d}{A} = \varrho\ \vec{g} \cdot \vec{s} \tag{83}$$

If the momentum convection term is smaller than the viscous term and the flow conditions are laminar, then the free-flow momentum equation can be simplified to Eq. 84:

$$\tau_w \frac{\pi d}{A} = -\frac{\partial p}{\partial s} + \varrho\ \vec{g} \cdot \vec{s} \tag{84}$$

$$\tau_w\ =\ \frac{\zeta}{8}\ \varrho\ \bar{u}_s^2, \text{ for laminar flow } \zeta = \frac{64}{Re}, \ \zeta = \frac{64\nu}{\bar{u}_s\ d} \tag{85}$$

$$\Rightarrow\ \tau_w\ =\ \frac{8\ \bar{u}_s\ \nu\ \varrho}{d}\text{ , by inserting } \tau_w \text{ in Eq. 84 one can get:} \tag{86}$$

$$\frac{32\bar{u}_s\nu\varrho}{d^2} = -\frac{\partial p}{\partial s} + \varrho\ \vec{g} \cdot \vec{s} \tag{87}$$

Eq. 87 is the well-known Hagen-Poiseuille equation (Hagen (1839) and Poiseuille (1841)). 1D-averaged velocity ($\bar{u}_s$) can be explicitly written as a function of pressure gradient (Eq. 88):

$$\bar{u}_s = -\left(\frac{d^2}{32\mu}\ (\frac{\partial p}{\partial s} - \varrho\ \vec{g} \cdot \vec{s})\right) \tag{88}$$

If Eq. 88 is inserted into Eq. 82, one can get the conservation equation of incompressible Hagen-Poiseuille flow accounting for both mass and momentum balances:

$$-\frac{\partial}{\partial s}\left(\frac{\varrho}{\mu}\ \frac{d^2}{32}\ (\frac{\partial p}{\partial s} - \varrho\ \vec{g} \cdot \vec{s})\right) = q \tag{89}$$

Discretization of Hagen-Poiseuille flow equation:

For the discretization of Hagen-Poiseuille flow the node-centered finite-volume method is chosen. It is more appropriate than the cell-centered finite-volume method for coupling with the box-method, because the centers of gravity of each discretization volume overlap each another.

Hagen-Poiseuille flow has one primary variable, i.e. pressure. Fig. 16 shows the control volumes and primary variables for the node-centered finite-volume method discretization in Hagen-Poiseuille flow.

Eq. 89 can be written in integral form to obtain Eq. 90:

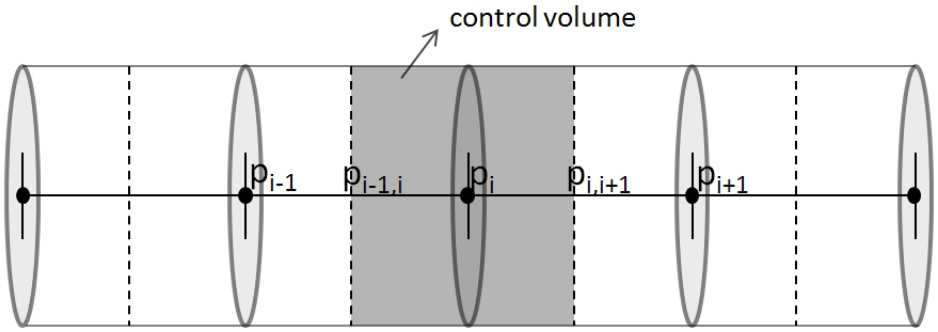

Figure 16: Node-centered finite-volume method discretization in Hagen-Poiseuille flow

$$\int_{\Omega} -\frac{\partial}{\partial s}\left(\frac{\varrho}{\mu}\,\frac{d^2}{32}\,(\frac{\partial p}{\partial s} - \varrho\,\vec{g}\cdot\vec{s})\right) d\Omega + \int_{\Omega} -q\; d\Omega = 0 \tag{90}$$

If the Green-Gauss theorem is used to convert volume integral to surface integral, one gets Eq. 91

$$\int_{\Gamma} -\left(\frac{\varrho}{\mu}\,\frac{d^2}{32}\,(\frac{\partial p}{\partial s} - \varrho\,\vec{g}\cdot\vec{s})\right)\cdot\vec{n}\; d\Gamma + \int_{\Omega} -q\; d\Omega = 0 \tag{91}$$

Eq. 91 can be written in fully discretized form as follows:

$$\sum_{i}\sum_{j\in n_i} -\left(\frac{\varrho_{ij}}{\mu_{ij}}\,\frac{d_{ij}^2}{32}((\frac{\partial p}{\partial s})_{ij} - \varrho_{ij}\,\vec{g}\cdot\vec{s})\right)\cdot\vec{n}\; dA_{ij} + \sum_{i} -q_i\; dV_i = 0 \tag{92}$$

The terms appearing with subscript ij in Eq. 92 need to be calculated at the interfaces between control volumes, i.e. ϱ_{ij}, μ_{ij} are arithmetically and d_{ij}^2 is harmonically averaged.

b) Compressible 1D pipe flow

Discretization of compressible 1D pipe flow:

The staggered finite volume method is chosen for the discretization of the pipe flow equation. The staggered arrangements offer several advantages over the colocated arrangements. Several terms that require interpolation with the colocated arrangement can here be calculated without interpolation. The biggest advantage of the staggered arrangement is the strong coupling between the velocities and the pressures. This helps to avoid some types of convergence problems and oscillations in the pressure and velocity fields (Ferziger and Peric (1999)). Fig. 17 shows a cell-centered finite volume discretization on a staggered grid, where the control volumes of the mass and the momentum equations are shifted half a cell distance from each other. In Fig. 17 the subscript "a" denotes the primary variables defined on the mass balance grid and the subscript "b" denotes the primary variables defined on the momentum balance grid. The pipe flow equation has two primary variables: Pressure (p) and velocity (u). Pressures are defined in the cell centers of mass-balance grid and velocities

are defined in the cell centers of the momentum-balance grid. The center of gravity of each control volume of the mass balance grid overlaps with the center of gravity of the linked box control volume in the porous media grid, which is also advantageous from the coupling point of view.

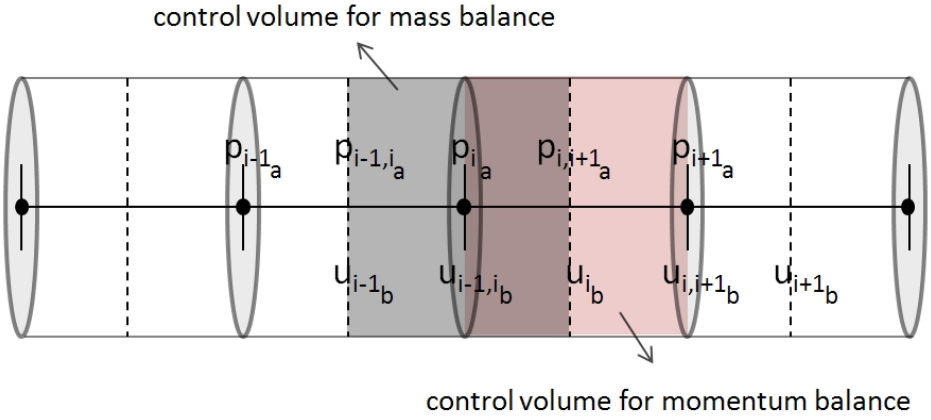

Figure 17: Cell-centered finite volume discretization on a staggered grid

Eq. 65 and Eq. 66 can be written in integral form to obtain Eq. 93 and Eq. 94

$$\int_\Omega \frac{\partial \varrho}{\partial t}\, d\Omega + \int_\Omega \frac{\partial}{\partial s}(\varrho\, \bar{u}_s)\, d\Omega + \int_\Omega -q\, d\Omega = 0 \tag{93}$$

$$\int_\Omega \frac{\partial(\varrho\, \bar{u}_s)}{\partial t}\, d\Omega + \int_\Omega \frac{\partial(\, \varrho\, \bar{u}_s\, \bar{u}_s)}{\partial s}\, d\Omega + \int_\Omega \frac{\partial p}{\partial s}\, d\Omega + \int_\Omega \tau_w \frac{\pi d}{A}\, d\Omega - \int_\Omega \varrho\, \vec{g} \cdot \vec{s}\, d\Omega = 0 \tag{94}$$

, where $\tau_w = \frac{\zeta}{8}\, \varrho\, \bar{u}_s^2$, and $\varrho = \frac{p}{R_{ind}\, T}$

Mass Balance

If Eq. 93 is discretized in time with the backward Euler method and the Green-Gauss theorem is used, one can get Eq. 95:

$$\frac{1}{\Delta t} \int_\Omega (\varrho_{i_a}^{t+\Delta t} - \varrho_{i_a}^{t})\, d\Omega + \int_\Gamma (\varrho\, \bar{u}_s)_{ij_a}^{t+\Delta t} \cdot \vec{n}\, d\Gamma + \int_\Omega -q_{i_a}^{t+\Delta t}\, d\Omega = 0 \tag{95}$$

Eq. 95 can be written in a fully discretized form as follows:

$$\frac{1}{\Delta t} \sum_i (\varrho_{i_a}^{t+\Delta t} - \varrho_{i_a}^{t})\, dV_i + \sum_i \sum_{j \in n_i} (\varrho_{ij_a}\, (\bar{u}_{s,ij})_a)^{t+\Delta t} \cdot \vec{n}\, dA_{ij} + \sum_i -q_{i_a}^{t+\Delta t}\, dV_i = 0 \tag{96}$$

Densities at the interfaces of the mass balance grid (ϱ_{ij_a}) are arithmetically averaged between nodes i and j. Note that $(\bar{u}_{s,ij})_a = (\bar{u}_{s,i})_b$, i.e. velocities at the interfaces of the mass

balance grid don't need to be interpolated, since it is explicitly defined on the momentum balance grid.

Momentum Balance

If Eq. 94 is discretized in time with the backward Euler method and the Green-Gauss theorem is used, one ends up with Eq. 97:

$$\frac{1}{\Delta t}\int_{\Omega}\left((\varrho\ \bar{u}_s)_{i_b}^{t+\Delta t}-(\varrho\ \bar{u}_s)_{i_b}^{t}\right)\ d\Omega+\int_{\Gamma}(\varrho\ \bar{u}_s\ \bar{u}_s)_{ij_b}^{t+\Delta t}\cdot\vec{n}\ d\Gamma$$
$$+\int_{\Gamma}p_{ij_b}\cdot\vec{n}\ d\Gamma+\int_{\Omega}\tau_{wi_b}^{t+\Delta t}\frac{\pi d_i}{A_i}\ d\Omega-\int_{\Omega}\varrho_{i_b}^{t+\Delta t}\ \vec{g}\cdot\vec{s}\ d\Omega=0 \tag{97}$$

Eq. 97 can be written in a fully discretized form as follows:

$$\frac{1}{\Delta t}\sum_{i}\left((\varrho_{i_b}\ (\bar{u}_{s,i})_b)^{t+\Delta t}-(\varrho_{i_b}\ (\bar{u}_{s,i})_b)^{t}\right)\ dV_i+\sum_{i}\sum_{j\in n_i}(\varrho_{ij_b}\ (\bar{u}_{s,ij})_b\ (\bar{u}_{s,ij})_b)^{t+\Delta t}\cdot\vec{n}\ dA_{ij}$$
$$+\sum_{i}\sum_{j\in n_i}p_{ij_b}^{t+\Delta t}\cdot\vec{n}\ dA_{ij}+\sum_{i}\tau_{wi_b}^{t+\Delta t}\frac{\pi d_i}{A_i}\ dV_i-\sum_{i}\varrho_{i_b}^{t+\Delta t}\ \vec{g}\cdot\vec{s}\ dV_i=0 \tag{98}$$

The densities and pressures appearing in Eq. 98 are either interpolated or directly substituted from the mass balance grid, i.e. $\varrho_{i_b}=(\varrho_{i_a}+\varrho_{i+1_a})/2$, $p_{ij_b}=p_{i_a}$ and $\varrho_{ij_b}=\varrho_{i_a}$. The wall shear stress term (τ_{wi_b}) is a function of velocity ($(\bar{u}_{s,i})_b$) and density (ϱ_{i_b}). The velocities ($(\bar{u}_{s,ij})_b$) appearing in the momentum convection term are fully upwinded either from node i or node j according to the following condition:

Upwinding node:

$\vec{n}$ is the normal face vector pointing from node i to node j.

$$Upwinding(i,j)=\begin{cases}upwinding\ node\ \ i & if\ ([\bar{u}_{s,i}\cdot\vec{n}]\geq 0\ )\\ upwinding\ node\ \ j & if\ ([\bar{u}_{s,j}\cdot\vec{n}]<0\ )\end{cases}$$

2.3.3 Boundary conditions

In order to render a unique solution of the partial differential equation, the continuous problem requires information about the solution at the domain boundaries. Therefore, at the inner or outer borders of the domain the boundary conditions need to be imposed, which basically represent physical conditions at the boundaries of the real system. In general, there are three types of boundary conditions:

- Dirichlet boundary: The value of the primary variable at the boundary is fixed.

- Neumann boundary: The gradient of the primary variable in normal direction to the boundary is given.
- Cauchy boundary: A linear combination of Dirichlet and Neumann boundaries is imposed at the border of the domain.

The physical meanings of the boundary conditions differ for the same type of boundary condition depending on the primary variables of the considered system. In the following the physical meanings of the boundary conditions for the porous-media flow and pipe flow are explained separately.

Boundary conditions in porous-media flow

In single-phase porous media flow the primary variable is usually pressure. However, in some models the pressure head is also chosen as a primary variable. In multi-phase multi-component models beside the pressure of a phase, saturation of a phase and concentration of a component can also be chosen as primary variables. The physical meanings of Dirichlet boundaries of a porous media flow problem are easy to grasp. They can represent a fixed pressure, a fixed saturation or a fixed concentration. The Neumann boundary condition describes a pressure gradient or more generally a mass flux across the boundary. When pressure and its normal derivate are described with a linear combination at the boundary, a Cauchy boundary value problem occurs. A typical example of such a physical situation in porous media are leaky aquifers (Bear (1988)).

Boundary conditions in pipe flow

In the pipe flow model, Dirichlet and Neumann boundaries can have different physical meanings depending on the primary variables. The pipe flow model has two primary variables, i.e. pressure and velocity. The pressure needs to be fixed at one node of the pipe flow model, which can be a boundary node as well as an inner node. The boundaries of a free flow problem can be categorized as follows (Ferziger and Peric (1999)):

at the inlet: Usually, at an inlet boundary, all quantities have to be prescribed. Since the velocity ($\bar{u}_s$) and pressure (p) are given (Dirichlet boundary), fluxes across the boundary are defined explicitly. The Dirichlet velocity boundary combined with the Dirichlet pressure boundary is enough to define a fixed mass flux boundary, whereas in porous media flow the Neumann boundary is necessary to define a fixed mass flux boundary.

at the outlet: At an outlet boundary usually little is known about the mass fluxes. At the out flow of a pipe the velocity gradient is fixed to zero, to satisfy a free flow boundary condition, i.e. $\partial \bar{u}_s \,/\, \partial n \;=\; 0$.

impermeable wall: The impermeable walls of the 1D-averaged pipe flow model are no flow boundaries. Therefore, it is necessary to set the pipe-flow velocity to zero ($\bar{u}_s \;=\; 0$).

2.3.4 Discretization in time

For the time discretization, a first order fully-implicit backward Euler scheme is applied for each particular model.

$$\begin{aligned} \frac{d\mathbf{u}}{dt} &= \mathbf{F}(\mathbf{u}) \\ \\ \frac{\mathbf{u}^{n+1} - \mathbf{u}^{n}}{\Delta t} &= \mathbf{F}(\mathbf{u}^{n+1}) \end{aligned} \tag{99}$$

The flow and transport processes in porous media and free flow are running in different time scales. In general, the free flow models require smaller time steps and finer grids than the porous media models, due to the fact that the flow velocities in porous media regions are much slower than the velocities in pipe flow regions. For the coupled models, the free flow model (in this case the pipe flow model) is decisive in the determination of the discretization size in time. The time-step size is kept the same for both models, and it is chosen as small as required by the pipe flow model.

2.3.5 Linearization of the partial differential equation system

The systems of partial differential equations arising from the mathematical description of multi-phase porous media flow and one dimensional pipe flow are generally highly non-linear. They are linearized using a damped inexact Newton-Raphson method, as described in Dennis and Schnabel (1996).

The non-linear partial differential equation can be written as in Eq. 100:

$$\mathbf{F}(\mathbf{u}) \; = \; 0 \tag{100}$$

In general an infinitely differentiable function f(x) can be expressed by the Taylor series expansion as in the Eq. 101 around a point x_c:

$$f(x) \; = \; f(x_c) \; + \; f^{'}(x_c)\,(x - x_c) \; + \; \frac{f^{''}(x_c)\,(x - x_c)^2}{2!} \; + \; .... \tag{101}$$

One can use the same principle for the partial differential equation system by approximating it around $\mathbf{u}^{t+\Delta t,r}$. After neglecting higher order terms, one can get Eq. 102:

$$\mathbf{F}\left(\mathbf{u}^{t+\Delta t,r+1}\right) \approx \mathbf{F}\left(\mathbf{u}^{t+\Delta t,r}\right) \; + \; \left(\frac{\partial \mathbf{F}}{\partial \mathbf{u}}\right)^{\mathbf{u}^{t+\Delta t,r}} \left(\mathbf{u}^{t+\Delta t,r+1} - \mathbf{u}^{t+\Delta t,r}\right) \tag{102}$$

If Jacobian matrix is defined as $\mathbf{J} \; = \; \partial \mathbf{F}/\partial \mathbf{u}$ and $-\Delta \mathbf{u}^{t+\Delta t,r \leftrightarrow r+1} \; = \; \left(\mathbf{u}^{t+\Delta t,r} - \mathbf{u}^{t+\Delta t,r+1}\right)$ is inserted into Eq. 102, the following equation is obtained:

$$\mathbf{J} \cdot \left(-\Delta \mathbf{u}^{t+\Delta t, r \leftrightarrow r+1}\right) = \mathbf{F}\left(\mathbf{u}^{t+\Delta t, r}\right) \tag{103}$$

Finally, Eq. 103 can be solved for $-\Delta \mathbf{u}$ and the next iterative solution can be obtained by:

$$\mathbf{u}^{t+\Delta t, r+1} = \mathbf{u}^{t+\Delta t, r} - \left(-\Delta \mathbf{u}^{t+\Delta t, r \leftrightarrow r+1}\right) \tag{104}$$

The method is called inexact Newton-Raphson method because the Jacobian matrix is calculated numerically as in Eq. 105:

$$\mathbf{J}_{ij}^{t+\Delta t, r} \approx \frac{\mathbf{F}\left(..., \mathbf{u}_{j-1}^{t+\Delta t, r}, \mathbf{u}_{j}^{t+\Delta t, r} + \xi, \mathbf{u}_{j+1}^{t+\Delta t, r}, ...\right) - \mathbf{F}\left(..., \mathbf{u}_{j-1}^{t+\Delta t, r}, \mathbf{u}_{j}^{t+\Delta t, r} - \xi, \mathbf{u}_{j+1}^{t+\Delta t, r}, ...\right)}{2\xi} \tag{105}$$

, where ξ is a very small number.

For the numerical implementation of coupled problems a special grid is necessary. Therefore, in the next chapter the grid generation techniques are explained.

3 1D pipe network grid embedded in a 3D porous media grid

The numerical modeling of coupled one-dimensional pipe flow with three-dimensional porous media flow requires a special grid concept that allows the representation of interactions between the pipe network grid and the porous media grid. Although this is a rather technical issue, it is the basis for the implementation of the model concept and detailed explanations are necessary. The basic idea is to isolate a pipe network grid within the three-dimensional porous media grid in such a way that each node of the pipe network grid is assigned to a node of the porous media grid.

The generation of 1D pipe network grid embedded in a 3D porous grid is performed according to the following sequence:

- First, a fully three-dimensional grid is generated by using a mesh generator.
- Next, the 3D grid information is saved in a csp data format.
- Then, a pps (pipe position) file is created, which defines the geometry of the pipe network grid.
- After that, the 3D grid information in the csp file and the pipe network information in the pps file are linked to each other into a dgf file.
- Although the dgf file assigns each node of the pipe network grid to a node of the porous media grid, it does not yet provide the connectivity information of the pipe network grid. Therefore, the coupled numerical model needs a preprocessing step called as an isolation step.

Each of the above steps is explained in the following section.

3.1 Explanation of the grid generation steps

3.1.1 Generation of a 3D porous media grid

For the generation of a 3D porous media grid a commercial program called $Ansys - Icem$ mesh generator is used. $Icem$ is a powerful tool which is capable of meshing complex geometries. If the domain geometries are simple, they can be easily created within the Icem

A summary of Chapter 3 is published in Dogan *et al.* (2009)

tool. On the other hand, if the geometries are complex, they need to be created in an external CAD drawing software, e.g. $Rhinoceros$ and then the geometry information needs to be imported into the $Icem$ mesh generator. However, this work has only focused on simple structured grids. First, the simple geometry is drawn within $Icem$. Then, appropriate grid sizes are defined on each edge of the geometry. After that, a boundary identity number is assigned to each boundary face of the geometry. Finally, the mesh is generated and saved in an external file in csp format.

3.1.2 Pipe network geometry

The geometry of the pipe networks needs to be defined in a structured way. For this purpose, a pps (pipe position) file is created where the positions of the starting and the end points of each pipe section, the property identities of the sections, and the boundary identities of each end point for each pipe section are defined. Fig. 18 shows an example of such a pps file structure with 41 pipe sections. The first section starts at point (5, 5, 3.6), ends at point (5, 5, 5), and has the property identity (id.) of 8. The starting point has the boundary id. 99 (denoting an internal boundary) and the ending point has the boundary id. 2.

3.1.3 Linking the nodes of the pipe network grid with the nodes of the porous media grid

The models are developed under $DuMu^x$ (Multi-Scale Multi-Physics Toolbox for the Simulation of Flow and Transport Processes in Porous Media) (Flemisch *et al.* (2007)), which is based on $DUNE$ (Distributed and Unified Numerics Environment) (Bastian *et al.* (2006)). $DUNE$ can read grids in dgf format (dune grid format). Therefore, the 3D porous media grid information in the csp format needs to be converted to the dgf format and the pipe network information in the pps format needs to be merged with the porous media grid information. This is achieved by programming a converter, which merges the information in the csp and the pps files into a dgf file. The starting and ending points of each pipe section in the pps file should be in very close proximity of a porous media grid node and the tolerance in the converter program can be chosen depending on the distance between successive porous media grid nodes, so that porous media nodes along each pipe section can be marked as pipe nodes. Fig. 19 shows a section of a dgf file. The first three columns in a dgf file store the x, y and z coordinates of the nodes in the porous media grid. The fourth and the fifth columns store the node properties and the boundary identities of the nodes in the pipe network grid. If both the fourth and the fifth columns are zero, this means that the related porous media grid nodes are not assigned to any pipe network grid node. The rectangles in Fig. 19 show the regions in the dgf file, where the pipe network grid nodes are linked to the porous media grid nodes.

```
41 # PIPES X1, Y1, Z1, X2, Y2, Z2, PIPEPARAMETER1, BOUNDARYCONDITION[0], BOUNDARYCONDITION[1],
 5   5   3.6   5   5   5   8   99    2
 3.6 5   3.6   5   5   3.6 8   99   99
 3.6 5   2.4   3.6 5   3.6 8   99   99
 2.4 5   2.4   3.6 5   2.4 8   99   99
 4.8 5   2.4   3.6 5   2.4 8   99   99
 4.8 5   0     4.8 5   2.4 8    1   99
 2.4 5   1.2   2.4 5   2.4 8   99   99
 1.2 5   1.2   2.4 5   1.2 8   99   99
 3.6 5   1.2   2.4 5   1.2 8   99   99
 1.2 5   0     1.2 5   1.2 8    1   99
 3.6 5   0     3.6 5   1.2 8    1   99
 6.4 5   3.6   5   5   3.6 8   99   99
 6.4 5   2.4   6.4 5   3.6 8   99   99
 5.2 5   2.4   6.4 5   2.4 8   99   99
 7.6 5   2.4   6.4 5   2.4 8   99   99
 5.2 5   0     5.2 5   2.4 8    1   99
 7.6 5   1.2   7.6 5   2.4 8   99   99
 6.4 5   1.2   7.6 5   1.2 8   99   99
 8.8 5   1.2   7.6 5   1.2 8   99   99
 6.4 5   0     6.4 5   1.2 8    1   99
 8.8 5   0     8.8 5   1.2 8    1   99
 5   3.6 3.6   5   5   3.6 8   99   99
 5   3.6 2.4   5   3.6 3.6 8   99   99
 5   2.4 2.4   5   3.6 2.4 8   99   99
 5   4.8 2.4   5   3.6 2.4 8   99   99
 5   4.8 0     5   4.8 2.4 8    1   99
 5   2.4 1.2   5   2.4 2.4 8   99   99
 5   1.2 1.2   5   2.4 1.2 8   99   99
 5   3.6 1.2   5   2.4 1.2 8   99   99
 5   1.2 0     5   1.2 1.2 8    1   99
 5   3.6 0     5   3.6 1.2 8    1   99
 5   6.4 3.6   5   5   3.6 8   99   99
 5   6.4 2.4   5   6.4 3.6 8   99   99
 5   5.2 2.4   5   6.4 2.4 8   99   99
 5   7.6 2.4   5   6.4 2.4 8   99   99
 5   5.2 0     5   5.2 2.4 8    1   99
 5   7.6 1.2   5   7.6 2.4 8   99   99
 5   6.4 1.2   5   7.6 1.2 8   99   99
 5   8.8 1.2   5   7.6 1.2 8   99   99
 5   6.4 0     5   6.4 1.2 8    1   99
 5   8.8 0     5   8.8 1.2 8    1   99
```

Figure 18: An example *pps* file for defining 1D network sections

3.1.4 Isolation process

The dgf file does not provide yet the connectivity information of the pipe network nodes required for the assembly of the stiffness matrix and the right-hand side vectors during the simulation of the pipe flow model. In order to solve this problem, an isolation algorithm is developed, which not only stores the connectivity information in a vector data structure, but also maps the nodes of the porous media grid to the nodes of the pipe network grid.

The isolated pipe network grid is stored in a simple vector data structure. The entries of the vector data structure are of a structure data type and named vertex. Each vertex data structure represents a pipe node. The members of the vertex data structure are, for example, the indices of the neighboring pipe nodes, the property identity and the boundary identity of the pipe node and the global identities of the linked porous-media grid node as well as some methods to calculate the normal vectors at the interface between the pipe control volumes. At the current state, the isolation algorithm can generate a pipe network grid only from

```
6.4000000e+00 4.8000000e+00 4.8000000e+00 0 0 % 43081
6.4000000e+00 4.8000000e+00 5.0000000e+00 0 0 % 43082
6.4000000e+00 5.0000000e+00 0.0000000e+00 8 1 % 43083
6.4000000e+00 5.0000000e+00 2.0000000e-01 8 0 % 43084
6.4000000e+00 5.0000000e+00 4.0000000e-01 8 0 % 43085
6.4000000e+00 5.0000000e+00 6.0000000e-01 8 0 % 43086
6.4000000e+00 5.0000000e+00 8.0000000e-01 8 0 % 43087
6.4000000e+00 5.0000000e+00 1.0000000e+00 8 0 % 43088
6.4000000e+00 5.0000000e+00 1.2000000e+00 8 99 % 43089
6.4000000e+00 5.0000000e+00 1.4000000e+00 0 0 % 43090
6.4000000e+00 5.0000000e+00 1.6000000e+00 0 0 % 43091
6.4000000e+00 5.0000000e+00 1.8000000e+00 0 0 % 43092
6.4000000e+00 5.0000000e+00 2.0000000e+00 0 0 % 43093
6.4000000e+00 5.0000000e+00 2.2000000e+00 0 0 % 43094
6.4000000e+00 5.0000000e+00 2.4000000e+00 8 99 % 43095
6.4000000e+00 5.0000000e+00 2.6000000e+00 8 0 % 43096
6.4000000e+00 5.0000000e+00 2.8000000e+00 8 0 % 43097
6.4000000e+00 5.0000000e+00 3.0000000e+00 8 0 % 43098
6.4000000e+00 5.0000000e+00 3.2000000e+00 8 0 % 43099
6.4000000e+00 5.0000000e+00 3.4000000e+00 8 0 % 43100
6.4000000e+00 5.0000000e+00 3.6000000e+00 8 99 % 43101
6.4000000e+00 5.0000000e+00 3.8000000e+00 0 0 % 43102
```

Figure 19: A section of a dgf file format including the 1D network grid information

a structured 3D grid. The isolation process needs to be run once in the beginning of each simulation, so that the vector data structure is filled with the pipe network grid information.

The parallel computation of a coupled lower dimensional dual-continuum model not only requires a pipe network gird, which is capable of running parallel simulations but also requires complex parallelized mapping of the porous media grid nodes with the nodes of the pipe network grid. That kind of work is beyond the scope of this thesis. For modeling more complex geometries, the current 1D pipe-network grid in a 3D grid needs to be further developed for unstructured grid implementations, and for large scale simulations both the models and the 1D pipe-network grid need to be modified for parallel computation.

With the help of the postprocessing tool $Paraview$, the resulting 1D pipe-network grid embedded in a 3D domain can be visualized (see Fig. 20).

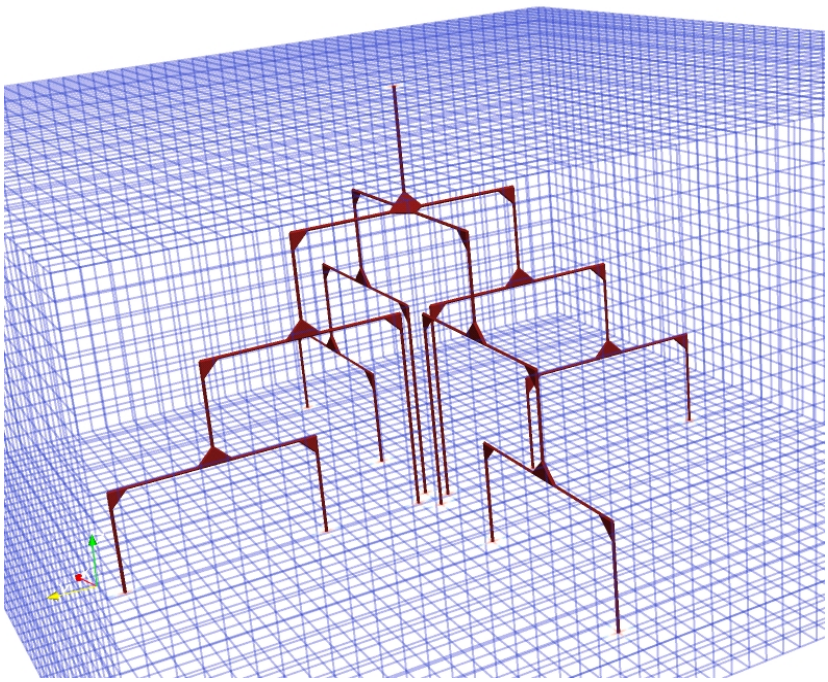

Figure 20: A 1D network grid in a 3D domain

The focus of this work is to develop numerical models, which are capable of simulating coupled systems. Therefore, in the following chapter the implemented numerical models for coupled single-phase flow systems are discussed in detail.

4 Numerical models for single-phase flow systems

This section is devoted to the introduction of the numerical models which are developed in this study for modeling single-phase flow systems. First, each model is described mathematically by introducing the governing equations. Subsequently, the numerical models are tested for the related problem cases. Before introducing the coupled models for single-phase flow systems, a stand alone compressible pipe flow model is introduced. After that, several lower-dimensional dual-continuum models for coupled single-phase flow systems are presented.

4.1 Compressible pipe flow model

In this study, the pipe flow system is described with a quasi-1D flow behavior. If the free flow equations are written for cross-sectionally averaged 1D pipe flow, for the conservation of mass, Eq. 106 and for the conservation of momentum, Eq. 107 are obtained. The vector $\vec{s}$ stands for the unit positive direction of the pipe and τ_w is the wall shear stress, which can be described by the Darcy-Weisbach approach as in Eq. 108.

$$\frac{\partial \varrho}{\partial t} + \frac{\partial}{\partial s}(\varrho\, \bar{u}_s) = q \tag{106}$$

$$\frac{\partial(\varrho\, \bar{u}_s)}{\partial t} + \frac{\partial(\varrho\, \bar{u}_s\, \bar{u}_s)}{\partial s} + \frac{\partial p}{\partial s} + \tau_w \frac{\pi d}{A} = \varrho\, \vec{g} \cdot \vec{s}, \tag{107}$$

The system has 4 unknowns (ϱ, p, $\bar{u}_s$ and τ_w) but 2 equations. To close the system it is assumed that the ideal gas law is valid; i.e. density and pressure are related with each other (Eq. 109) and the wall friction is described by the Darcy-Weisbach approach (Eq. 108). The term ζ in Eq. 108 is called the Darcy-Weisbach friction factor and is a function of $f(Re, \frac{\epsilon}{d})$, where Re is the Reynolds number and ϵ is an equivalent sand grain roughness. A detailed description of the discretization scheme is given in Section 2.3.2.2.

$$\tau_w \;=\; \frac{\zeta}{8}\, \varrho\, (\bar{u}_s)^2 \tag{108}$$

$$\varrho \;=\; \frac{p}{R_{ind}\, T} \tag{109}$$

A test problem of the pipe flow model:

A numerical test example is run to illustrate the results of the pipe flow model. Air is flowing along a $20\ m$ long L-shaped pipe (Fig. 21) with a diameter of $10\ cm$. The pipe is closed at the left boundary ($\bar{u}_s = 0$) and at the top boundary the pressure is fixed to $1.0\ bar$. There is a continuous source term ($0.25\ kg/(m^3 \cdot s)$) along the horizontal pipe. The parameters and the boundary conditions chosen for the test problem are listed in Tab. 2.

Fig. 22 shows the steady state velocity distribution. As a result of the source term, velocity increases along the horizontal pipe. Since there is no source term along the vertical pipe, flow conditions hardly vary along the vertical pipe compared to the horizontal pipe.

fluid	air
parameters	temperature = 15 [°C] diameter = 10 [cm] ε / d = 1/90 [-]
initial condition	pressure = 1.0*10^5 [Pa] velocity = 0 [m/s]
source term	0.25 [kg/(m^3*s)]
boundary conditions left boundary top boundary	 no flow ($\bar{u}_s$ = 0 [m/s]) out flow boundary Dirichlet - pressure = 1.0*10^5 [Pa]

Table 2: The parameters and the boundary conditions of the pipe flow model problem

At steady state, the total balance of ingoing and outgoing mass fluxes can be checked as follows:

$$q_{source}\ L\ A = \varrho_{air}\ \bar{u}_{s\_out}\ A\ [kg/s] \ => \ \bar{u}_{s\_out} = \frac{q_{source}\ L}{\varrho_{air}}\ [m/s] \tag{110}$$

$$\bar{u}_{s\_out} = \frac{0.25 \cdot 10.0}{1.21} \approx 2.07\ [m/s]$$

The steady state condition can be also be checked by calculating the mass balance of a control volume in the vertical pipe as follows:

$$\frac{p_1}{R_{ind}\ T}\ \bar{u}_{s1}\ A - \frac{p_2}{R_{ind}\ T}\ \bar{u}_{s2}\ A \ = \ \frac{(p_1\ \bar{u}_{s1} - p_2\ \bar{u}_{s2})}{R_{ind}\ T}\ A \tag{111}$$

$$\frac{(100013.15432 \cdot 2.068949) - (100000.00000 \cdot 2.069221)}{(286.991 \cdot 288.15)} \cdot (\pi \cdot \frac{0.1^2}{4})$$

$$\approx 1.48 \cdot 10^{-9}\ [kg/s]$$

Since the difference between the incoming and outgoing flux is negligible, steady state condition is reached.

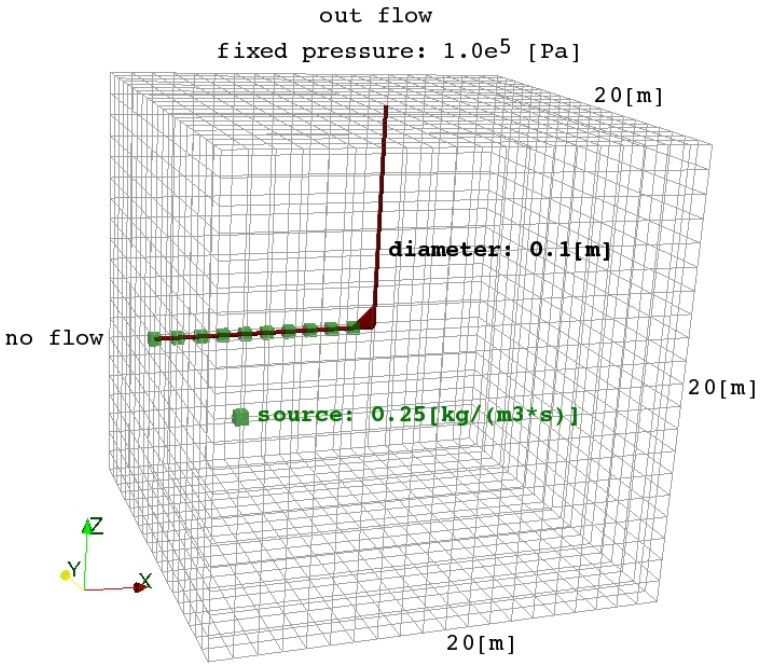

Figure 21: The pipe flow problem

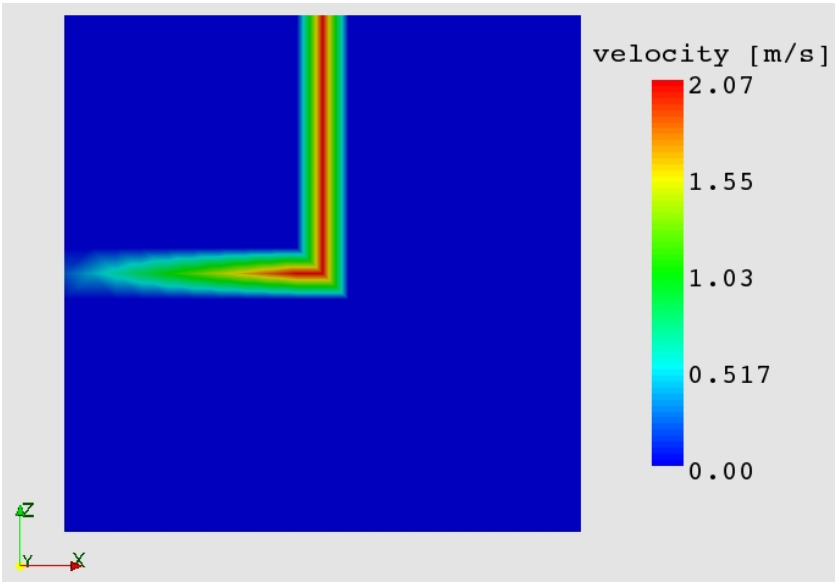

Figure 22: Velocity distribution along the pipe in a cut plane at $y = 10\ m$

In the following section single-phase lower-dimensional dual-continuum models and their numerical test examples are discussed.

4.2 Lower-dimensional dual-continuum models for single-phase flow systems

In this section several numerical models for coupled single-phase flow systems are introduced. The lower-dimensional dual-continuum coupling strategy (see Section 2.2.5) accounts only for the mass transfers between the two continua and requires source/sink mass exchange terms, which are described in each mathematical model in detail. The chosen sequence of example applications follows the order of increasing complexity of the applied model concepts.

4.2.1 Coupling single-phase flow in porous media with Hagen-Poiseuille flow

As a first step, a coupled single-phase model is implemented for simulating steady-state incompressible flow conditions. The multi-phase mass balance equation (Eq. 31) simplifies to Eq. 112 and Darcy's law (Eq. 113) holds for single-phase porous media flow:

$$\vec{\nabla} \cdot (\varrho \vec{u}) = q + \boxed{q_{ex}}, \text{, where } q_{ex} \text{ is the mass exchange term} \tag{112}$$

$$\vec{u} = -\frac{\bar{\bar{K}}}{\mu}(\nabla p - \varrho \vec{g}) \tag{113}$$

The mass balance equation of pipe flow (Eq. 114) has the same mass exchange term as the porous media mass balance equation, but it appears with a different sign. If the momentum storage and the momentum convection terms are smaller than the viscous term and the flow conditions are laminar, then the momentum equation of pipe flow (Eq. 66) can be simplified to the well-known Hagen-Poiseuille equation (Eq. 115):

$$\frac{\partial}{\partial s}(\varrho\, \bar{u}_s) = q - \boxed{q_{ex}} \tag{114}$$

$$\bar{u}_s = -\left(\frac{d^2}{32\mu}\,(\frac{\partial p}{\partial s} - \varrho\, \vec{g} \cdot \vec{s})\right) \tag{115}$$

For the calculation of the mass exchange term (Eq. 116), one has to take the fluid properties (density(ϱ) and dynamic viscosity (μ)), the porous media properties (the exchange coefficient (α_{ex})), the pipe geometry (the outer surface of the pipe element ($A_{outerface}$) and the pipe diameter (d)), as well as the pressure difference between the two continua into account:

$$\int q_{ex}\, dV \;=\; \varrho\, \frac{\alpha_{ex}}{\mu}\, \frac{A_{outerface}}{d}\, (p_{pipe} - p_{pm}) \tag{116}$$

The Sections 4.2.1 and 4.2.5 are published in Dogan *et al.* (2009)

A test problem for coupling porous medium flow with Hagen-Poiseuille flow:

A problem is set up where a pipe with a diameter of 2 cm is embedded into a porous medium in the longitudinal direction and the flowing fluid is water. The porous domain is 2 m high, 2 m wide and 10 m long. The grid is only refined along the pipe line to save computation time. In this example, gravity is set to zero in order to see the effect of the exchange term clearly. The parameters and the boundary conditions chosen for the problem are listed in Tab. 3. At the left and right boundaries of the porous domain, Dirichlet boundaries are set to $p_{left} = 1.004$ bar and $p_{right} = 1.000$ bar. The permeability of the porous medium is $5.0 \cdot 10^{-10}$ m^2. At the left boundary of the pipe, a no flow boundary is set and at the right boundary, the pressure is fixed at 1.000 bar. The exchange coefficient is chosen to $1.2 \cdot 10^{-11}$ m^2 (see Fig. 23).

common parameters	α_{ex} = 1.2*10-11 [m²]	temperature = 10 [°C]
domain	Porous media	Pipe
fluid parameters	water permeability = 5.0*10-10 [m²] porosity = 0.4 [-]	water diameter = 2 [cm]
initial condition	-	-
boundary conditions left boundary right boundary other boundaries	 Dirichlet - pressure = 1.004*10^5 [Pa] Dirichlet - pressure = 1.0*10^5 [Pa] Neumann : no flow	 Neumann : no flow Dirichlet - pressure = 1.0*10^5 [Pa] -

Table 3: The parameters and the boundary conditions of the coupled porous medium flow - Hagen-Poiseuille flow problem

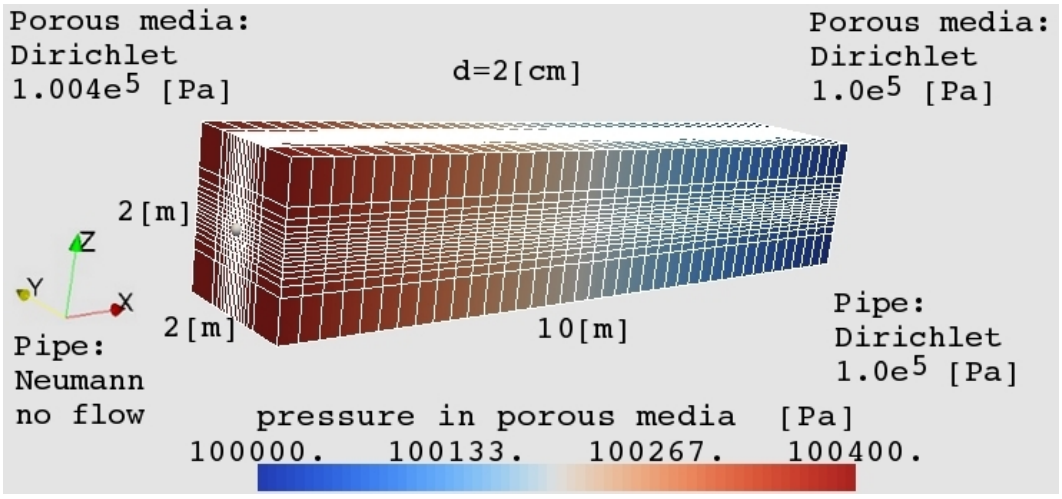

Figure 23: The coupled porous medium flow - pipe flow problem

The left part in Fig. 24 shows the steady state pressure distribution along the pipe for both porous medium and pipe flow continua. The right side of the same figure shows the velocity distribution along the pipe. At the outflow section of the pipe the Reynolds number (Re)

reaches to $1752 < 2300$, i.e. laminar flow condition required by Hagen-Poiseuille flow is satisfied. To examine the effect of coupled flow on the porous medium pressure distribution, a cut plane at y = 1 m is shown in Fig. 25. If there were no coupled flow, one would expect to see a linear pressure distribution in the porous medium since the flow is incompressible. As Fig. 25 shows, there is a pressure gradient towards the pipe and the pressure isolines are not linear. This indicates the influence of the pipe flow coupling on the hydraulics in the porous medium.

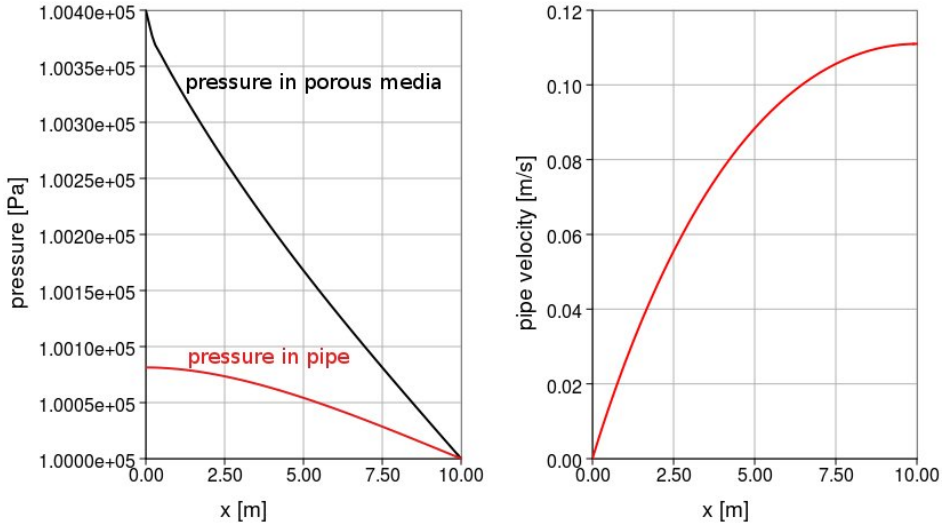

Figure 24: Pressure and velocity distributions along the pipe

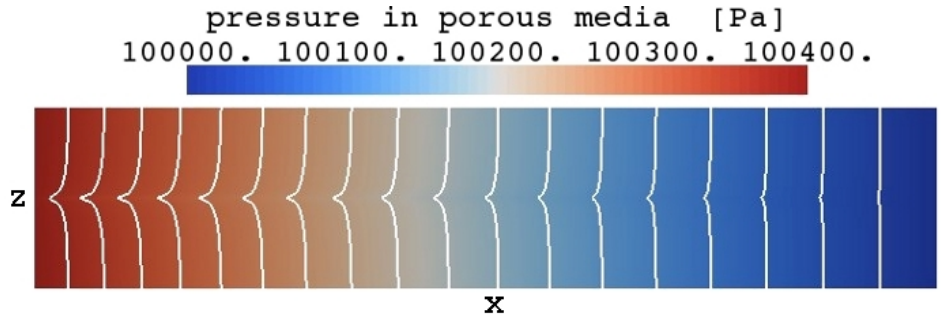

Figure 25: Pressure distribution in a cut plane at y = 1 m in the porous medium

A test problem for coupling porous medium flow with the flow in a pipe network:

Another problem is simulated where a pipe network is embedded into a porous medium and flowing fluid is water (see Fig. 20 for the exact geometry of the pipe network system). Analogous to the first example, gravity is neglected. The porous medium has a rectangular prism shape with $x = 10$ m, $y = 10$ m and $z = 5$ m. All pipes have a diameter of 2 cm. The parameters and the boundary conditions of the system are listed in Tab. 4. The sides of

the porous domain are no-flow Neumann boundaries, whereas the top boundary is set to a constant pressure of 1.004 bar and at the bottom boundary the pressure is set to 1.000 bar. The pipe network system has a no-flow boundary at the top and a fixed pressure of 1.000 bar at the bottom. The permeability of the porous medium is $5.0 \cdot 10^{-10}$ m^2 and the exchange coefficient is chosen to be $1.2 \cdot 10^{-11}$ m^2. Fig. 26 shows the porous media pressure distribution. The gradients of the pressure isolines show clearly that there is a considerable flow from the porous medium into the pipe network system, which could be described by the model.

common parameters	$\propto_{ex}$ = 1.2*10-11 [m²]	temperature = 10 [°C]
	Porous media	Pipe network
fluid parameters	water permeability = 5.0*10-10 [m²] porosity = 0.4 [-]	water diameter = 2 [cm]
initial condition	-	-
boundary conditions top boundary bottom boundary other boundaries	 Dirichlet - pressure = 1.004*10^5 [Pa] Dirichlet - pressure = 1.0*10^5 [Pa] Neumann : no flow	 Neumann : no flow Dirichlet - pressure = 1.0*10^5 [Pa] -

Table 4: The parameters and the boundary conditions of the coupled porous medium - pipe network flow problem

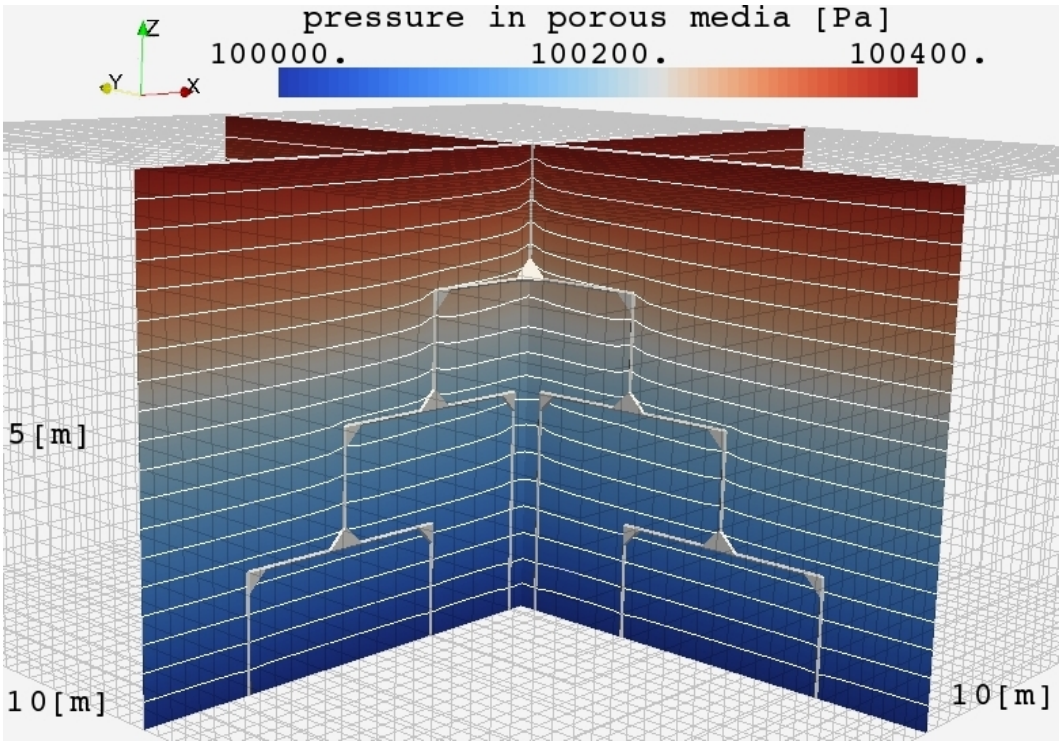

Figure 26: Pressure distribution in the porous medium for the coupled pipe network system

In the next three sections, the coupled lower dimensional dual-continuum model will be analyzed, considering the computational cost (CPU time), the sensitivity of the results depending on the exchange coefficient (α_{ex}) and the grid density.

4.2.2 CPU time in coupled lower dimensional dual-continuum models

Since coupled models are simulating more complex physical processes, they need more computational power, i.e. more CPU time, than not coupled models. In this section, the test problems in Fig. 23 and Fig. 26 are analyzed with respect to the required CPU time. The implemented lower dimensional dual-continuum model can be divided into two parts. In the first part, the required CPU time for the isolation process is calculated. Each simulation starts with an isolation process, which generates a pipe network grid from a structured 3D grid and maps the nodes of the porous media grid to the nodes of the pipe network grid. The isolation process is done only once at the beginning of each simulation. In the second part, the required CPU time for the rest of the simulation, which also includes the iterations between the coupled models, is calculated. For the ease of understanding, the test problems in Fig. 23 and Fig. 26 are called "simple problem" and "complex problem" respectively.

The simulations are computed with Intel Pentium E5200 processor running at 2.5 GHz. Tab. 5 shows the grid information of both problems. The grid size of the complex problem is about 6 to 7 times bigger than the grid size of the simple problem. Tab. 6 shows the CPU time required to calculate the standalone (not coupled) porous medium flow problems. As expected, the simulation time is non-linearly increasing with increasing node numbers (see Tab. 6), i.e. more nodes means more connectivity and bigger matrices. Tab. 7 shows the CPU time required to calculate the coupled problems. Keeping in mind that the isolation process is calculated only once for each simulation, it is a good idea to calculate the CPU time required by the isolation process. The isolation process takes 2.4 seconds for the simple problem and 50.6 seconds for the complex problem, i.e. it takes 21 times more time for an about 7 times bigger grid. The simulation time of the not coupled simple problem takes 8.4 seconds, whereas the coupled simple problem takes 24.7 seconds. The not coupled complex problem takes 108.7 seconds and the coupled complex problem takes 277.1 seconds. These numbers show that coupled problems require about 2.5 to 3 times more time than not coupled models, which is most of the time due to the isolation process and the iterations between the coupled models. The extra computation time required by the coupled models is acceptable, considering the geometrical complexity and iterative loops implemented in the coupled models.

	# of elements	# of faces	# of lines	# of nodes	# of pipe nodes
simple problem	10240	32256	33864	11849	41
complex problem	62500	192500	197625	67626	276

Table 5: The number of the grid entities in the analysed problems

	total simulation time
simple problem	8.4 $[s]$
complex problem	108.7 $[s]$

Table 6: The CPU times for the standalone (not coupled) porous medium flow problems

	isolation time	the rest of the simulation time	total simulation time
simple problem	2.4 $[s]$	22.3 $[s]$	24.7 $[s]$
complex problem	50.6 $[s]$	226.5 $[s]$	277.1 $[s]$

Table 7: The required CPU times for the coupled problems

4.2.3 Sensitivity of the coupled model on the variation of the exchange coefficient (α_{ex})

In coupled dual-continuum models the exchanged mass between the continua is calculated via the mass exchange term (see Eq. 116), which is similar to a source/sink term. In the mass exchange term there is a parameter called exchange coefficient (α_{ex}), which eventually determines how strong the continua are coupled. Therefore, the most important parameter in the lower dimensional dual-continuum model is the exchange coefficient.

If closely investigated, the mass exchange term (Eq. 116) is formulated like an advective flux between two control volumes. Like the permeability, the exchange coefficient (α_{ex}) has a unit in m^2. Although α_{ex} can be defined as a property of the porous medium, there are no values of α_{ex} coefficients related to porous material in the literature. Therefore, the exchange coefficient is most of the time chosen by the modeler. However, the correct α_{ex} value needs to be determined by fitting the simulation results to the experimental results.

The response of the coupled numerical model to the variation of the exchange parameter needs to be investigated. For that purpose, the test problem in Fig. 23 is calculated for 7 different α_{ex} values, ranging from $1.0 \cdot 10^{-11}$ m^2 to $3.2 \cdot 10^{-10}$ m^2. Each time the value of the α_{ex} parameter is doubled. Fig. 27 shows the averaged velocity profiles along the pipe line. As expected, with increasing α_{ex} values, the continua are more strongly coupled and more water flows from porous media into the pipe, which results in higher velocities in the pipe continua. As Fig. 27 shows, the increase in the exchanged mass flux is non-linearly related to the α_{ex} parameter. From $1.0 \cdot 10^{-11}$ m^2 to $4.0 \cdot 10^{-11}$ m^2 the α_{ex} is quadrupled but the exchanged mass is only doubled. For a 32 times bigger exchange coefficient (from $1.0 \cdot 10^{-11}$ m^2 to $3.2 \cdot 10^{-10}$ m^2) the exchanged mass has only increased 2.8 times. Assuming that in Eq. 116 all the other values except the α_{ex} parameter stay constant, one would expect a linear relationship between the total exchanged mass and the exchange coefficient. However, this is not the case, since the pressure difference between the continua changes with changing α_{ex} parameter. Fig. 28 shows the pressure differences between the continua for exchange coefficients $1.0 \cdot 10^{-11}$ m^2 and $4.0 \cdot 10^{-11}$ m^2. With increasing exchange coefficient, the pressure difference between the continua decreases. The results denote that the total exchanged mass between the continua is not only a function of α_{ex} parameter but also the

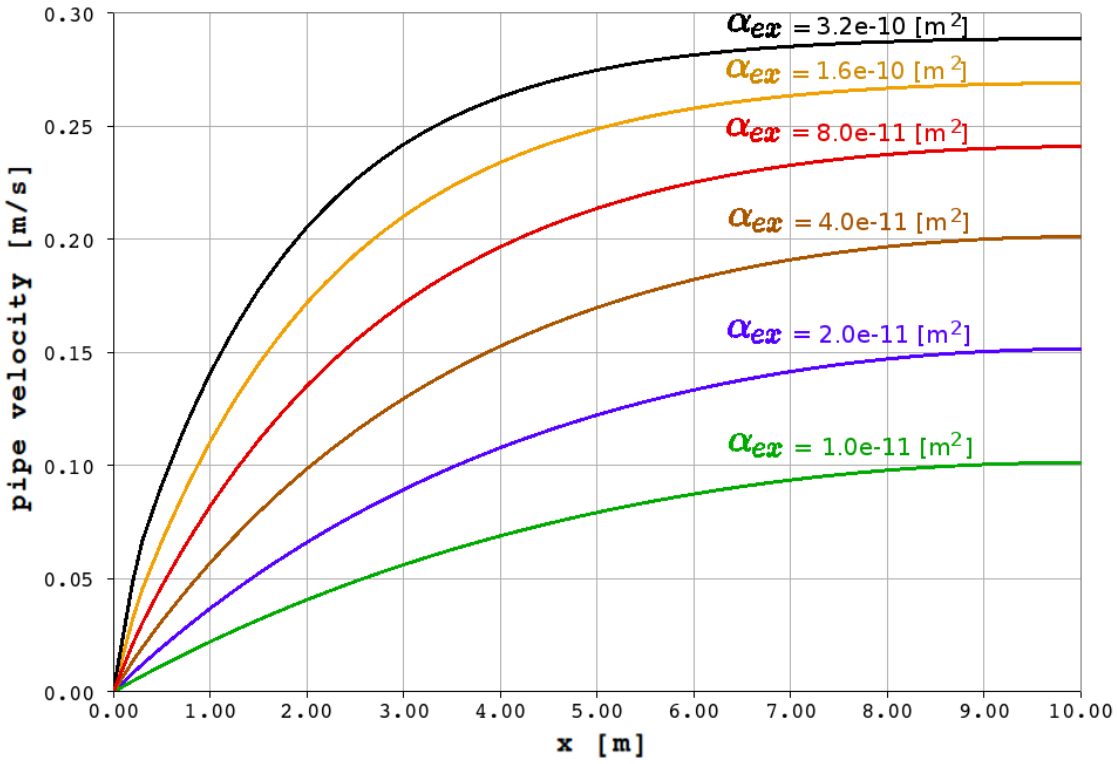

Figure 27: Sensitivity of the coupled model on the variation of the exchange coefficient (α_{ex})

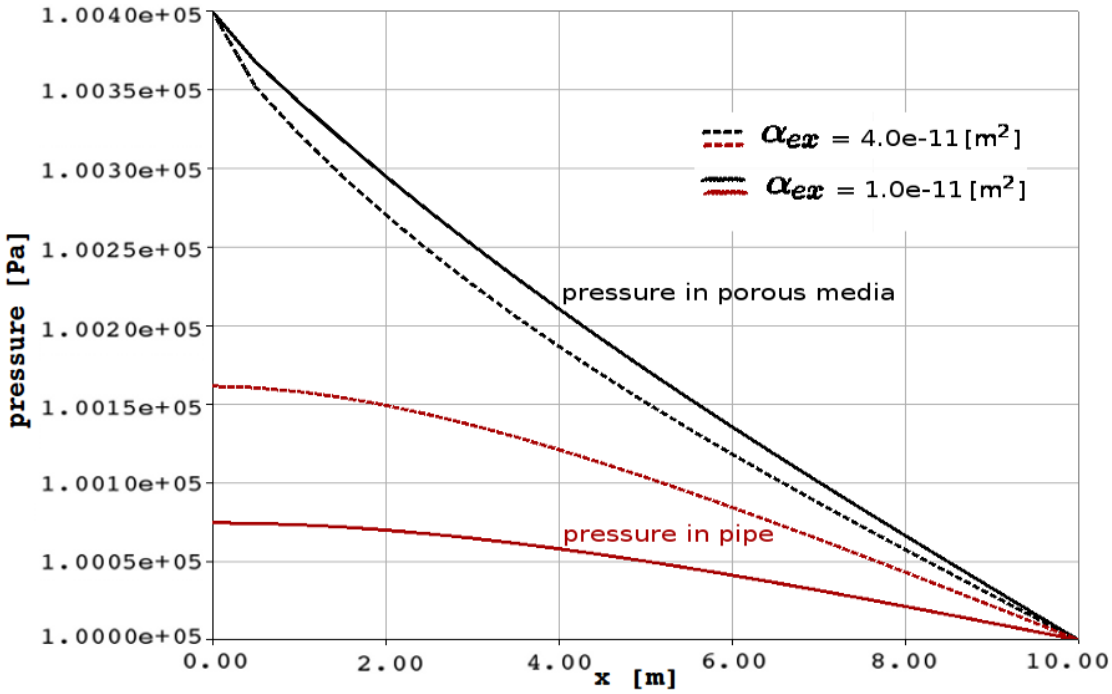

Figure 28: Pressure differences between the continua for different exchange coefficients

pressure difference between the continua, which does not stay constant. This effect results in a non-linear α_{ex} - total exchanged mass relationship.

4.2.4 Grid convergence test

A grid convergence test is necessary to see the dependence of the numerical solution on the grid size. For this purpose, a problem similar to the problem in Fig. 23 is set up. The parameters and boundary conditions of the problem are described in Fig. 29.

common parameters	α_{ex} = 1.2*10-11 [m²]	temperature = 10 [°C]
	Porous media	Pipe
fluid parameters	water permeability = 5.0*10-10 [m²] porosity = 0.4 [-]	water diameter = 2 [cm]
initial condition	-	-
boundary conditions left boundary right boundary other boundaries	 Dirichlet - pressure = 1.004*10^5 [Pa] Dirichlet - pressure = 1.0*10^5 [Pa] Neumann : no flow	 Neumann : no flow Dirichlet - pressure = 1.0*10^5 [Pa] -

Table 8: The parameters and the boundary conditions of the grid convergence test problem

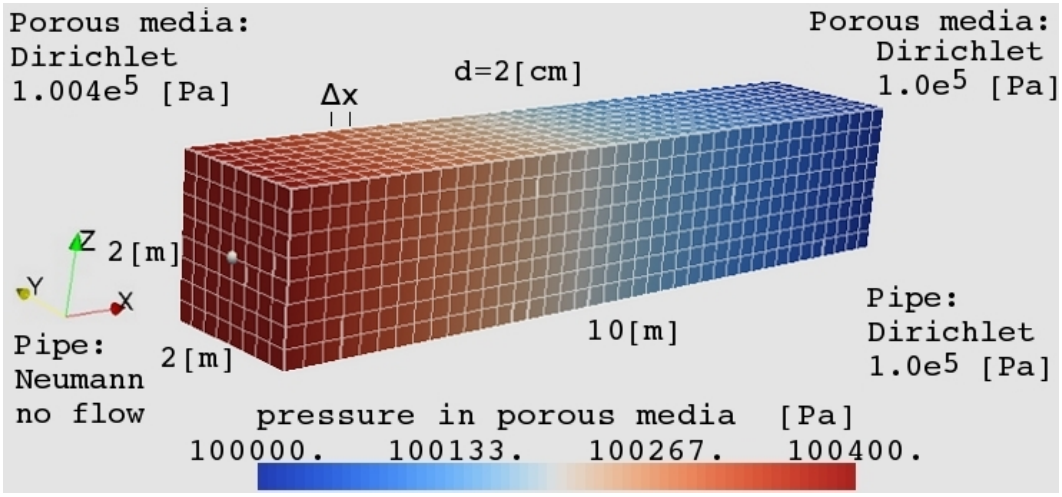

Figure 29: The grid convergence test boundary conditions of the coupled porous media flow - pipe flow problem

The same problem is simulated for four different grid sizes. The grid spacings (Δx) from coarse to fine are 1.0 m, 0.5 m, 0.25 m and 0.125 m. As Fig. 30 shows, the grid size doesn't play a big role in the steady state pressure distributions along the pipe line. This behavior can be simply explained by going through the mass exchange term. As Eq. 116 shows, the mass transfer between the two continua depends on the pressure gradient, which is expressed by the ratio ($\frac{p_{pipe} - p_{pm}}{d}$). In contrast to the discrete fracture models, where the

pressure gradient around the fractures highly depends on the grid refinement, in dual-continuum models the grid spacing has minimal effect on the pressure gradient between the two continua, since the exchange distance is fixed with the diameter of the pipe. In discrete fracture models the fluxes towards the fractures are calculated between the fracture node and the neighboring porous media node. The distance between the fracture node and the neighboring porous media node is highly grid dependent. On the other hand, in the dual-continuum model there are two overlapping continua, i.e. a node in the pipe grid and the linked node in the porous media grid are on top of each other and the virtual distance (pipe diameter) between those nodes is grid size independent. However, the grid size still has an effect, i.e. in coarser grids the exchanged mass is distributed for lager regions at once in contrast to the finer grids. That is the reason, why the lines in Fig. 30 are not fully overlapping.

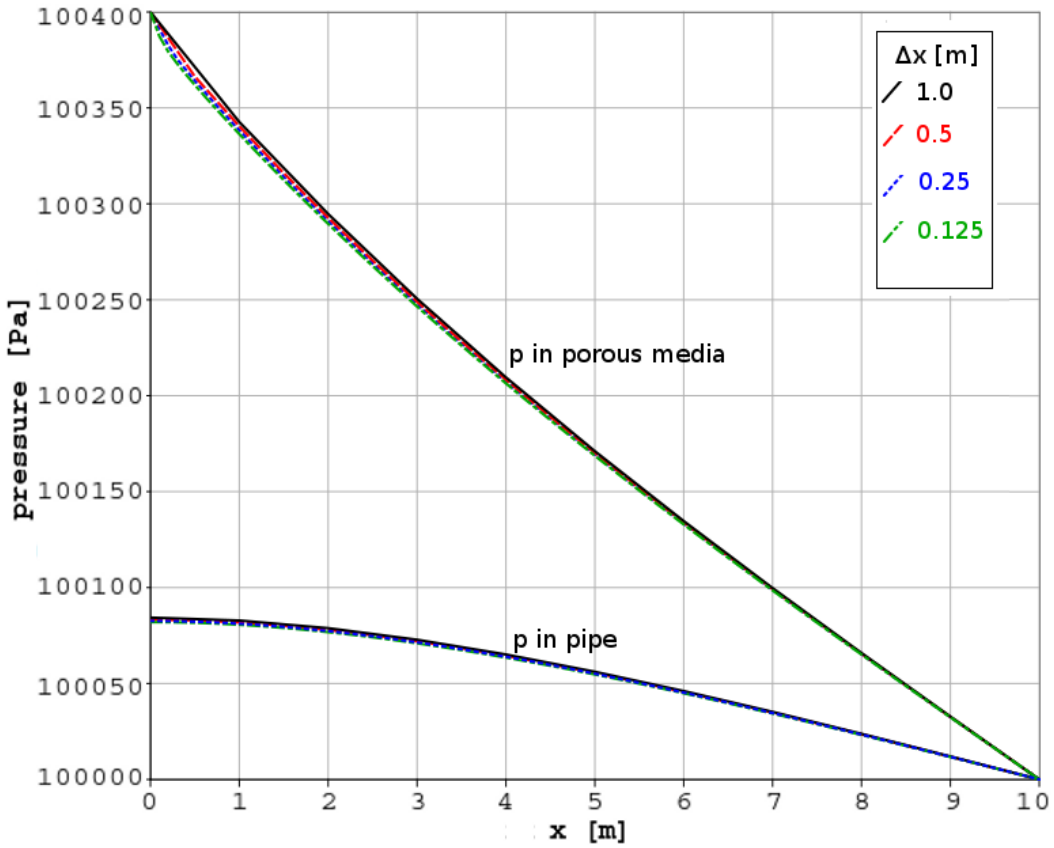

Figure 30: Grid convergence test: Pressure distributions of both porous media and pipe flow continua along the pipe line

4.2.5 Coupling single-phase flow in porous media with single-phase pipe flow

In the next step, the numerical models are extended for transient, compressible flow conditions. The conservation equations for compressible one-phase flow in porous media can be written as:

$$\frac{\partial(\phi\varrho)}{\partial t} + \vec{\nabla}\cdot(\varrho\vec{u}) = q + \boxed{q_{ex}} \tag{117}$$

, where q_{ex} is the mass exchange term, and $\varrho = \dfrac{p}{R_{ind}\,T}$.

$$\vec{u} = -\frac{\bar{\bar{K}}}{\mu}(\nabla p - \varrho\vec{g}) \tag{118}$$

The conservation equations of the pipe flow are:

$$\frac{\partial\varrho}{\partial t} + \frac{\partial}{\partial s}(\varrho\ \bar{u}_s) = q - \boxed{q_{ex}} \tag{119}$$

$$\frac{\partial(\varrho\ \bar{u}_s)}{\partial t} + \frac{\partial(\varrho\ \bar{u}_s\ \bar{u}_s)}{\partial s} + \frac{\partial p}{\partial s} + \tau_w\frac{\pi d}{A} = \varrho\ \vec{g}\cdot\vec{s} \tag{120}$$

Exchange term:

$$\int q_{ex}\ dV\ =\ \varrho_{ex}\ \frac{\alpha_{ex}}{\mu}\frac{A_{outerface}}{d}\ (p_{pipe} - p_{pm}) \tag{121}$$

Since in compressible flow conditions density changes as a function of the pressure, ϱ_{ex} in the mass exchange term needs to be determined. The density exchange term is upwinded, i.e.

if $p_{pipe} < p_{pm} \Rightarrow \varrho_{ex} = \varrho_{pm}$;

else $\Rightarrow \varrho_{ex} = \varrho_{pipe}$

A test problem for coupling single-phase porous medium flow with pipe flow:

A test problem is set up as described in the upper part of Fig. 31 and the flowing fluid is air. As seen in the setup a pipe with a diameter of $2\ cm$ is embedded into the porous medium in the longitudinal direction. Tab. 9 shows the parameters and the boundary conditions of the test problem. At the left and right boundaries of the porous domain, Dirichlet boundaries are set to $p_{left} = 1.004$ bar and $p_{right} = 1.0$ bar. The permeability of the porous medium is $5.0 \cdot 10^{-10}$ m^2. At the left boundary of the pipe, a no flow boundary is set and at the right boundary, the pressure is fixed at 1.0 bar. The exchange coefficient is chosen to be $1.2 \cdot 10^{-11}$ m^2

The lower left and lower right parts of Fig. 31 show the pressure distributions in both domains. The difference between this test problem and the test problem in Fig. 23 lies in the flowing fluid. The boundary conditions are the same as before, but this time air is flowing instead of water. If one compares the left part of Fig. 24 with the lower left part of Fig. 31, one can see that the pressure difference is higher in the second case. This doesn't necessarily mean that the mass exchange rate is higher in the second case because the mass exchange rate also depends on the kinematic viscosity of the fluid ($1/\nu = 1/(\mu/\varrho)$). Although the same boundary conditions are set for both problem cases, they are not directly comparable

to each other. Different amounts of mass are stored in each problem, depending on the fluid properties, and the governing equations for the two problems are not identical. However, the problem given in Fig. 31 will be further discussed in Section 6.1.2, where the coupling of two-phase porous medium flow with single-phase pipe flow is presented.

common parameters	α_{ex} = 1.2*10-11 [m²]	temperature = 10 [°C]
	Porous media	Pipe
fluid parameters	air permeability = 5.0*10-10 [m²] porosity = 0.4 [-]	air diameter = 2 [cm] ε / d = 1/90 [-]
initial condition	pressure = 1.0*10^5 [Pa] -	pressure = 1.0*10^5 [Pa] velocity ($\bar{u}_s$) = 0 [m/s]
boundary conditions left boundary right boundary other boundaries	 Dirichlet - pressure = 1.004*10^5 [Pa] Dirichlet - pressure = 1.0*10^5 [Pa] - Neumann : no flow	 no flow ($\bar{u}_s$ = 0 [m/s]) out flow boundary Dirichlet - pressure = 1.0*10^5 [Pa] -

Table 9: The parameters and the boundary conditions of the coupled single-phase porous medium flow - single-phase pipe flow problem

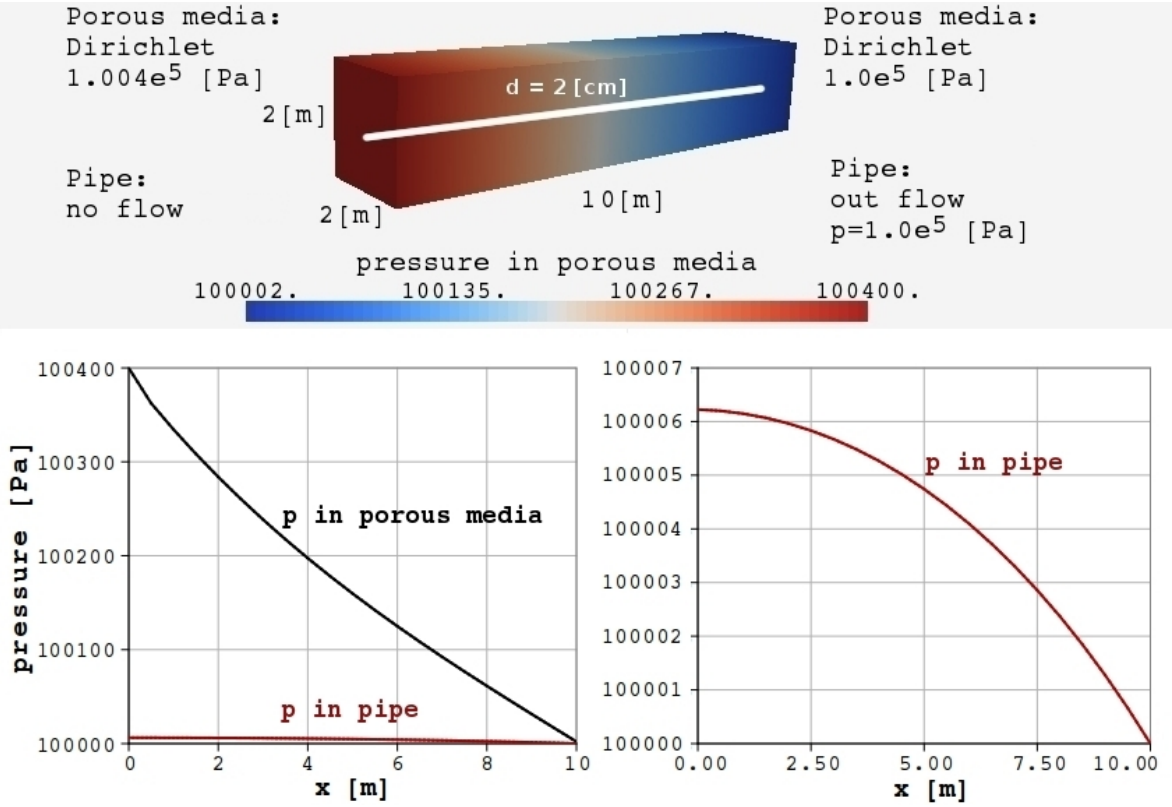

Figure 31: The boundary conditions and the pressure distribution of the coupled single-phase porous medium flow - single-phase pipe flow problem

5 An attempt to validate the coupled single-phase model

5.1 Aim

At this stage, the validation of the lower-dimensional dual-continuum coupling strategy for single-phase flow systems was necessary, before developing numerical models for more complex multi-phase flow and transport systems. For this reason an experiment is carried out to observe the coupled single-phase porous media flow - pipe flow system under controlled laboratory conditions. At the end of this chapter the results of the experiment are compared with the results of the numerical model in order to determine, whether the numerical model can reproduce the experimental results. Therefore, a simple experiment is set up to observe the mass balance of air for a coupled system.

The setup consists of an airtight plastic box, a glass-tube flow meter, a prandtl tube, an electronic pressure meter, a pressure regulator, a digital thermometer, an air storage cylinder, sand, an air distributor and a perforated L-shaped metal pipe.

5.2 Setup of the experiment

The plastic box is $50\ cm$ long, $50\ cm$ wide and $45\ cm$ high in the inner dimensions. Pressurized air is supplied from the central air compressor of the laboratory. In order to obtain a regular air source without fluctuations, there is a need to install an air storage cylinder and a pressure regulator between the air source and glass-tube flow meter. At the bottom of the box an air distributor is installed. The air distributor is embedded within a filtering layer, which has a total thickness of $8\ cm$. The glass-tube flow meter is connected to the air distributor in the plastic box from outside. The purpose of the air distributor is to distribute the inflowing air homogeneously in the filtering layer and to create an uniform air supply (uniform Neumann boundary) at the bottom of the porous media. The L-shaped pipe is $3\ cm$ in diameter, $25\ cm$ long in the horizontal direction and $14\ cm$ long in the vertical direction. One end of the L-shaped pipe, which is inside the porous medium, is closed and the whole pipe is covered with thin metal wire fabric to prevent sand getting into the pipe. The box is filled with sand and the L-shaped pipe is buried within the sand layer. The air-tight box is closed at the top leaving a $6\ cm$ space for the porous medium out flow (see Fig. 32). Air is first flowing from the source into the filtering layer at the bottom of the box. Then, it flows from the filtering layer into the main sand. Inflowing air has two ways out. Air can either

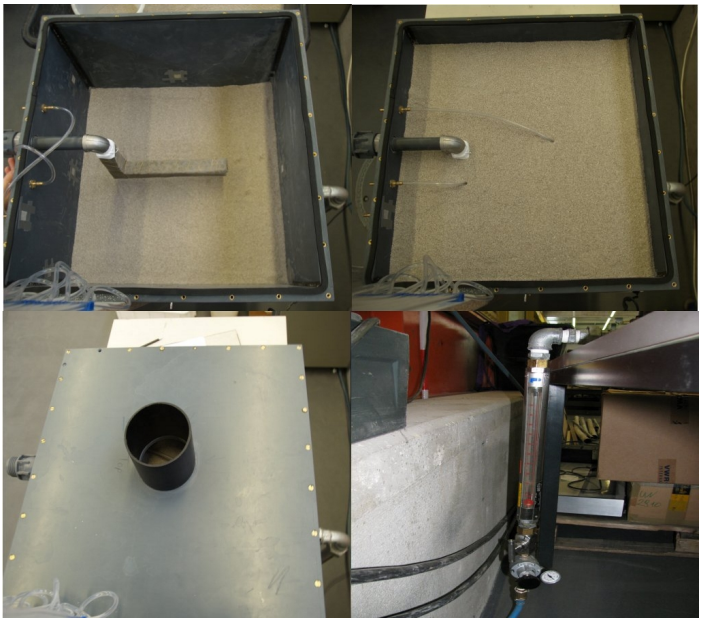

Figure 32: The setup of the experiment

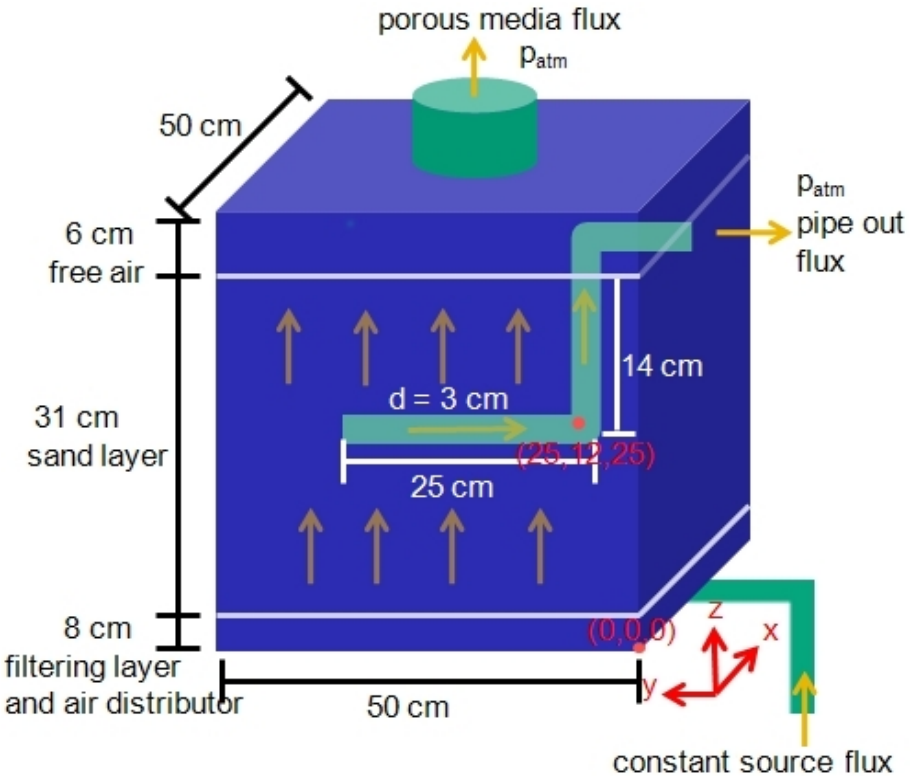

Figure 33: Physical dimensions of the experimental setup

flow through the porous medium out of the box or it can flow through the porous medium into the L-shaped pipe and then from the pipe out of the box (see Fig. 33).

The experiment is repeated for two different kinds of sand samples. The first setup contains coarse dorsilit sand. The second setup contains fine dorsilit sand. Inflowing air volume flux is measured with the help of the glass-tube flow meter and the pipe outflow velocity is measured via prandtl tube and an electronic pressure meter.

5.3 Results of the experiment and discussion

The experiment is repeated for two different kinds of setups. The first setup contains dorsilit sand with grain size varying from $0.6\,mm$ to $1.2\,mm$, whereas the sand in the second setup has a grain size from $0.1\ mm$ to $0.5\ mm$. The coarse sand has a porosity of 0.42 and a permeability of $2.57 \cdot 10^{-10} m^2$. The fine sand has a porosity of 0.44 and a permeability of $6.27 \cdot 10^{-11} m^2$ (see Tab. 10).

sand type	grain size $[mm]$	permeability $[m^2]$	porosity $[-]$
coarse dorsilit	0.6 - 1.2	$2.57 \cdot 10^{-10}$	0.42
fine dorsilit	0.1 - 0.5	$6.27 \cdot 10^{-11}$	0.44

Table 10: Properties of the sand types used in the experiment

The experiment is repeated for each setup at 7 different air sources. Fig. 34 shows the source and the pipe out volume fluxes for the fine and coarse sand setups. At each source the figure shows the corresponding pipe out flux of air, which is leaving the system through the L-shaped pipe. The rest of the air is leaving the system through the porous medium.

As the Fig. 34 shows there are two kinds of tendencies. The first one depends on the source flux, the second one depends on the sand permeability:

- The slope of the pipe out flux v.s. source flux curve is decreasing with increasing source fluxes; i.e. the share of the pipe out flux from the source flux is decreasing. Consequently, as the source flux is increasing, the air is preferentially flowing through the porous medium. This behavior can be explained by the vertical velocity components of flowing air. Corresponding to the increase in the source flux, the velocity component in vertical direction is increasing, which results in a reduction in the catchment zone of the pipe.
- As the permeability of the sand is decreasing, air is flowing preferentially through the L-shaped pipe. If one introduces more resistance against the flow in the porous medium by decreasing the permeability, air chooses to flow through the less resistance area, i.e. pipe.

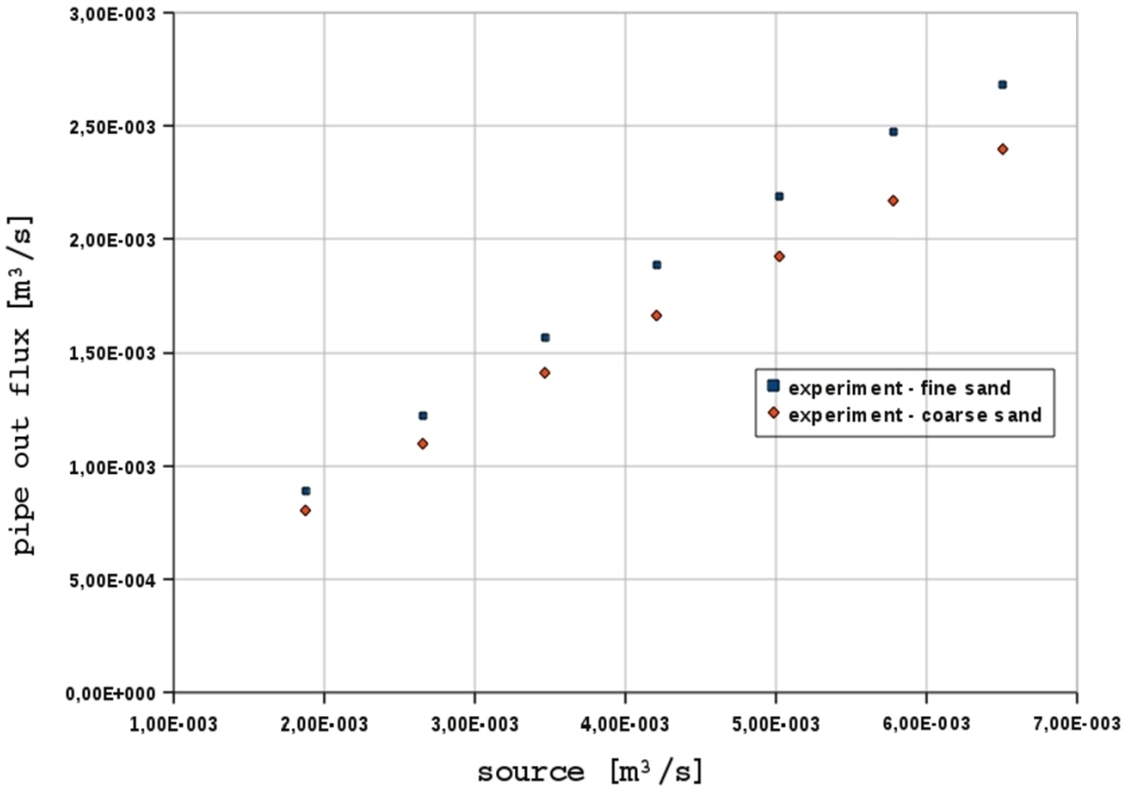

Figure 34: The pipe out fluxes v.s. the source fluxes of the fine and coarse sand setups

5.4 Numerical model

The experiment is modeled with the numerical model introduced in Section 4.2.5. The experiment is carried out at 7 different source terms for each sand type. The model needs the α_{ex} parameter which cannot be measured directly. The α_{ex} parameter mainly depends on the porous media properties, such as pore structure and grain size at the interface between the porous media and the pipe. The approach of determination of α_{ex} is as follows:

- α_{ex} parameter is fitted for one type of sand at a fixed source flux, which is the middle source flux.
- Then, the same α_{ex} parameter is used for the remaining 6 different source terms.
- Since pore structures and grain sizes are different for each sand type, the α_{ex} parameter fitted for one type of sand cannot be used for the other type.
- The same procedure is repeated for the other type of sand.

5.4.1 The parameters and the boundary conditions of the model setup

Tab. 11 and Tab. 12 show the parameters and the boundary conditions in the numerical model. The pipe has an outflow boundary and fixed atmospheric pressure at the top of the

box, and the closed end of the pipe in the box is a no flow boundary. The porous medium has a constant Neumann flux boundary at the bottom and a fixed Dirichlet pressure boundary at the top of the box. The sides of the box are Neumann no flow boundaries.

exchange term	$\propto_{ex}$ = 2.45*10^{-9} [m^2]	
	Porous media	Pipe
fluid parameters	air permeability = 6.27*10^{-11} [m^2] porosity = 0.44 [-]	air diameter = 3 [cm] ε / d = 4.0*10^{-2} [-]
initial condition	pressure = p_{atm} -	pressure = p_{atm} velocity ($\bar{u}_s$)= 0 [m/s]
boundary conditions top boundary closed end inside the box bottom boundary other boundaries	 Dirichlet - pressure = p_{atm} - - Neumann : fixed source flux Neumann : no flow	 Dirichlet - pressure = p_{atm} out flow boundary no flow ($\bar{u}_s$ = 0 [m/s]) - -

Table 11: The parameters and the boundary conditions of the numerical model for the fine sand setup

exchange term	$\propto_{ex}$ = 4.01*10^{-9} [m^2]	
	Porous media	Pipe
fluid parameters	air permeability = 2.57*10^{-10} [m^2] porosity = 0.42 [-]	air diameter = 3 [cm] ε / d = 4.0*10^{-2} [-]
initial condition	pressure = p_{atm} -	pressure = p_{atm} velocity ($\bar{u}_s$)= 0 [m/s]
boundary conditions top boundary closed end inside the box bottom boundary other boundaries	 Dirichlet - pressure = p_{atm} - - Neumann : fixed source flux Neumann : no flow	 Dirichlet - pressure = p_{atm} out flow boundary no flow ($\bar{u}_s$ = 0 [m/s]) - -

Table 12: The parameters and the boundary conditions of the numerical model for the coarse sand setup

For the fine sand experiment at a source flux of $4.21 \cdot 10^{-3}\ m^3/s$ the fitted α_{ex} parameter is $2.45 \cdot 10^{-9}\ m^2$. For the coarse sand experiment at the same source flux the fitted α_{ex} parameter is $4.01 \cdot 10^{-9}\ m^2$.

5.4.2 Comparison of the numerical results with the experimental results

In Fig. 35 the blue square dots show the experimental data and the red diamond dots show the model results. The first result of the experiment was that as the source flux is increasing, the air is preferentially flowing through the porous media. This effect can also be seen in the simulation results. That means the percentage share of the pipe out flow from the source flux is decreasing for increasing source fluxes. Fig. 36 shows the experimental data and model results for the coarse sand experiment. The percentage share drop of the pipe out flow for increasing source fluxes can also be seen in the coarse sand simulation results. If one compares the modeling results of the fine and coarse sand setups, one can easily see that in the fine sand setup more air is preferentially flowing through the L-shaped pipe than in the coarse sand setup. This also corresponds with the experimental results.

The exchange coefficient (α_{ex}) can be defined as a property of the porous medium. Therefore, α_{ex} should not depend on the value of the source flux or the pressure difference between the continua. The numerical simulations are repeated using the same α_{ex} coefficient at 7 different source fluxes, and the numerical results match closely with the experimental results (see Fig. 35 and Fig. 36). This implies that the α_{ex} coefficient does not depend on the value of the source flux.

Although the tendencies in the experimental results can be reproduced by the model, the measured data and modeling results don't overlap exactly. For increasing source fluxes the model underestimates and for decreasing source fluxes the model overestimates the experimental data. The possible reasons for that can be, for example, not accounting for the momentum transfer in the model or a systematic measurement error. As explained in Section 2.2.2, the coupling strategy doesn't include the momentum transfer between both continua, i.e. the slip boundary at the interface is neglected.

Although the model doesn't match the experimental data one to one, the model is successful in reproducing close results. That means, the dual-continuum modeling approach can be used for coupled porous-media pipe-flow systems and the difficulties lie mostly in the parameter determination.

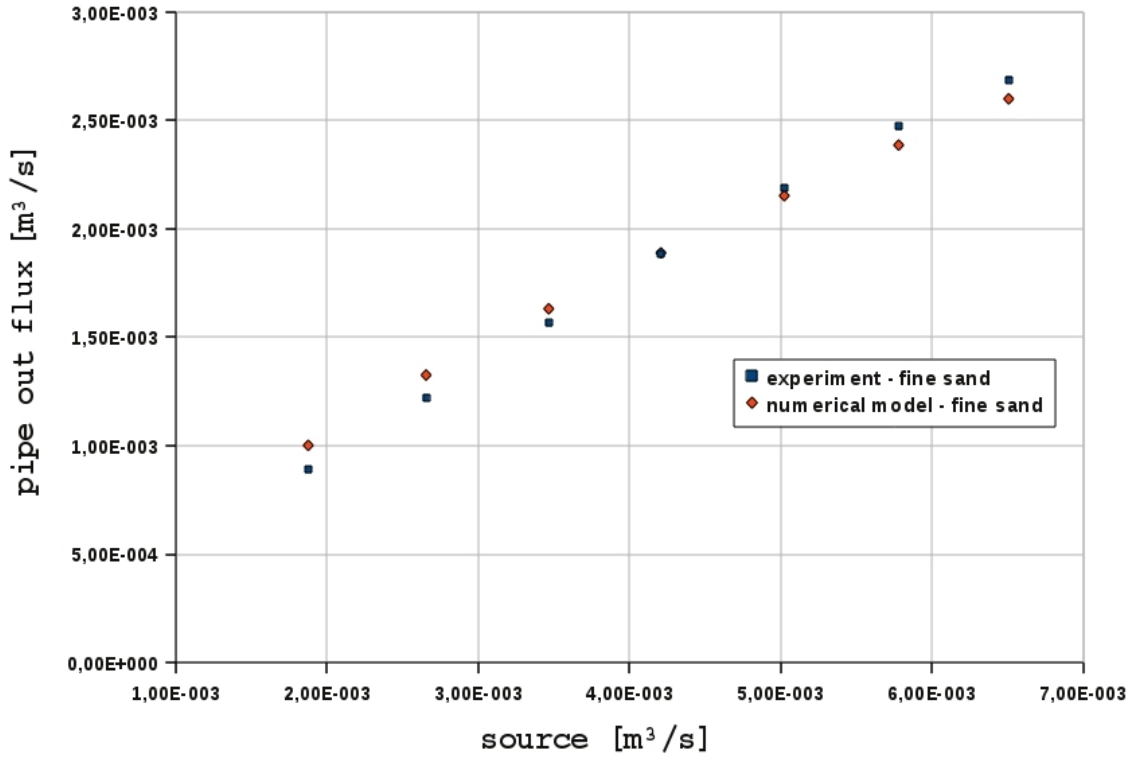

Figure 35: The pipe out fluxes v.s. the source fluxes of the fine sand setup

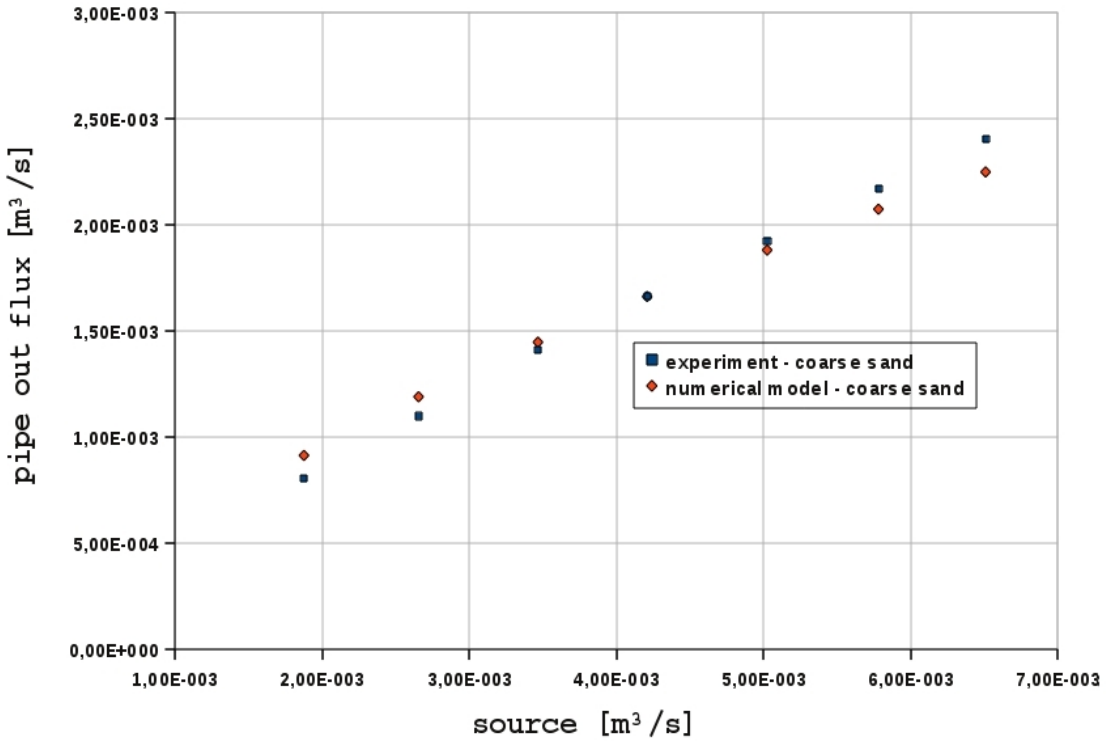

Figure 36: The pipe out fluxes v.s. the source fluxes of the coarse sand setup

6 Numerical models for coupled multi-phase flow and transport systems

6.1 Lower-dimensional dual-continuum models related to different problem cases

This section introduces a couple of numerical models for the simulation of coupled multi-phase flow and transport systems. In the porous media continuum multi-phase flow equations are solved, whereas the pipe flow is modeled as a single-phase multi-component system. First, each model is described mathematically by introducing the governing equations. Subsequently, the numerical models are tested by simulating a related problem case. The lower-dimensional dual-continuum coupling strategy accounts only for the mass transfers between both continua and requires source/sink mass exchange terms. As the coupled systems get more complex, new coupling terms need to be introduced in order to better express the total system. The chosen sequence of the example applications follows the order of increasing complexity of the applied model concepts.

6.1.1 Richards equation - Hagen Poiseuille coupling

The coupling of the Richards equation in the porous medium with the Hagen-Poiseuille equation in the pipe is implemented as an intermediate step towards considering multi-phase flow in the porous medium. This increase in complexity (compared to the previous model) enables us to show the influence of the capillary effects in the porous domain during the dual-continuum coupling. Such a flow system could become relevant, for example, in a macropore flow problem. Water can flow relatively fast in so-called macropore structures like root channels or wormholes, and there is an exchange of water between the macropores (the soil pipes) and the unsaturated zone (the porous medium), where capillary effects are important.

The unsaturated soil zone can be modeled with a two-phase flow model, where the fluid phases are water and air. The presence of gas in the soil causes some additional resistance to the water flow in the porous media. However, the dynamic viscosity of air is only about 2% of the dynamic viscosity of water, making the gas phase highly mobile. Therefore, a simplified approach to the two-phase flow problem could be the reduction of the multi-phase flow equation to the Richards problem (Richards (1931)), where the mobility of the

The Sections 6.1.1 and 6.1.2 in Chapter 6 are published in Dogan *et al.* (2009)

gas phase is assumed to be infinite. The Richards equation not only considers the water phase but also the capillary effects, where the pressure of the gas phase is set to a reference pressure ($p_{n_{ref}}$), which can be chosen freely. In some of the models $p_{n_{ref}}$ is set to null, which leads to negative water pressure in the unsaturated zone due to the capillary pressure effect. However, in the following formulation $p_{n_{ref}}$ is set to $1.0\ bar$:

$$\varrho\ \phi\ \frac{\partial S_w}{\partial p_c}\frac{\partial p_c}{\partial t} - \vec{\nabla}\cdot(\frac{k_{rw}}{\mu_w}\ \varrho_w\ \bar{\bar{K}}\ (\nabla p_w - \varrho_w\ \vec{g}))\ =\ q + \boxed{q_{ex}} \tag{122}$$

, where $p_w = p_{nref} - p_c$ and $p_{nref} = 1.0\ bar$.

The macropores are modeled with the Hagen-Poiseuille formulation (Eq. 89).

In addition to the single-phase flow coupling exchange terms, the mass exchange term here (Eq. 123) includes a mobility exchange term (λ_{ex}) to account for the relative permeability of water in the unsaturated zone :

$$\int q_{ex}\ dV\ =\ \varrho\ \lambda_{ex}\ \alpha_{ex}\frac{A_{outerface}}{d}\ (p_{pipe} - p_{w_{pm}}) \tag{123}$$

The mobility exchange term (λ_{ex}) is upwinded, i.e.

if $p_{pipe} < p_{pm}\ \Rightarrow\ \lambda_{ex} = \frac{k_{rw}}{\mu}$;

else $\Rightarrow\ \lambda_{ex} = \frac{1}{\mu}$

A test problem for coupling Richards equation with macropores

A numerical experiment is set up, where four unconnected macropores are embedded into a porous medium and the flowing fluid is water (see Fig. 37). Analogous to the previous examples, gravity is set to zero. The porous medium has the shape of a cube with sides $x = y = z = 1.2$ m. The macropores have a diameter of 1 cm. Tab. 13 shows the parameters and the boundary conditions used in the test problem. The porous medium is initially unsaturated and the macropores are full of water. The sides of the porous domain are unsaturated, whereas the top and the bottom boundaries are set to a no-flow condition. The macropores have a fixed pressure of 1.0 bar at the top and at the bottom boundaries (see Fig. 37). The permeability of the porous medium is $5.0 \cdot 10^{-10}$ m^2 and the exchange coefficient is chosen to be the same as the permeability.

In Fig. 38, the top figure shows the saturation distribution and the bottom figure shows the pressure distribution along the pipes. After 11 seconds, the saturation at the nodes of the porous medium, which have direct contact to the macropores, increases from 0 to 0.6 and water pressure in the unsaturated zone increases accordingly, whereas macropore pressure decreases. After 5 minutes, as the unsaturated zone fills with water, the capillary pressure in the porous media decreases, which results in an increase in water pressure (p_w) and the

common parameters	α_{ex} = 5.0*10-10 [m²]	temperature = 10 [°C]
	Porous media	Macropores
fluid parameters	water permeability = 5.0*10-10 [m²] porosity = 0.4 [-] linear $p_c - S_w$ relationship, $S_{wr} = 0$, $S_{nr} = 0$	water diameter = 1 [cm] - -
initial condition	p_w = 9.9000*10^4 [Pa] (S_w = 0 [-])	-
boundary conditions top boundary bottom boundary other boundaries	 Neumann : no flow Neumann : no flow Dirichlet - p_w = 9.9000*10^4 [Pa] (S_w = 0 [-])	 Dirichlet - pressure = 1.0*10^5 [Pa] Dirichlet - pressure = 1.0*10^5 [Pa] -

Table 13: The parameters and the boundary conditions for coupled Richards - macropore problem

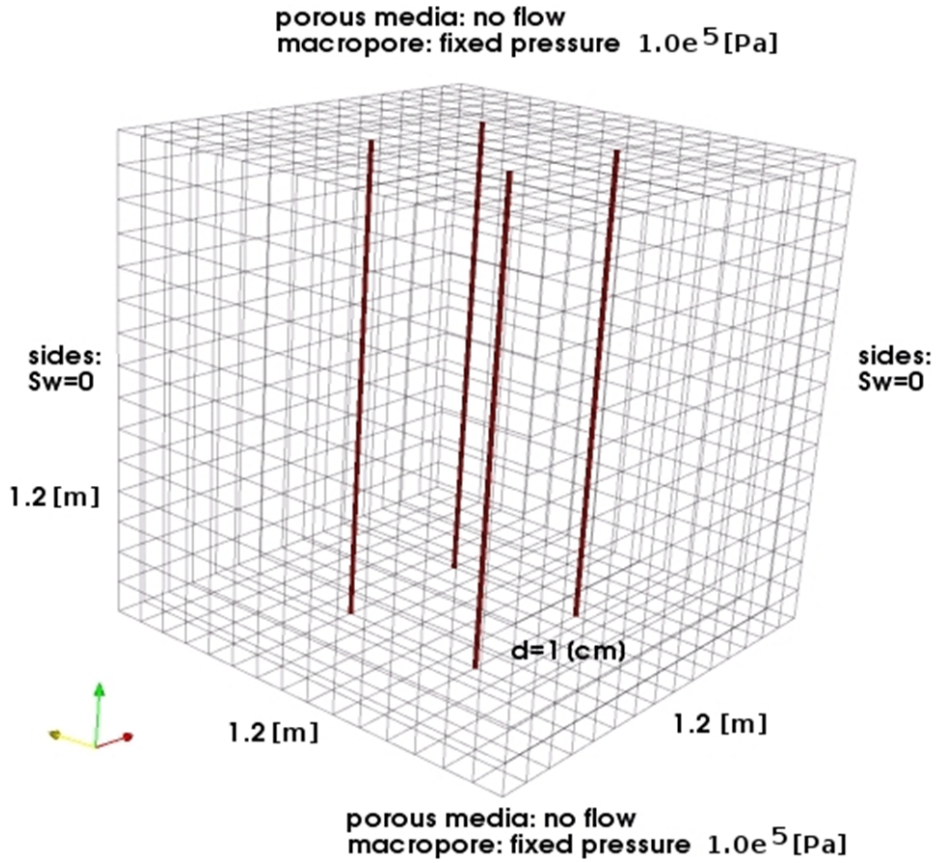

Figure 37: The coupled Richards - macropore problem

pressure difference between macropore and porous medium decreases as a consequence (see Fig. 39). Subsequently, this decrease results in a smaller pressure difference and accordingly a smaller mass transfer rate between the macropore and the unsaturated zone. This eventually shows that a variation in saturation results in a change in the capillary pressure,

which has a considerable influence on the mass exchange rate between the two continua.

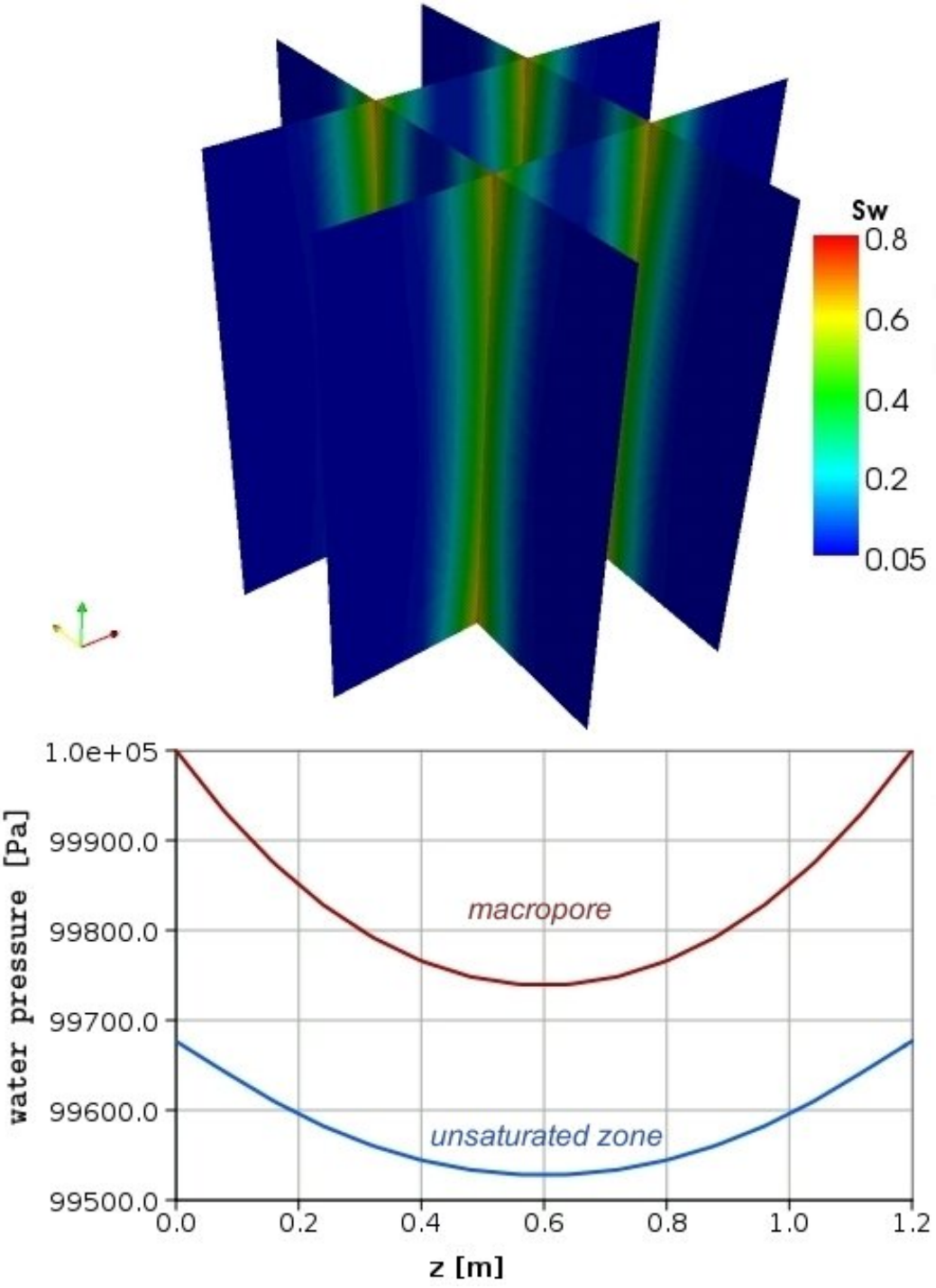

Figure 38: Saturation distribution and pressure distributions after t=11 seconds

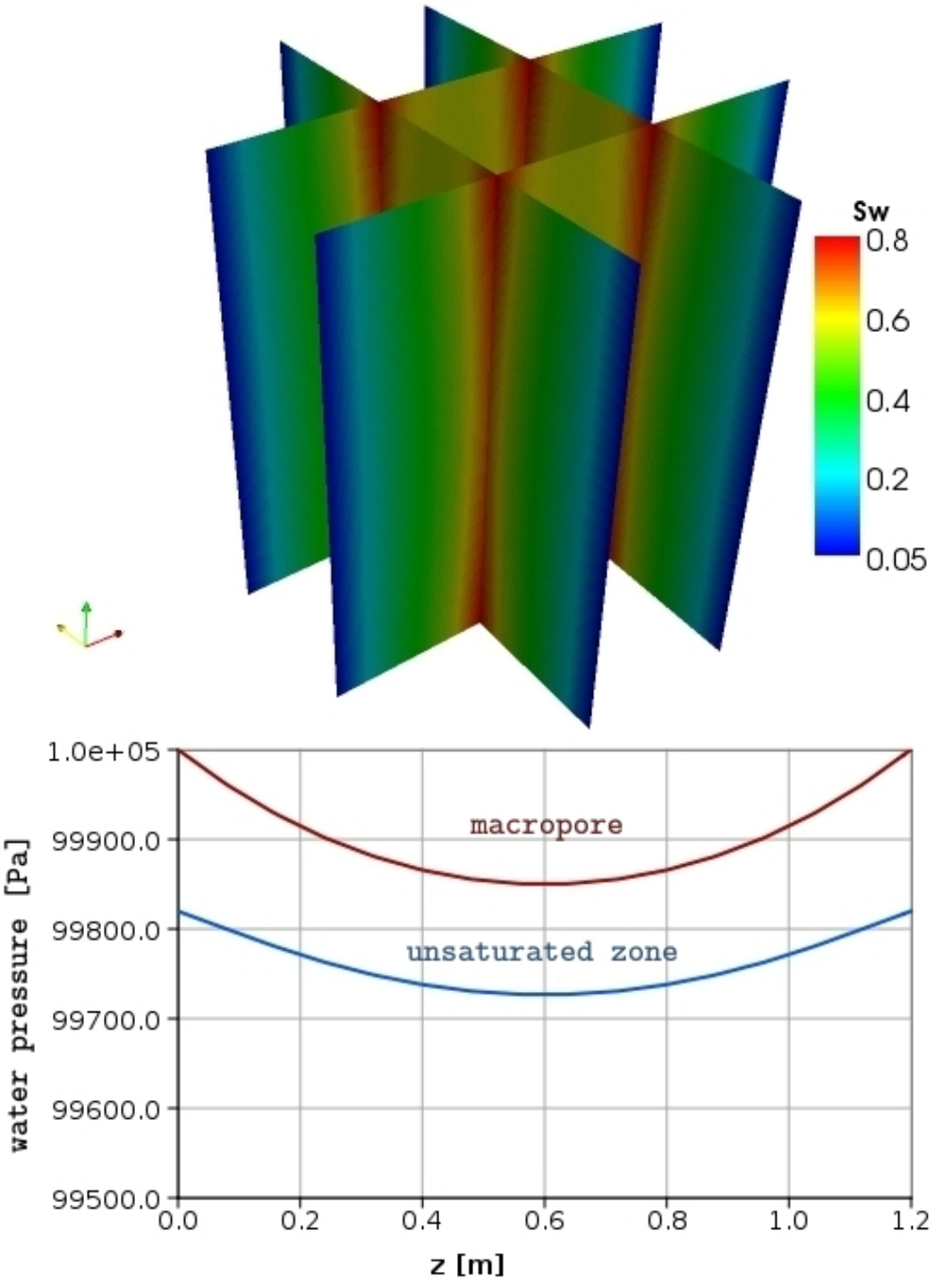

Figure 39: Saturation distribution and pressure distributions after t=5 minutes

6.1.2 Coupling of two-phase porous media flow with single-phase pipe flow

The example application presented in the following is motivated by gas migration in abandoned coal mines. The coal seams in the mines contain adsorbed methane gas. However, the methane desorbs from the coal seams as a result of the pressure decrease during and after the mining activity. Methane accumulates in the gas phase of the porous rock or soil and then migrates to the surface through the rocks, but also through the shafts and tunnels of the old mine. Methane emissions to the surface need to be controlled to ensure safe living conditions, since it is suffocative and explosive. If the coal mine is not flooded with groundwater, the surroundings of the tunnels and shafts are relatively dry. Given such a case, the methane migration problem could be modeled as a two-phase porous media flow coupled with a single-phase pipe flow. The main assumption in this model concept is that the mass transfer between the porous medium and the pipe flow only takes place via the gas phase and that the water phase is assumed to stay in the porous medium (see Fig. 40).

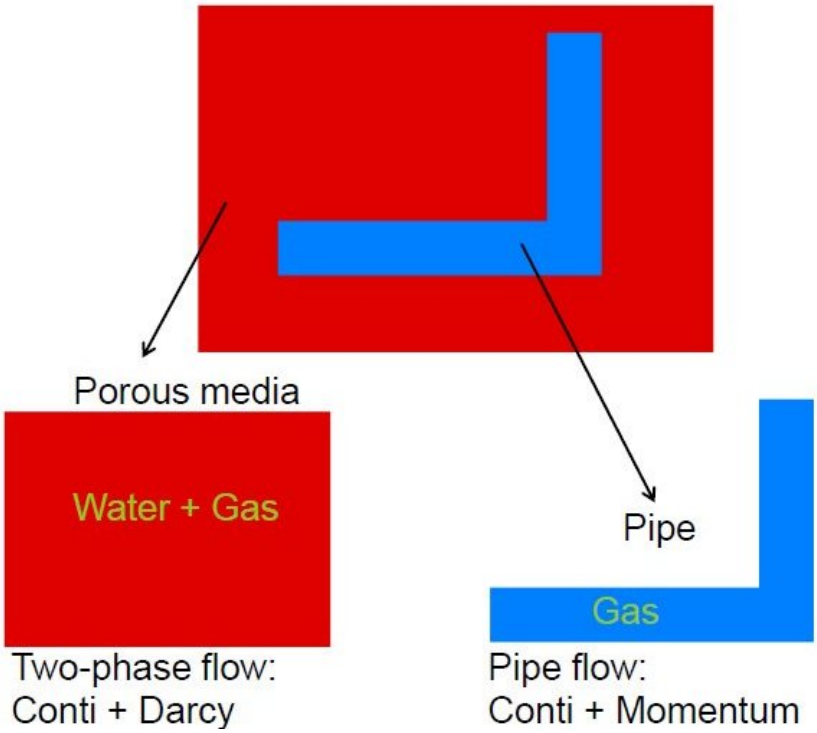

Figure 40: Dual-continuum coupling strategy for two-phase porous media flow - single-phase pipe flow system

The conservation equations of two-phase flow in porous media can be written for the gas phase (g) as in Eq. 124:

$$\frac{\partial(\phi S_g \varrho_g)}{\partial t} - \vec{\nabla} \cdot \left(\varrho_g \frac{k_{rg}}{\mu_g} \bar{\bar{K}} \cdot (\nabla p_g - \varrho_g \vec{g}) \right) = q_g + \boxed{q_{ex}} \tag{124}$$

and for the water phase (w) as in Eq. 125:

$$\frac{\partial(\phi S_w \varrho_w)}{\partial t} - \vec{\nabla} \cdot \left(\varrho_w \frac{k_{rw}}{\mu_w} \bar{\bar{K}} \cdot (\nabla p_w - \varrho_w \vec{g}) \right) = q_w \tag{125}$$

The conservation equations for the pipe flow are:

$$\frac{\partial \varrho}{\partial t} + \frac{\partial}{\partial s}(\varrho \, \bar{u}_s) = q - \boxed{q_{ex}} \tag{126}$$

$$\frac{\partial(\varrho \, \bar{u}_s)}{\partial t} + \frac{\partial(\varrho \, \bar{u}_s \, \bar{u}_s)}{\partial s} + \frac{\partial p}{\partial s} + \tau_w \frac{\pi d}{A} = \varrho \, \vec{g} \cdot \vec{s} \tag{127}$$

The exchange term includes a mobility term (λ_{ex}) to account for the relative permeability of gas in the unsaturated zone (Eq. 128).

Exchange term:

$$\int q_{ex} \, dV \; = \; \varrho_{ex} \, \lambda_{ex} \, \alpha_{ex} \frac{A_{outerface}}{d} \, (p_{pipe} - p_{g_{pm}}) \tag{128}$$

Density exchange (ϱ_{ex}) and mobility exchange (λ_{ex}) terms are upwinded, i.e.

if $p_{pipe} < p_{pm} \;\Rightarrow\; \varrho_{ex} = \varrho_{pm}, \; \lambda_{ex} = \frac{k_{rg}}{\mu}$;

else $\Rightarrow \; \varrho_{ex} = \varrho_{pipe}, \; \lambda_{ex} = \frac{1}{\mu}$

Two test problems for coupling two-phase porous medium flow with single-phase pipe flow:

Two numerical problems (setup A and setup B) are simulated to see the effects of the mobility-dependent exchange term on the coupled two-phase porous medium flow (water and air) - single-phase pipe flow (air) problem (Fig. 41). The same geometric setup as in the single-pipe examples is used. Tab. 14 shows the parameters and the boundary conditions used in the test problem. The pipe has a no-flow boundary condition at the left boundary and a fixed pressure of 1.0 bar at the right boundary. The exchange coefficient is chosen to be $1.2 \cdot 10^{-11}$ m^2. In both setups the porous medium is initially unsaturated and at the right boundary, the saturation of the water phase S_w is set to 0, while the pressure of the gas phase is fixed at 1.0 bar. In setup A, the saturation of the water phase S_w is set to 0 at the left boundary of the porous medium, and the pressure of the gas phase is fixed at 1.004 bar. In setup B, the saturation of the water phase S_w is set to 0.9 at the left boundary of the porous medium. This means that in setup B the porous medium is flooded, i.e. it is a two-phase system, while in setup A the porous medium remains dry and the model should behave like a single-phase system.

Because the boundary conditions, the geometry, and the flowing fluid (air) in setup A are the same as in the problem setup described in the upper part of Fig. 31, the two problems are comparable to each other. The pressure distributions in the lower left part of Fig. 31 and

common parameters	α_{ex} = 1.2*10-11 [m²]	temperature = 10 [°C]
	Porous media	Pipe
fluid parameters	water, air permeability = 5.0*10-10 [m²] porosity = 0.4 [-] linear $p_c - S_w$ relationship, S_{wr} = 0, S_{gr} = 0	air diameter = 2 [cm] ε / d = 1/90 [-] -
initial condition	S_w = 0 [-], p_g = 1.0*10^5 [Pa]	pressure = 1.0*10^5 [Pa], $\bar{u}_s$ = 0 [m/s]
boundary conditions left boundary right boundary other boundaries	 Dirichlet - p_g = 1.004*10^5 [Pa] Dirichlet - S_w = setup A) 0.0 [-]; setup B) 0.9 [-] Dirichlet - p_g = 1.0*10^5 [Pa] Dirichlet - S_w = 0 [-] Neumann : no flow	 no flow ($\bar{u}_s$ = 0 [m/s]) - Dirichlet - pressure = 1.0*10^5 [Pa] out flow boundary -

Table 14: The parameters and the boundary conditions for coupled two-phase porous medium flow - single-phase pipe flow problems (setup A and setup B)

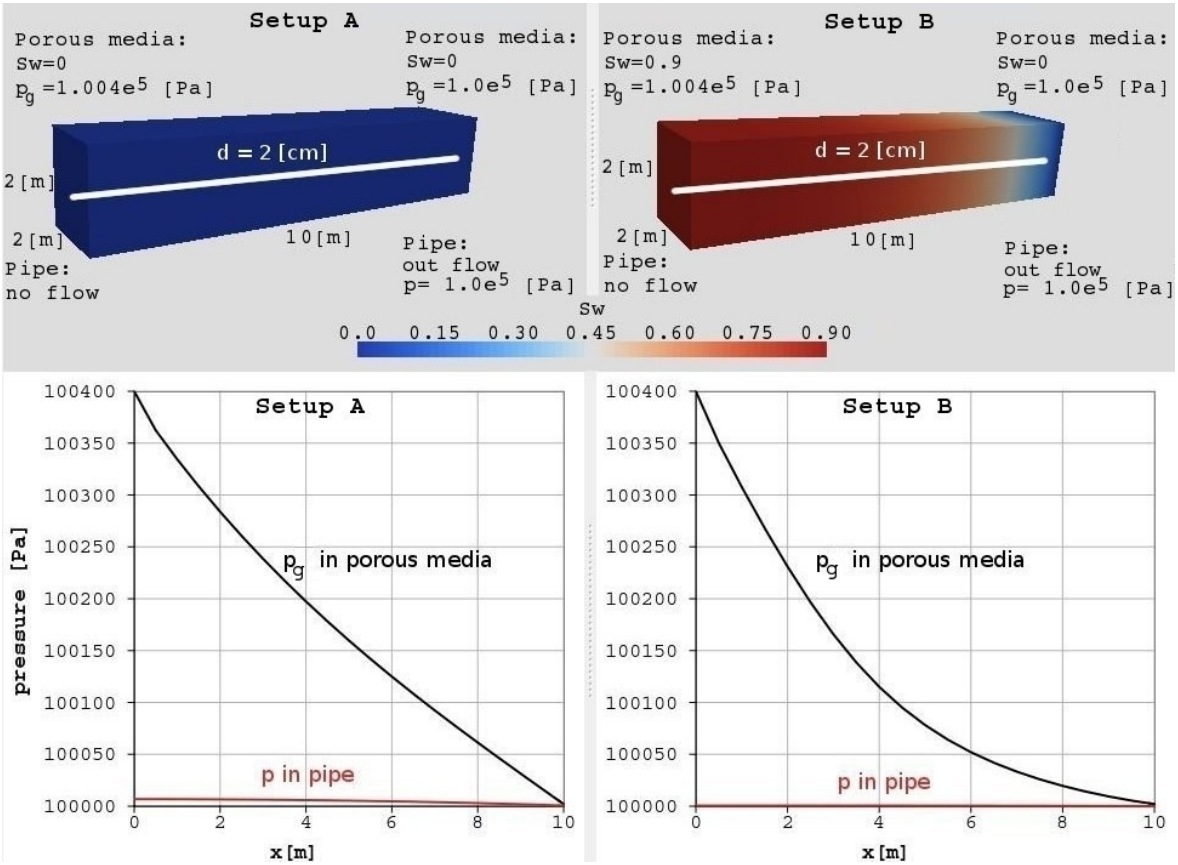

Figure 41: The coupled two-phase porous medium flow - single-phase pipe flow problem

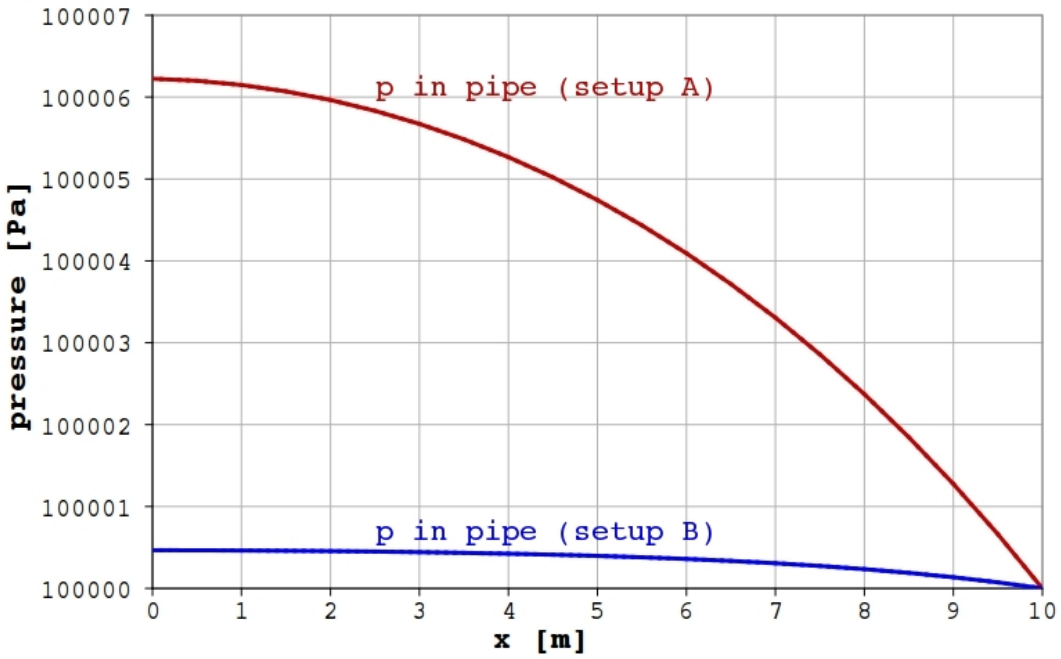

Figure 42: Comparison of the pipe pressure distributions along the pipe line for the setups A and B

in the lower left part of Fig. 41 are the same. The pipe pressures in setup A (upper curve in Fig. 42) and in the lower right part of Fig. 31 match. This comparison clearly shows that, as of course was expected, setup A behaves exactly like a single phase system.

In setup B, the porous medium is flooded with water due to the left boundary condition ($S_w = 0.9$). If the steady state pressure distributions along the pipe line for both setups are compared to each other, it can be clearly recognized that the pressure difference between both continua is lower in setup B than in setup A, which is a clear hint that less gas is flowing into the pipe when the domain is flooded with water (Fig. 42). The model is capable of representing this effect mainly due to the mobility exchange term ($\lambda_{ex} = k_{rgporous}/\mu$). In setup A, the relative permeability of the gas phase in the porous medium is 1.0. On the other hand, the relative permeability of the gas phase in setup B is only around 0.1. Therefore, at the steady state the mobility exchange term in setup A is approximately 10 times larger than in setup B.

6.1.3 Coupling of two-phase two-component porous media flow with one-phase two-component pipe flow

Until now the focus has been on the systems where the transport phenomenon is not decisive or negligible, i.e. the macropore flow problem and the methane migration problem, but for flow and transport dominant systems like fuel-cells, there are both water and gas transfers between the free flow and porous medium, i.e. it is not enough to describe the pipe flow only with one component. For such systems, there is a need to extend the dual-continuum coupling concept so that the resulting model should not only take into account

the transport of the components within each continuum (porous media, free flow), but also the mass transfers of each component between the continua.

In order to understand the effect of the transport processes in the dual-continuum coupling concept a hypothetical system is chosen, where pipe flow is described as a one-phase (gas) two-component (water vapor, air) system, and the porous medium is described as a two-phase (gas, water) two-component (water, air) system. Eq. 129 and Eq. 130 describe a multi-phase flow system in porous media with the exchange terms q^a_{ex} and q^w_{ex} respectively, where a stands for the air component and w stands for the water component. The pipe flow is described as a compressible one-phase (gas) two-component (water vapor , air) system. Equations 131, 132 and 133 describe a one-phase two-component pipe flow model. Eq. 131 is the total mass balance equation with the exchange terms (q^a_{ex} and q^w_{ex}). The total momentum balance is described by Eq. 133, and Eq. 132 describes the transport of the water vapor component along the pipe.

To close the pipe-flow system, 3 conditions are needed (see Eq. 136):

- The sum of all mass fractions for each component should be 1.
- The wall friction is described by Darcy-Weisbach approach.
- The ideal gas law relates the gas density to the gas pressure.

Air component in porous media:

$$\begin{aligned}
&\phi \frac{\partial(\varrho_g x^a_g S_g + \varrho_w x^a_w S_w)}{\partial t} \\
&-\vec{\nabla} \cdot \left[\varrho_g x^a_g \frac{k_{rg}}{\mu_g} \bar{\bar{K}} \cdot (\nabla p_g - \varrho_g \vec{g}) + \varrho_w x^a_w \frac{k_{rw}}{\mu_w} \bar{\bar{K}} \cdot (\nabla p_w - \varrho_w \vec{g}) \right] \\
&-\vec{\nabla} \cdot \left[D^a_g \nabla(\varrho_g x^a_g) + D^a_w \nabla(\varrho_w x^a_w) \right] = q^a_g + \boxed{q^a_{ex}}
\end{aligned} \tag{129}$$

Water component in porous media:

$$\begin{aligned}
&\phi \frac{\partial(\varrho_g x^w_g S_g + \varrho_w x^w_w S_w)}{\partial t} \\
&-\vec{\nabla} \cdot \left[\varrho_g x^w_g \frac{k_{rg}}{\mu_g} \bar{\bar{K}} \cdot (\nabla p_g - \varrho_g \vec{g}) + \varrho_w x^w_w \frac{k_{rw}}{\mu_w} \bar{\bar{K}} \cdot (\nabla p_w - \varrho_w \vec{g}) \right] \\
&-\vec{\nabla} \cdot \left[D^w_g \nabla(\varrho_g x^w_g) + D^w_w \nabla(\varrho_w x^w_w) \right] = q^w_g + \boxed{q^w_{ex}}
\end{aligned} \tag{130}$$

Pipe flow:

$$\frac{\partial \varrho_g}{\partial t} + \frac{\partial}{\partial s}(\varrho_g \, \bar{u}_{gs}) = q^a + q^w - \boxed{q^a_{ex}} - \boxed{q^w_{ex}} \tag{131}$$

$$\frac{\partial \varrho_g x_g^w}{\partial t} + \frac{\partial}{\partial s}(\varrho_g\, x_g^w \bar{u}_{gs}) - \frac{\partial}{\partial s}(D_g^w \frac{\partial(\varrho_g x_g^w)}{\partial s}) = q^w - \boxed{q_{ex}^w} \tag{132}$$

$$\frac{\partial(\varrho_g\, \bar{u}_{gs})}{\partial t} + \frac{\partial(\varrho_g\, \bar{u}_{gs}\, \bar{u}_{gs})}{\partial s} + \frac{\partial p_g}{\partial s} + \tau_w \frac{\pi d}{A} = \varrho_g\, \vec{g} \cdot \vec{s} \tag{133}$$

Exchange terms:

It is assumed that mass exchange only takes place between the gas phases of the two continua. Two mass exchange terms are necessary, because there are two components which can be transferred between the gas phases of the porous medium and the pipe. The exchange terms include gas-phase pressure differences between the continua. They both include the same α_{ex}, because α_{ex} depends on the porous media properties. The exchange terms are described with Eq. 134 and Eq. 135 for the air and water components respectively.

$$\int q_{ex}^a\, dV \;=\; \varrho_{g_{ex}}\, x_{g_{ex}}^a \lambda_{ex}\, \alpha_{ex} \frac{A_{outerface}}{d}\, (p_{g_{pipe}} - p_{g_{pm}}) \tag{134}$$

$$\int q_{ex}^w\, dV \;=\; \varrho_{g_{ex}}\, x_{g\ ex}^w \lambda_{ex}\, \alpha_{ex} \frac{A_{outerface}}{d}\, (p_{g_{pipe}} - p_{g_{pm}}) \tag{135}$$

Mobility exchange (λ_{ex}), density exchange ($\varrho_{g_{ex}}$) and concentration exchange ($x_g^{a,w}{}_{ex}$) terms are upwinded, i.e.

if $p_{g_{pipe}} < p_{g_{pm}} \Rightarrow \varrho_{g_{ex}} = \varrho_{g_{pm}},\ x_g^{a,w}{}_{ex} = x_g^{a,w}{}_{pm},\ \lambda_{ex} = \frac{kr_g}{\mu}$;

else $\Rightarrow \varrho_{g_{ex}} = \varrho_{g_{pipe}},\ x_g^{a,w}{}_{ex} = x_g^{a,w}{}_{pipe},\ \lambda_{ex} = \frac{1}{\mu}$

Closing relations for the pipe flow system:

$$x_g^a + x_g^w = 1, \quad \tau_w \;=\; \frac{\zeta}{8}\, \varrho_g\, \bar{u}_{gs}^2, \quad \varrho_g \;=\; \frac{p_g}{R_{ind}\, T} \tag{136}$$

A test problem for coupling two-phase - two-component porous medium flow with single-phase two component pipe flow:

A test problem is setup, where a pipe is embedded into the porous medium. Analogous to the previous examples gravity is neglected. The porous medium has a rectangular prism shape with $x = 10$ m, $y = 2$ m and $z = 2$ m. The pipe has a diameter of 5 cm. Tab. 15 shows the parameters and the boundary conditions used in the test problem. The sides of the porous domain and the left boundary are no flow Neumann boundaries, whereas at the right boundary the pressure is fixed to 1.001 bar and the water saturation is fixed to 0.5. Initial conditions are identical to the right boundary conditions. The pipe has a no flow boundary on the left side of the domain, and an out flow boundary and a fixed pressure of 1.0 bar on the right side of the domain. The concentration of air (X_{ag}) at the right boundary

of the pipe is fixed to 0.1 kg/kg and initially X_{ag} is set to 0.1 kg/kg along the pipe. The permeability of the porous medium is $5.0 \cdot 10^{-10}$ m^2 and the exchange coefficient is chosen as $5.0 \cdot 10^{-11}$ m^2. The boundary conditions and the geometry of the system are shown in the upper part of Fig. 43.

common parameters	α_{ex} = 5.0*10-11 [m²]	temperature = 10 [°C]
	Porous media	Pipe
fluid parameters	water, air permeability = 5.0*10-10 [m²] porosity = 0.4 [-] linear $p_c - S_w$ relationship, $S_{wr} = 0$, $S_{gr} = 0$	water vapor, air diameter = 5 [cm] ε / d = 1/90 [-] -
initial condition	S_w = 0 [-] p_g = 1.00100*10^5 [Pa]	p = 1.0*10^5 [Pa], $\bar{u}_s$ = 0 [m/s] X_{ag} = 0.1 [kg/kg]
boundary conditions		
left boundary	Neumann : no flow Neumann : no flow	no flow ($\bar{u}_s$ = 0 [m/s]) -
right boundary	Dirichlet - p_g = 1.00100*10^5 [Pa] Dirichlet - S_w = 0.5 [-] -	Dirichlet - pressure = 1.0*10^5 [Pa] out flow boundary Dirichlet - X_{ag} = 0.1 [kg/kg]
other boundaries	Neumann : no flow	-

Table 15: The parameters and the boundary conditions for the coupled two-phase two-component porous medium - single-phase two-component pipe flow and transport problem

Initially, the concentration of air in the gas phase of the porous medium is around 0.99 kg/kg, whereas the concentration of air in the pipe is 0.1 kg/kg.

The middle left part of Fig. 43 shows the pressure distribution of the gas phases in both continua along the x-axis at an intermediate time. Since the mass transfer direction is solely determined by the gas-phase pressure difference, it can be clearly seen that the mass transfer direction is from the porous medium to the pipe continuum. The gas-phase pressure difference not only determines the direction, but also the amount of the mass transfer. However, this amount is scaled with the concentration of the related component as described with $x^a_{g\,ex}$ and $x^w_{g\,ex}$ in Eq. 134 and Eq. 135 respectively.

Although both air and water vapor is flowing from the porous medium to the pipe, more air is entering the pipe than water vapor. This can simply be explained by the higher concentrations of air in the porous medium continuum. After 8 seconds, the concentration of air in the pipe increases from 0.1 kg/kg to 0.6 kg/kg (see the middle right part of Fig. 43). At the steady state, there is a decrease in the gas-phase pressure difference between the continua. The concentration of air in the pipe has reached its maximum 0.988 kg/kg (see the lower right part of the Fig. 43).

This test example shows how significant the concentration of the components in each continua are for the compositional ratio of the exchanged mass. The coupled two-phase two-component porous medium - single-phase two-component pipe flow and transport model

is able to model complicated transport systems by accounting not only for the mobility exchange term but also for the concentrations of the exchanged components between the continua.

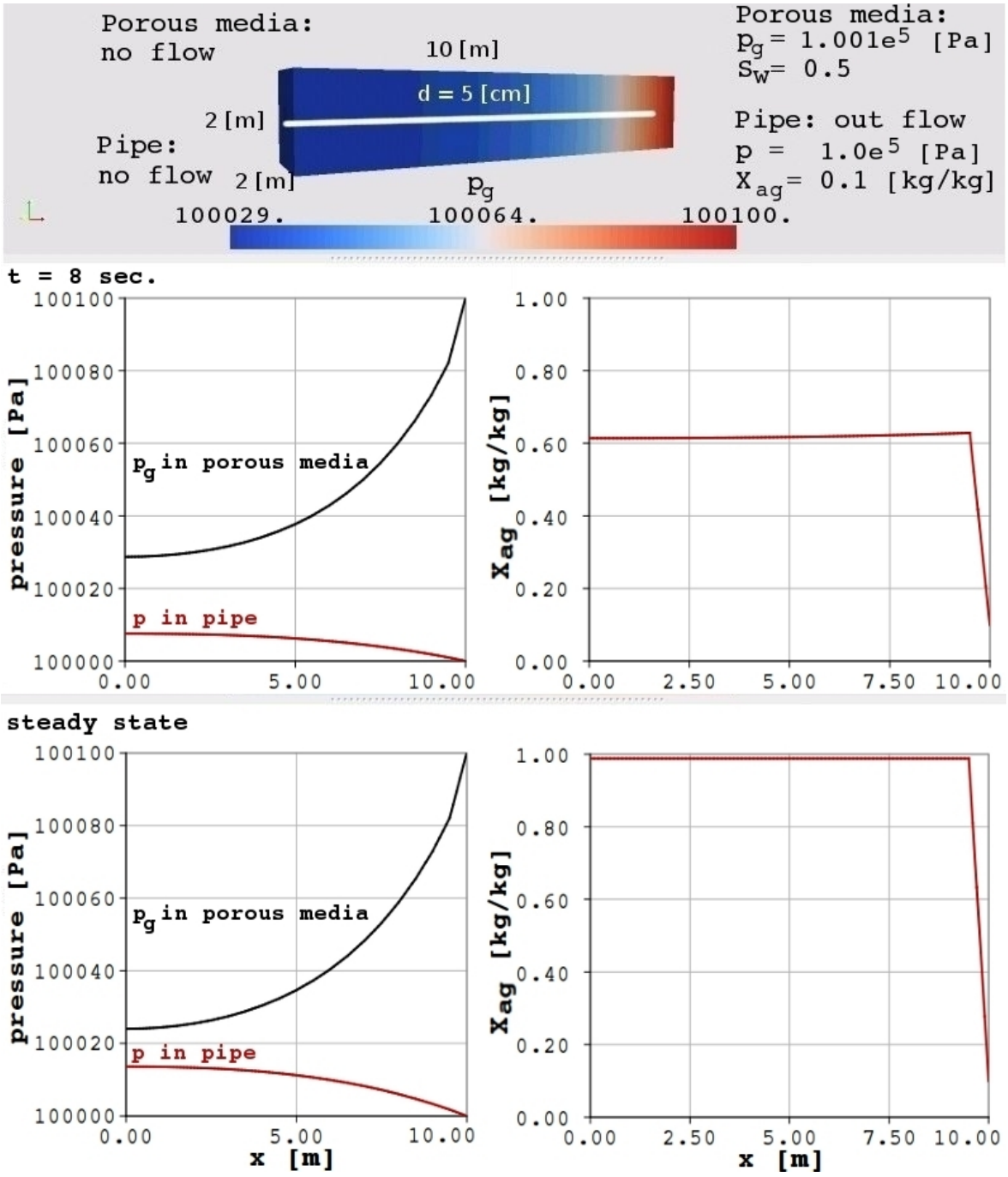

Figure 43: The coupled two-phase two-component porous medium - single-phase two-component pipe flow and transport problem

7 Final Remarks

7.1 Summary and Conclusion

Many flow problems in environmental, technical and biological systems are characterized by a distinct interaction between a flow region in porous media and a free flow region in quasi-one-dimensional hollow structures, such as abandoned coal mines, landslides, polymer electrolyte membrane fuel cells and cancer therapy. The objective of this study consists in the development of different model concepts for the interaction of multi-phase flow processes in porous media with single-phase free flow in quasi-one-dimensional structures, which can form a basis for further studies to model such complex systems. This is achieved on the basis of a lower-dimensional dual-continuum coupling approach, where the interaction between the two continua is restricted to mass transfers only. The flow velocity along the pipe network is cross-sectionally averaged, i.e. there is no finite velocity gradient perpendicular to the pipe direction which would be required in order to implement coupling approaches as, for example, suggested by Beavers and Joseph (1967). Although the dual-continuum coupling strategy is easy to implement, it reveals difficulties in the determination of the exchange coefficient (α_{ex}).

For the numerical modeling of coupled systems a special grid implementation is necessary, which is capable of representing one-dimensional network structures in a three-dimensional grid. Therefore, in the frame work of this study a special grid called 1D network grid in a 3D domain is developed.

A series of coupled numerical models are implemented, while the complexity of each model and the related coupling terms are gradually increased , which eventually helps in understanding the newly introduced coupling terms.

In the beginning, coupled single-phase systems are investigated. First, a simple model is implemented which is capable of modeling steady state coupled single-phase porous media flow with (also single-phase) Hagen-Poiseuille flow. This model could show that the mutual influence of the coupled flow systems on the pressure distributions in both domains can be clearly represented with the lower-dimensional dual-continuum coupling strategy. Before implementing more complex models, a grid convergence test is conducted for different grid sizes, to determine the grid dependence of the solution. In discrete fracture models the pressure gradient around the fractures highly depends on the grid refinement, whereas in dual-continuum models the grid spacing has minimal effect on the steady state pressure gradient between the two continua, since in lower dimensional dual-continuum models the virtual exchange distance is fixed with the diameter of the pipe. Then, the model complexity is increased by introducing compressible flow with time dependent storage terms in both

continua. This model is capable of modeling gas (air in this case) flow in both continua, where the coupling terms are nothing else than the exchange terms in the coupled Hagen-Poiseuille flow model with the exception of the pressure dependent density exchange term (ϱ_{ex}).

At this stage, the validation of the coupling strategy for single-phase flow coupling is necessary , before developing numerical models for more complex multi-phase systems. For this reason, an experiment is carried out to observe the mass balance of air for a coupled air flow system. The experiment consists of an airtight box filled with sand and a perforated L-shaped pipe was installed in the middle of the porous medium. Constant air source feeds the box from the bottom boundary of the box and air can either flow through the porous medium out of the box or it can flow through the porous medium into the L-shaped pipe and then out. In the second case, air flow in the porous medium is coupled with the pipe flow. The experiment is conducted for two different types of sand and seven different source flux terms. The comparison of the experimental data with the results of the numerical model is a close match, which reveals that the model is capable of reproducing the effects of the changes in the sand permeabilities and the variations in the source flux. This shows that the dual-continuum modeling approach can be used for the coupled porous media - pipe flow systems and the difficulties lie mostly in the parameter determination.

Then, the coupling of the Richards equation in the porous medium with the Hagen-Poiseuille equation in the pipe is implemented as an intermediate step towards considering multi-phase flow in the porous medium. Such a flow system could become relevant, for example, in a macropore flow problem, where water can flow relatively fast in so-called macropore structures like root channels or wormholes, and there is an exchange of water between the macropores (the pipes) and the unsaturated zone (the porous medium). The results of the model indicate that the capillary forces in the unsaturated zone play a decisive role in the determination of the mass exchange rate.

In the next step, the model complexity is increased by introducing a coupled two-phase porous-medium flow with the single-phase pipe flow model. Similar systems can be found in abandoned coal mines, where methane gas desorbs from coal seams and migrates to the surface through the shafts and tunnels of the old mine. If the coal mine is not flooded with groundwater, the surroundings of the tunnels and shafts are relatively dry. In such a case, the methane migration problem could be modeled as a two-phase porous media flow coupled with a single-phase pipe flow. The results of the model reveals that the mobility exchange term (λ_{ex}) is a key term in the model, since it significantly affects the mass exchange rate between the two continua.

Flow and transport systems as in fuel cells or cancer therapy need to be modeled with more complex models, since the transport of the components, for example oxygen or the therapeutic agent respectively, in both media is significant. Therefore, the last step in this study is the inclusion of the transport processes by introducing coupled two-phase two-component porous media flow with single-phase two-component pipe flow model. From the coupling perspective, the difference between this model and the previous model lies in the number of exchange terms (for each component a separate exchange term is necessary). The mass exchange term includes a concentration exchange term, which scales the total exchanged mass

with respect to the concentrations of the exchanged components between the continua. The direction of the exchanged mass between the continua is determined by the total gas phase pressure differences not by the partial pressures differences of the components. The results of the model show that the concentrations of the components in each continua play an important role for the compositional ratio of the exchanged mass.

The implemented numerical models and presented examples are kept as simple as possible to show the basic features and characteristics of the model concepts that address the processes of different complexity.

7.2 Outlook

This study focused on the development of different model concepts for the interaction of multi-phase flow processes in porous media with single-phase free flow in quasi-one-dimensional structures, which can eventually form a basis for further studies to model such complex systems. The numerical models presented do not comprise one to one implementation for the physical problems mentioned in the beginning. That means, there is still much room for further research, which is highlighted in the following:

- The macropore model can be further developed for modeling landslides by coupling the current model with a soil deformation model, which can eventually model the triggering effects of macropores on landslides.
- The coupled two-phase porous media flow with single-phase pipe flow model can be further developed for the methane migration problem by implementing isotherms (e.g. Langmuir isotherm) for describing adsorption and desorption of methane from coal seams.
- The coupled two-phase two-component porous media flow with one-phase two-component pipe flow model can be further developed for fuel cell systems by implementing the reaction kinetics at the anode and cathode of the fuel cell.
- For modeling more complex geometries, the current 1D pipe-network grid in a 3D porous grid needs to be further developed for unstructured grid implementations, and for large scale simulations both the models and the 1D pipe-network grid need to be modified for parallel computations.
- In this study, the flow and transport in the pipe flow continuum is considered as single-phase flow. For a better description of coupled multi-phase flow systems, new concepts need to be developed to describe quasi-one-dimensional multi-phase flow in pipes. This can be possibly achieved on the basis of modified open channel flow equations.
- In dual-continuum coupling strategy the decisive part is the determination of the lumped exchange coefficient (α_{EX}). Generally, the α_{EX} coefficient is determined for

each specific problem case. However, in this work the mass exchange term is described more explicitly by isolating the fluid properties, the pipe geometry and the porous media properties (α_{ex}), as it is described in Eq. 116. In this case, α_{ex} depends only on the porous media properties and should be determined for different porous materials in further experimental studies, which could not only ease the effort of the parameter determination for each specific case but also reduce the uncertainties in parameter estimations for lower-dimensional dual-continuum models.

- In this study, lower-dimensional dual-continuum coupling strategy accounts only for the mass transfer between the continua. One could add another exchange term for the momentum transfer, which can account for the slip boundary condition at the interface. However, for the one-dimensional pipe flow model the determination of the momentum exchange rate would require an averaging technique, which will eventually introduce new terms to the pipe flow model. If the theoretical work can be accomplished, the effect of the slip boundary at the interface can also be introduced into the coupled model.

Bibliography

Acosta, M., Merten, C., Eigenberger, G., Class, H., Helmig, R., Thoben, B., and Müller-Steinhagen, H. (2006). Modeling non-isothermal two-phase multicomponent flow in the cathode of PEM fuel cells. *Journal of Power Sources*, **159**(2), 1123–1141.

Assteerawatt, A. (2008). *Flow and transport modelling of fractured aquifers based on a geostatistical approach*. Dissertation, Mitteilungen / Institut für Wasserbau, Universität Stuttgart ; 176.

Barenblatt, G. I., Zheltov, I. P., and Kochina, I. N. (1960). Basic concepts in the theory of seepage of homogeneous liquids in fissured rocks [strata]. *Journal of Applied Mathematics and Mechanics*, **24**(5), 1286–1303.

Barnard, A. C. L., Hunt, W. A., Timlake, W. P., and Varley, E. (1966). A theory of fluid flow in compliant tubes. *Biophysical Journal*, **6**(6), 717–724.

Bastian, P. and Helmig, R. (1999). Efficient fully-coupled solution techniques for two-phase flow in porous media: Parallel multigrid solution and large scale computations. *Advances in Water Resources*, **23**(3), 199–216.

Bastian, P., Blatt, M., Engwer, C., Dedner, A., Klöfkorn, R., Kuttanikkad, S. P., Ohlberger, M., and Sander, O. (2006). The distributed and unified numerics environment (DUNE). In *Proc. of 19th Symposium on Simulation Technique in Hannover*.

Basu, A. J. and Khalili, A. (1999). Computation of flow through a fluid-sediment interface in a benthic chamber. *Physics of Fluids*, **11**(6), 1395.

Bauer, S. (2003). Modeling of karst aquifer genesis: Influence of exchange flow. *Water Resources Research*, **39**(10).

Bear, J. (1988). *Dynamics of fluids in porous media*. Courier Dover Publications.

Bear, J., Tsang, C., and Marsily, G. D. (1993). *Flow and Contaminant Transport in Fractured Rock*. Academic Press, San Diego, CA (United States).

Beavers, G. S. and Joseph, D. D. (1967). Boundary conditions at a naturally permeable wall. *Journal of Fluid Mechanics Digital Archive*, **30**(01), 197–207.

Beavers, G. S., Sparrow, E. M., and Magnuson, R. A. (1970). Experiments on coupled parallel flows in a channel and a bounding porous medium. *Journal of Basic Engineering*, **92**, 843–848.

Bibby, R. (1981). Mass transport of solutes in dual-porosity media. *Water Resources Research*, **17**(4), 1075–1081.

Breiting, T., Reinhard, H., and Helmig, R. (2000). Modellierung und Analyse von Gas-Wasser-Strömungen zur Simulation von Methanmigrationsvorgängen im Untergrund. Technischer bericht, Institut für Computer Anwendungen im Bauingenieurwesen - Technische Universität Braunschweig.

Brill, J. P. and Mukherjee, H. (1999). *Multiphase flow in wells*. SPE monograph series / Society of Petroleum Engineers ; 17. Society of Petroleum Engineers, Richardson, Tex., 1. print. edition.

Brinkman, H. C. (1949). A calculation of the viscous force exerted by a flowing fluid on a dense swarm of particles. *Applied Scientific Research*, **1**(1), 27–34.

Canic, S. and Kim, E. H. (2003). Mathematical analysis of the quasilinear effects in a hyperbolic model blood flow through compliant axi-symmetric vessels. *Mathematical Methods in the Applied Sciences*, **26**(14), 1161–1186.

Class, H., Helmig, R., and Bastian, P. (2002). Numerical simulation of non-isothermal multiphase multicomponent processes in porous media.: 1. an efficient solution technique. *Advances in Water Resources*, **25**(5), 533–550.

Colebrook, C. F. (1939). Turbulent flow in pipes, with particular reference to the transition region between the smooth and rough pipe laws. *Journal of the ICE*, **11**(4), 133–156.

Darcy, H. P. G. (1856). *Les fontaines publiques de la ville de dijon*. Victor Dalmont, Paris.

Darcy, H. P. G. (1857). *Recherches expérimentales relatives au mouvement de l'eau dans les tuyaux*. Impr. Impériale.

Dennis, J. E. and Schnabel, R. B. (1996). *Numerical methods for unconstrained optimization and nonlinear equations*. SIAM.

Dietrich, P., Helmig, R., Sauter, M., Hötzl, H., Köngeter, J., and Teutsch, G. (2005). *Flow and transport in fractured porous media*.

Dogan, M. O., Class, H., and Helmig, R. (2009). Different concepts for the coupling of porous-media flow with lower-dimensional pipe flow. *Computer Modeling in Engineering & Sciences*, **53**(3), 207–233.

Ferziger, J. H. and Peric, M. (1999). *Computational methods for fluid dynamics*. Springer, Berlin [etc.], 2nd revised edition.

Flemisch, B., Fritz, J., Helmig, R., Niessner, J., and Wohlmuth, B. I. (2007). DUMUX: A multi-scale multi-physics toolbox for flow and transport processes in porous media. In *ECCOMAS Thematic Conference on Multi-scale Computational Methods for Solids and Fluids in Paris*.

Gebauer, S., Neunhäuserer, L., Kornhuber, R., Ochs, S. O., Hinkelmann, R., and Helmig, R. (2002). Equidimensional modelling of flow and transport processes in fractured porous systems I. In *14. International Conference on Computational Methods in Water Resources*, Delft, The Netherlands.

Gerke, H. H. and van Genuchten, M. T. (1993). A dual-porosity model for simulating the preferential movement of water and solutes in structured porous media. *Water Resources Research*, **29**(2), 305–319.

Gijsen, F. J. H., van de Vosse, F. N., and Janssen, J. D. (1999). The influence of the non-Newtonian properties of blood on the flow in large arteries: steady flow in a carotid bifurcation model. *Journal of Biomechanics*, **32**(6), 601–608.

Givler, R. C. and Altobelli, S. A. (1994). A determination of the effective viscosity for the Brinkman–Forchheimer flow model. *Journal of Fluid Mechanics*, **258**, 355–370.

Granger, R. A. (1995). *Fluid mechanics*. Courier Dover Publications.

Gupte, S. K. and Advani, S. G. (1997). Flow near the permeable boundary of a porous medium: An experimental investigation using LDA. *Experiments in Fluids*, **22**(5), 408–422.

Hagen, G. (1839). Über die Bewegung des Wassers in engen cylindrischen Röhren. *Annalen der Physik und Chemie*, **122**(3), 423–442.

Helmig, R. (1993). *Theorie und Numerik der Mehrphasenströmungen in geklüftet-porösen Medien*. Dissertation, Institut für Strömungsmechanik und Elektronisches Rechnen im Bauwesen der Universität Hannover, ISSN 0177-9028. Hannover.

Helmig, R. (1997). *Multiphase flow and transport processes in the subsurface: A contribution to the modeling of hydrosystems*. Springer, Berlin, 1'st edition.

Hirsch, C. (2007). *Numerical computation of internal and external flows: fundamentals of computational fluid dynamics*. Butterworth-Heinemann.

Howells, I. D. (1974). Drag due to the motion of a newtonian fluid through a sparse random array of small fixed rigid objects. *Journal of Fluid Mechanics*, **64**(03), 449–475.

Huber, R. and Helmig, R. (1999). Multiphase flow in heterogeneous porous media: A classical finite element method versus an implicit pressure-explicit saturation-based mixed finite element-finite volume approach. *International Journal for Numerical Methods in Fluids*, **29**(8), 899–920.

IEA Coal Industry Advisory Board (1994). *Global methane and the coal industry : A two-part report on methane emissions from the coal industry and coalbed methane recovery and use*. OECD Publications and Information Centre [distributor], Paris, Washington D.C.

Jain, R. K. (1989). Delivery of novel therapeutic agents in tumors: Physiological barriers and strategies. *Journal of the National Cancer Institute*, **81**(8), 570–576.

Jakobs, H. (2004). *Simulation nicht-isothermer Gas-Wasser-Prozesse in komplexen Kluft-Matrix-Systemen*. Mitteilungen / Institut für Wasserbau, Universität Stuttgart ; 128.

James, D. F. and Davis, A. M. J. (2001). Flow at the interface of a model fibrous porous medium. *Journal of Fluid Mechanics*, **426**, 47–72.

Kaviany, M. (1995). *Principles of heat transfer in porous media*. Springer, 2nd edition.

Kim, S. and Russel, W. B. (1985). Modelling of porous media by renormalization of the stokes equations. *Journal of Fluid Mechanics*, **154**, 269–286.

Kolditz, O. (1997). *Strömung, Stoff- und Wärmetransport im Kluftgestein : mit 72 Tabellen*. Borntraeger, Berlin.

Koplik, J., Levine, H., and Zee, A. (1983). Viscosity renormalization in the Brinkman equation. *Physics of Fluids*, **26**(10), 2864.

Kröhn, K. P. (1991). *Simulation von Transportvorgängen im klüftigen Gestein mit der Methode der finiten Elemente*. Dissertation, Institut für Strömungsmechanik und Elektronisches Rechnen im Bauwesen der Universität Hannover, ISSN 0177-9028. Hannover.

Larson, R. E. and Higdon, J. J. L. (1986). Microscopic flow near the surface of two-dimensional porous media. part 1. axial flow. *Journal of Fluid Mechanics*, **166**, 449–472.

Larson, R. E. and Higdon, J. J. L. (1987). Microscopic flow near the surface of two-dimensional porous media. part 2. transverse flow. *Journal of Fluid Mechanics*, **178**, 119–136.

Layton, W. J., Schieweck, F., and Yotov, I. (2003). Coupling fluid flow with porous media flow. *SIAM Journal on Numerical Analysis*, **40**(6), 2195–2218.

Martys, N., Bentz, D. P., and Garboczi, E. J. (1994). Computer simulation study of the effective viscosity in brinkman's equation. *Physics of Fluids*, **6**(4), 1434.

Mikelic, A. and Jäger, W. (2000). On the interface boundary condition of Beavers, Joseph, and Saffman. *SIAM Journal on Applied Mathematics*, **60**(4), 1111.

Mosthaf, K., Baber, K., Flemisch, B., Helmig, R., Leijnse, T., Rybak, I., and Wohlmuth, B. I. (2010). A new coupling concept for two-phase compositional porous media and single-phase compositional free flow. *submitted to Journal of Fluid Mechanics*.

Murdoch, A. I. and Soliman, A. (1999). On the slip-boundary condition for liquid flow over planar porous boundaries. *Proceedings of the Royal Society A: Mathematical, Physical and Engineering Sciences*, **455**(1984), 1315–1340.

Neunhäuserer, L. (2003). *Diskretisierungsansätze zur Modellierung von Strömungs- und Transportprozessen in geklüftet-porösen Medien*. Dissertation, Mitteilungen / Institut für Wasserbau, Universität Stuttgart ; 119.

Neunhäuserer, L., Gebauer, S., Kornhuber, R., Ochs, S. O., Hinkelmann, R., and Helmig, R. (2002). Equidimensional modelling of flow and transport processes in fractured porous systems II. In *14. International Conference on Computational Methods in Water Resources*, Delft, The Netherlands.

Nikuradse, J. (1933). *Strömungsgesetze in rauhen Rohren*. Forschungsheft ; 361. VDI-Verl., Berlin.

Ochoa-Tapia, J. A. and Whitaker, S. (1995). Momentum transfer at the boundary between a porous medium and a homogeneous fluid–I. theoretical development. *International Journal of Heat and Mass Transfer*, **38**(14), 2635–2646.

Ochs, S. O., Hinkelmann, R., Neunhäuserer, L., Süß, M., Helmig, R., Gebauer, S., and Kornhuber, R. (2002). Adaptive methods for the equidimensional modelling of flow and transport processes in fractured aquifers. In *5. International Conference on Hydroscience and Engineering, ICHE2002, Advances in Hydro-Science and -Engineering*, Warschau, Poland.

Pierson, T. C. (1983). Soil pipes and slope stability. *Quarterly Journal of Engineering Geology and Hydrogeology*, **16**(1), 1–11.

Poiseuille, J. L. M. (1841). *Recherches expérimentales sur le mouvement des liquides dans les tubes de très-petit diamètres, comptes rendus*. Académie des sciences, Paris.

Prinos, P., Sofialidis, D., and Keramaris, E. (2003). Turbulent flow over and within a porous bed. *Journal of Hydraulic Engineering*, **129**(9), 720–733.

Pruess, K. and Narasimhan, T. N. (1985). A practical method for modeling fluid and heat flow in fractured porous media. *Society of Petroleum Engineers Journal*, **25**(1).

Reichenberger, V. (2004). *Numerical simulation of multiphase flow in fractured porous media*. Dissertation, Heidelberg University.

Reichenberger, V., Jakobs, H., Bastian, P., and Helmig, R. (2006). A mixed-dimensional finite volume method for two-phase flow in fractured porous media. *Advances in Water Resources*, **29**(7), 1020–1036.

Richards, L. A. (1931). Capillary conduction of liquids through porous mediums. *Physics*, **1**, 318–333.

Rosenzweig, R. and Shavit, U. (2007). The laminar flow field at the interface of a Sierpinski carpet configuration. *Water Resources Research*, **43**(10).

Saffman, P. (1971). On the boundary condition at the surface of a porous media. *Studies in Applied Mathematics*, **50**, 93–101.

Sahraoui, M. and Kaviany, M. (1992). Slip and no-slip velocity boundary conditions at interface of porous, plain media. *International Journal of Heat and Mass Transfer*, **35**(4), 927–943.

Sheta, H., Breiting, T., Hinkelmann, R., and Helmig, R. (2004). Dreidimensionale Modellierung von Methanmigrationsprozessen im Untergrund. Technischer Bericht Nr. 02, Institut für Wasserbau, Lehrstuhl für Hydromechanik und Hydrosystemmodellierung, Universität Stuttgart.

Sidle, R. C., Tsuboyama, Y., Noguchi, S., Hosoda, I., Fujieda, M., and Shimizu, T. (2000). Stormflow generation in steep forested headwaters: A linked hydrogeomorphic paradigm. *Hydrological Processes*, **14**(3), 369–385.

Starov, V. (2001). Effective viscosity and permeability of porous media. *Colloids and Surfaces A: Physicochemical and Engineering Aspects*, **192**(1-3), 363–375.

Süß, M. (2005). *Analysis of the influence of structures and boundaries on flow and transport processes in fractured porous media*. Mitteilungen / Institut für Wasserbau der Universität Stuttgart ; 135.

Taylor, G. I. (2006). A model for the boundary condition of a porous material. part 1. *Journal of Fluid Mechanics*, **49**(02), 319.

Thoben, B. (2006). *Untersuchungen des Wasserhaushaltes an der Kathode einer Polymer-Elektrolyt-Brennstoffzelle*. Dissertation, Universität Stuttgart, Logos Verlag Berlin GmbH.

Uchida, T. and Mizuyama, T. (2002). The contribution of pipeflow on shallow landslides initiation at steep hillslopes. In *Interpraevent 2002 in the Pacific Rim*, volume 2, pages 559–569.

Uchida, T., Kosugi, K., and Mizuyama, T. (2001). Effects of pipeflow on hydrological process and its relation to landslide: A review of pipeflow studies in forested headwater catchments. *Hydrological Processes*, **15**(11), 2151–2174.

Warren, J. E. and Root, P. J. (1963). The behavior of naturally fractured reservoirs. *Society of Petroleum Engineers Journal*, **3**(3).

Weisbach, J. L. (1855). *Lehrbuch der Ingenieur- und Maschinen-Mechanik*. F. Vieweg und Sohn.

You, L. and Liu, H. (2006). A two-phase flow and transport model for PEM fuel cells. *Journal of Power Sources*, **155**(2), 219–230.

Zhou, D. and Mendoza, C. (1993). Flow through porous bed of turbulent stream. *Journal of Engineering Mechanics*, **119**(2), 365–383.

Zigrang, D. J. and Sylvester, N. D. (1985). A review of explicit friction factor equations. *Journal of Energy Resources Technology*, **107**(2), 280.

Institut für Wasserbau
Universität Stuttgart

Pfaffenwaldring 61
70569 Stuttgart (Vaihingen)
Telefon (0711) 685 - 64717/64749/64752/64679
Telefax (0711) 685 - 67020 o. 64746 o. 64681
E-Mail: iws@iws.uni-stuttgart.de
http://www.iws.uni-stuttgart.de

Direktoren
Prof. Dr. rer. nat. Dr.-Ing. András Bárdossy
Prof. Dr.-Ing. Rainer Helmig
Prof. Dr.-Ing. Silke Wieprecht

Vorstand *(Stand 01.04.2009)*
Prof. Dr. rer. nat. Dr.-Ing. A. Bárdossy
Prof. Dr.-Ing. R. Helmig
Prof. Dr.-Ing. S. Wieprecht
Jürgen Braun, PhD
Dr.-Ing. H. Class
Dr.-Ing. S. Hartmann
Dr.-Ing. H.-P. Koschitzky
PD Dr.-Ing. W. Marx
Dr. rer. nat. J. Seidel

Emeriti
Prof. Dr.-Ing. habil. Dr.-Ing. E.h. Jürgen Giesecke
Prof. Dr.h.c. Dr.-Ing. E.h. Helmut Kobus, PhD

Lehrstuhl für Wasserbau und Wassermengenwirtschaft
Leiter: Prof. Dr.-Ing. Silke Wieprecht
Stellv.: PD Dr.-Ing. Walter Marx, AOR

Versuchsanstalt für Wasserbau
Leiter: Dr.-Ing. Sven Hartmann, AOR

Lehrstuhl für Hydromechanik und Hydrosystemmodellierung
Leiter: Prof. Dr.-Ing. Rainer Helmig
Stellv.: Dr.-Ing. Holger Class, AOR

Lehrstuhl für Hydrologie und Geohydrologie
Leiter: Prof. Dr. rer. nat. Dr.-Ing. András Bárdossy
Stellv.: Dr. rer. nat. Jochen Seidel

***VEGAS,* Versuchseinrichtung zur Grundwasser- und Altlastensanierung**
Leitung: Jürgen Braun, PhD
Dr.-Ing. Hans-Peter Koschitzky, AD

Verzeichnis der Mitteilungshefte

5 Plate, Erich: *Beitrag zur Bestimmung der Windgeschwindigkeitsverteilung in der durch eine Wand gestörten bodennahen Luftschicht*,
und
Röhnisch, Arthur; Marotz, Günter: *Neue Baustoffe und Bauausführungen für den Schutz der Böschungen und der Sohle von Kanälen, Flüssen und Häfen; Gestehungskosten und jeweilige Vorteile*, sowie Unny, T.E.: *Schwingungsuntersuchungen am Kegelstrahlschieber*, 1967

6 Seiler, Erich: *Die Ermittlung des Anlagenwertes der bundeseigenen Binnenschiffahrtsstraßen und Talsperren und des Anteils der Binnenschiffahrt an diesem Wert*, 1967

7 *Sonderheft anläßlich des 65. Geburtstages von Prof. Arthur Röhnisch mit Beiträgen von* Benk, Dieter; Breitling, J.; Gurr, Siegfried; Haberhauer, Robert; Honekamp, Hermann; Kuz, Klaus Dieter; Marotz, Günter; Mayer-Vorfelder, Hans-Jörg; Miller, Rudolf; Plate, Erich J.; Radomski, Helge; Schwarz, Helmut; Vollmer, Ernst; Wildenhahn, Eberhard; 1967

8 Jumikis, Alfred: *Beitrag zur experimentellen Untersuchung des Wassernachschubs in einem gefrierenden Boden und die Beurteilung der Ergebnisse*, 1968

9 Marotz, Günter: *Technische Grundlagen einer Wasserspeicherung im natürlichen Untergrund*, 1968

10 Radomski, Helge: *Untersuchungen über den Einfluß der Querschnittsform wellenförmiger Spundwände auf die statischen und rammtechnischen Eigenschaften*, 1968

11 Schwarz, Helmut: *Die Grenztragfähigkeit des Baugrundes bei Einwirkung vertikal gezogener Ankerplatten als zweidimensionales Bruchproblem*, 1969

12 Erbel, Klaus: *Ein Beitrag zur Untersuchung der Metamorphose von Mittelgebirgsschneedecken unter besonderer Berücksichtigung eines Verfahrens zur Bestimmung der thermischen Schneequalität*, 1969

13 Westhaus, Karl-Heinz: *Der Strukturwandel in der Binnenschiffahrt und sein Einfluß auf den Ausbau der Binnenschiffskanäle*, 1969

14 Mayer-Vorfelder, Hans-Jörg: *Ein Beitrag zur Berechnung des Erdwiderstandes unter Ansatz der logarithmischen Spirale als Gleitflächenfunktion*, 1970

15 Schulz, Manfred: *Berechnung des räumlichen Erddruckes auf die Wandung kreiszylindrischer Körper*, 1970

16 Mobasseri, Manoutschehr: *Die Rippenstützmauer. Konstruktion und Grenzen ihrer Standsicherheit*, 1970

17 Benk, Dieter: *Ein Beitrag zum Betrieb und zur Bemessung von Hochwasserrückhaltebecken*, 1970

18 Gàl, Attila: *Bestimmung der mitschwingenden Wassermasse bei überströmten Fischbauchklappen mit kreiszylindrischem Staublech*, 1971, vergriffen

19 Kuz, Klaus Dieter: *Ein Beitrag zur Frage des Einsetzens von Kavitationserscheinungen in einer Düsenströmung bei Berücksichtigung der im Wasser gelösten Gase*, 1971, vergriffen

20 Schaak, Hartmut: *Verteilleitungen von Wasserkraftanlagen*, 1971

21 *Sonderheft zur Eröffnung der neuen Versuchsanstalt des Instituts für Wasserbau der Universität Stuttgart mit Beiträgen von* Brombach, Hansjörg; Dirksen, Wolfram; Gàl, Attila; Gerlach, Reinhard; Giesecke, Jürgen; Holthoff, Franz-Josef; Kuz, Klaus Dieter; Marotz, Günter; Minor, Hans-Erwin; Petrikat, Kurt; Röhnisch, Arthur; Rueff, Helge; Schwarz, Helmut; Vollmer, Ernst; Wildenhahn, Eberhard; 1972

22 Wang, Chung-su: *Ein Beitrag zur Berechnung der Schwingungen an Kegelstrahlschiebern*, 1972

23 Mayer-Vorfelder, Hans-Jörg: *Erdwiderstandsbeiwerte nach dem Ohde-Variationsverfahren*, 1972

24 Minor, Hans-Erwin: *Beitrag zur Bestimmung der Schwingungsanfachungsfunktionen überströmter Stauklappen*, 1972, vergriffen

25 Brombach, Hansjörg: *Untersuchung strömungsmechanischer Elemente (Fluidik) und die Möglichkeit der Anwendung von Wirbelkammerelementen im Wasserbau*, 1972, vergriffen

26 Wildenhahn, Eberhard: *Beitrag zur Berechnung von Horizontalfilterbrunnen*, 1972

27 Steinlein, Helmut: *Die Eliminierung der Schwebstoffe aus Flußwasser zum Zweck der unterirdischen Wasserspeicherung, gezeigt am Beispiel der Iller*, 1972

28 Holthoff, Franz Josef: *Die Überwindung großer Hubhöhen in der Binnenschiffahrt durch Schwimmerhebewerke*, 1973

29 Röder, Karl: *Einwirkungen aus Baugrundbewegungen auf trog- und kastenförmige Konstruktionen des Wasser- und Tunnelbaues*, 1973

30 Kretschmer, Heinz: *Die Bemessung von Bogenstaumauern in Abhängigkeit von der Talform*, 1973

31 Honekamp, Hermann: *Beitrag zur Berechnung der Montage von Unterwasserpipelines*, 1973

32 Giesecke, Jürgen: *Die Wirbelkammertriode als neuartiges Steuerorgan im Wasserbau*, und Brombach, Hansjörg: *Entwicklung, Bauformen, Wirkungsweise und Steuereigenschaften von Wirbelkammerverstärkern*, 1974

33 Rueff, Helge: *Untersuchung der schwingungserregenden Kräfte an zwei hintereinander angeordneten Tiefschützen unter besonderer Berücksichtigung von Kavitation*, 1974

34 Röhnisch, Arthur: *Einpreßversuche mit Zementmörtel für Spannbeton - Vergleich der Ergebnisse von Modellversuchen mit Ausführungen in Hüllwellrohren*, 1975

35 *Sonderheft anläßlich des 65. Geburtstages von Prof. Dr.-Ing. Kurt Petrikat mit Beiträgen von*: Brombach, Hansjörg; Erbel, Klaus; Flinspach, Dieter; Fischer jr., Richard; Gàl, Attila; Gerlach, Reinhard; Giesecke, Jürgen; Haberhauer, Robert; Hafner Edzard; Hausenblas, Bernhard; Horlacher, Hans-Burkhard; Hutarew, Andreas; Knoll, Manfred; Krummet, Ralph; Marotz, Günter; Merkle, Theodor; Miller, Christoph; Minor, Hans-Erwin; Neumayer, Hans; Rao, Syamala; Rath, Paul; Rueff, Helge; Ruppert, Jürgen; Schwarz, Wolfgang; Topal-Gökceli, Mehmet; Vollmer, Ernst; Wang, Chung-su; Weber, Hans-Georg; 1975

36 Berger, Jochum: *Beitrag zur Berechnung des Spannungszustandes in rotationssymmetrisch belasteten Kugelschalen veränderlicher Wandstärke unter Gas- und Flüssigkeitsdruck durch Integration schwach singulärer Differentialgleichungen*, 1975

37 Dirksen, Wolfram: *Berechnung instationärer Abflußvorgänge in gestauten Gerinnen mittels Differenzenverfahren und die Anwendung auf Hochwasserrückhaltebecken*, 1976

38 Horlacher, Hans-Burkhard: *Berechnung instationärer Temperatur- und Wärmespannungsfelder in langen mehrschichtigen Hohlzylindern*, 1976

39 Hafner, Edzard: *Untersuchung der hydrodynamischen Kräfte auf Baukörper im Tiefwasserbereich des Meeres*, 1977, ISBN 3-921694-39-6

40 Ruppert, Jürgen: *Über den Axialwirbelkammerverstärker für den Einsatz im Wasserbau*, 1977, ISBN 3-921694-40-X

41 Hutarew, Andreas: *Beitrag zur Beeinflußbarkeit des Sauerstoffgehalts in Fließgewässern an Abstürzen und Wehren*, 1977, ISBN 3-921694-41-8, vergriffen

42 Miller, Christoph: *Ein Beitrag zur Bestimmung der schwingungserregenden Kräfte an unterströmten Wehren*, 1977, ISBN 3-921694-42-6

43 Schwarz, Wolfgang: *Druckstoßberechnung unter Berücksichtigung der Radial- und Längsverschiebungen der Rohrwandung*, 1978, ISBN 3-921694-43-4

44 Kinzelbach, Wolfgang: *Numerische Untersuchungen über den optimalen Einsatz variabler Kühlsysteme einer Kraftwerkskette am Beispiel Oberrhein*, 1978, ISBN 3-921694-44-2

45 Barczewski, Baldur: *Neue Meßmethoden für Wasser-Luftgemische und deren Anwendung auf zweiphasige Auftriebsstrahlen*, 1979, ISBN 3-921694-45-0

46 Neumayer, Hans: *Untersuchung der Strömungsvorgänge in radialen Wirbelkammerverstärkern*, 1979, ISBN 3-921694-46-9

47 Elalfy, Youssef-Elhassan: *Untersuchung der Strömungsvorgänge in Wirbelkammerdioden und -drosseln*, 1979, ISBN 3-921694-47-7

48 Brombach, Hansjörg: *Automatisierung der Bewirtschaftung von Wasserspeichern*, 1981, ISBN 3-921694-48-5

49 Geldner, Peter: *Deterministische und stochastische Methoden zur Bestimmung der Selbstdichtung von Gewässern*, 1981, ISBN 3-921694-49-3, vergriffen

50 Mehlhorn, Hans: *Temperaturveränderungen im Grundwasser durch Brauchwassereinleitungen*, 1982, ISBN 3-921694-50-7, vergriffen

51 Hafner, Edzard: *Rohrleitungen und Behälter im Meer*, 1983, ISBN 3-921694-51-5

52 Rinnert, Bernd: *Hydrodynamische Dispersion in porösen Medien: Einfluß von Dichteunterschieden auf die Vertikalvermischung in horizontaler Strömung*, 1983, ISBN 3-921694-52-3, vergriffen

53 Lindner, Wulf: *Steuerung von Grundwasserentnahmen unter Einhaltung ökologischer Kriterien*, 1983, ISBN 3-921694-53-1, vergriffen

54 Herr, Michael; Herzer, Jörg; Kinzelbach, Wolfgang; Kobus, Helmut; Rinnert, Bernd: *Methoden zur rechnerischen Erfassung und hydraulischen Sanierung von Grundwasserkontaminationen*, 1983, ISBN 3-921694-54-X

55 Schmitt, Paul: *Wege zur Automatisierung der Niederschlagsermittlung*, 1984, ISBN 3-921694-55-8, vergriffen

56 Müller, Peter: *Transport und selektive Sedimentation von Schwebstoffen bei gestautem Abfluß*, 1985, ISBN 3-921694-56-6

57 El-Qawasmeh, Fuad: *Möglichkeiten und Grenzen der Tropfbewässerung unter besonderer Berücksichtigung der Verstopfungsanfälligkeit der Tropfelemente*, 1985, ISBN 3-921694-57-4, vergriffen

58 Kirchenbaur, Klaus: *Mikroprozessorgesteuerte Erfassung instationärer Druckfelder am Beispiel seegangsbelasteter Baukörper*, 1985, ISBN 3-921694-58-2

59 Kobus, Helmut (Hrsg.): *Modellierung des großräumigen Wärme- und Schadstofftransports im Grundwasser*, Tätigkeitsbericht 1984/85 (DFG-Forschergruppe an den Universitäten Hohenheim, Karlsruhe und Stuttgart), 1985, ISBN 3-921694-59-0, vergriffen

60 Spitz, Karlheinz: *Dispersion in porösen Medien: Einfluß von Inhomogenitäten und Dichteunterschieden*, 1985, ISBN 3-921694-60-4, vergriffen

61 Kobus, Helmut: *An Introduction to Air-Water Flows in Hydraulics*, 1985, ISBN 3-921694-61-2

62 Kaleris, Vassilios: *Erfassung des Austausches von Oberflächen- und Grundwasser in horizontalebenen Grundwassermodellen*, 1986, ISBN 3-921694-62-0

63 Herr, Michael: *Grundlagen der hydraulischen Sanierung verunreinigter Porengrundwasserleiter*, 1987, ISBN 3-921694-63-9

64 Marx, Walter: *Berechnung von Temperatur und Spannung in Massenbeton infolge Hydratation*, 1987, ISBN 3-921694-64-7

65 Koschitzky, Hans-Peter: *Dimensionierungskonzept für Sohlbelüfter in Schußrinnen zur Vermeidung von Kavitationsschäden*, 1987, ISBN 3-921694-65-5

66 Kobus, Helmut (Hrsg.): *Modellierung des großräumigen Wärme- und Schadstofftransports im Grundwasser*, Tätigkeitsbericht 1986/87 (DFG-Forschergruppe an den Universitäten Hohenheim, Karlsruhe und Stuttgart) 1987, ISBN 3-921694-66-3

67 Söll, Thomas: *Berechnungsverfahren zur Abschätzung anthropogener Temperaturanomalien im Grundwasser*, 1988, ISBN 3-921694-67-1

68 Dittrich, Andreas; Westrich, Bernd: *Bodenseeufererosion, Bestandsaufnahme und Bewertung*, 1988, ISBN 3-921694-68-X, vergriffen

69 Huwe, Bernd; van der Ploeg, Rienk R.: *Modelle zur Simulation des Stickstoffhaushaltes von Standorten mit unterschiedlicher landwirtschaftlicher Nutzung*, 1988, ISBN 3-921694-69-8, vergriffen

70 Stephan, Karl: *Integration elliptischer Funktionen*, 1988, ISBN 3-921694-70-1

71 Kobus, Helmut; Zilliox, Lothaire (Hrsg.): *Nitratbelastung des Grundwassers, Auswirkungen der Landwirtschaft auf die Grundwasser- und Rohwasserbeschaffenheit und Maßnahmen zum Schutz des Grundwassers*. Vorträge des deutsch-französischen Kolloquiums am 6. Oktober 1988, Universitäten Stuttgart und Louis Pasteur Strasbourg (Vorträge in deutsch oder französisch, Kurzfassungen zweisprachig), 1988, ISBN 3-921694-71-X

72 Soyeaux, Renald: *Unterströmung von Stauanlagen auf klüftigem Untergrund unter Berücksichtigung laminarer und turbulenter Fließzustände*,1991, ISBN 3-921694-72-8

73 Kohane, Roberto: *Berechnungsmethoden für Hochwasserabfluß in Fließgewässern mit überströmten Vorländern*, 1991, ISBN 3-921694-73-6

74 Hassinger, Reinhard: *Beitrag zur Hydraulik und Bemessung von Blocksteinrampen in flexibler Bauweise*, 1991, ISBN 3-921694-74-4, vergriffen

75 Schäfer, Gerhard: *Einfluß von Schichtenstrukturen und lokalen Einlagerungen auf die Längsdispersion in Porengrundwasserleitern*, 1991, ISBN 3-921694-75-2

76 Giesecke, Jürgen: *Vorträge, Wasserwirtschaft in stark besiedelten Regionen; Umweltforschung mit Schwerpunkt Wasserwirtschaft*, 1991, ISBN 3-921694-76-0

77 Huwe, Bernd: *Deterministische und stochastische Ansätze zur Modellierung des Stickstoffhaushalts landwirtschaftlich genutzter Flächen auf unterschiedlichem Skalenniveau*, 1992, ISBN 3-921694-77-9, vergriffen

78 Rommel, Michael: *Verwendung von Kluftdaten zur realitätsnahen Generierung von Kluftnetzen mit anschließender laminar-turbulenter Strömungsberechnung*, 1993, ISBN 3-92 1694-78-7

79 Marschall, Paul: *Die Ermittlung lokaler Stofffrachten im Grundwasser mit Hilfe von Einbohrloch-Meßverfahren*, 1993, ISBN 3-921694-79-5, vergriffen

80 Ptak, Thomas: *Stofftransport in heterogenen Porenaquiferen: Felduntersuchungen und stochastische Modellierung*, 1993, ISBN 3-921694-80-9, vergriffen

81 Haakh, Frieder: *Transientes Strömungsverhalten in Wirbelkammern,* 1993, ISBN 3-921694-81-7

82 Kobus, Helmut; Cirpka, Olaf; Barczewski, Baldur; Koschitzky, Hans-Peter: *Versucheinrichtung zur Grundwasser und Altlastensanierung VEGAS, Konzeption und Programmrahmen*, 1993, ISBN 3-921694-82-5

83 Zang, Weidong: *Optimaler Echtzeit-Betrieb eines Speichers mit aktueller Abflußregenerierung*, 1994, ISBN 3-921694-83-3, vergriffen

84 Franke, Hans-Jörg: *Stochastische Modellierung eines flächenhaften Stoffeintrages und Transports in Grundwasser am Beispiel der Pflanzenschutzmittelproblematik*, 1995, ISBN 3-921694-84-1

85 Lang, Ulrich: *Simulation regionaler Strömungs- und Transportvorgänge in Karstaquiferen mit Hilfe des Doppelkontinuum-Ansatzes: Methodenentwicklung und Parameteridentifikation*, 1995, ISBN 3-921694-85-X, vergriffen

86 Helmig, Rainer: *Einführung in die Numerischen Methoden der Hydromechanik*, 1996, ISBN 3-921694-86-8, vergriffen

87 Cirpka, Olaf: *CONTRACT: A Numerical Tool for Contaminant Transport and Chemical Transformations - Theory and Program Documentation* -, 1996, ISBN 3-921694-87-6

88 Haberlandt, Uwe: *Stochastische Synthese und Regionalisierung des Niederschlages für Schmutzfrachtberechnungen*, 1996, ISBN 3-921694-88-4

89 Croisé, Jean: *Extraktion von flüchtigen Chemikalien aus natürlichen Lockergesteinen mittels erzwungener Luftströmung*, 1996, ISBN 3-921694-89-2, vergriffen

90 Jorde, Klaus: *Ökologisch begründete, dynamische Mindestwasserregelungen bei Ausleitungskraftwerken*, 1997, ISBN 3-921694-90-6, vergriffen

91 Helmig, Rainer: *Gekoppelte Strömungs- und Transportprozesse im Untergrund - Ein Beitrag zur Hydrosystemmodellierung*-, 1998, ISBN 3-921694-91-4, vergriffen

92 Emmert, Martin: *Numerische Modellierung nichtisothermer Gas-Wasser Systeme in porösen Medien,* 1997, ISBN 3-921694-92-2

93 Kern, Ulrich: *Transport von Schweb- und Schadstoffen in staugeregelten Fließgewässern am Beispiel des Neckars*, 1997, ISBN 3-921694-93-0, vergriffen

94 Förster, Georg: *Druckstoßdämpfung durch große Luftblasen in Hochpunkten von Rohrleitungen 1997*, ISBN 3-921694-94-9

95 Cirpka, Olaf: *Numerische Methoden zur Simulation des reaktiven Mehrkomponententransports im Grundwasser*, 1997, ISBN 3-921694-95-7, vergriffen

96 Färber, Arne: *Wärmetransport in der ungesättigten Bodenzone: Entwicklung einer thermischen In-situ-Sanierungstechnologie*, 1997, ISBN 3-921694-96-5

97 Betz, Christoph: *Wasserdampfdestillation von Schadstoffen im porösen Medium: Entwicklung einer thermischen In-situ-Sanierungstechnologie*, 1998, ISBN 3-921694-97-3

98 Xu, Yichun: *Numerical Modeling of Suspended Sediment Transport in Rivers*, 1998, ISBN 3-921694-98-1, vergriffen

99 Wüst, Wolfgang: *Geochemische Untersuchungen zur Sanierung CKW-kontaminierter Aquifere mit Fe(0)-Reaktionswänden,* 2000, ISBN 3-933761-02-2

100 Sheta, Hussam: *Simulation von Mehrphasenvorgängen in porösen Medien unter Einbeziehung von Hysterese-Effekten*, 2000, ISBN 3-933761-03-4

101 Ayros, Edwin: *Regionalisierung extremer Abflüsse auf der Grundlage statistischer Verfahren*, 2000, ISBN 3-933761-04-2, vergriffen

102 Huber, Ralf: *Compositional Multiphase Flow and Transport in Heterogeneous Porous Media*, 2000, ISBN 3-933761-05-0

103 Braun, Christopherus: *Ein Upscaling-Verfahren für Mehrphasenströmungen in porösen Medien*, 2000, ISBN 3-933761-06-9

104 Hofmann, Bernd: *Entwicklung eines rechnergestützten Managementsystems zur Beurteilung von Grundwasserschadensfällen*, 2000, ISBN 3-933761-07-7

105 Class, Holger: *Theorie und numerische Modellierung nichtisothermer Mehrphasenprozesse in NAPL-kontaminierten porösen Medien,* 2001, ISBN 3-933761-08-5

106 Schmidt, Reinhard: *Wasserdampf- und Heißluftinjektion zur thermischen Sanierung kontaminierter Standorte*, 2001, ISBN 3-933761-09-3

107 Josef, Reinhold:, *Schadstoffextraktion mit hydraulischen Sanierungsverfahren unter Anwendung von grenzflächenaktiven Stoffen*, 2001, ISBN 3-933761-10-7

108 Schneider, Matthias: *Habitat- und Abflussmodellierung für Fließgewässer mit unscharfen Berechnungsansätzen*, 2001, ISBN 3-933761-11-5

109 Rathgeb, Andreas: *Hydrodynamische Bemessungsgrundlagen für Lockerdeckwerke an überströmbaren Erddämmen*, 2001, ISBN 3-933761-12-3

110 Lang, Stefan: *Parallele numerische Simulation instätionärer Probleme mit adaptiven Methoden auf unstrukturierten Gittern*, 2001, ISBN 3-933761-13-1

111 Appt, Jochen; Stumpp Simone: *Die Bodensee-Messkampagne 2001, IWS/CWR Lake Constance Measurement Program 2001*, 2002, ISBN 3-933761-14-X

112 Heimerl, Stephan: *Systematische Beurteilung von Wasserkraftprojekten,* 2002, ISBN 3-933761-15-8

113 Iqbal, Amin: *On the Management and Salinity Control of Drip Irrigation,* 2002, ISBN 3-933761-16-6

114 Silberhorn-Hemminger, Annette: *Modellierung von Kluftaquifersystemen: Geostatistische Analyse und deterministisch-stochastische Kluftgenerierung,* 2002, ISBN 3-933761-17-4

115 Winkler, Angela: *Prozesse des Wärme- und Stofftransports bei der In-situ-Sanierung mit festen Wärmequellen,* 2003, ISBN 3-933761-18-2

116 Marx, Walter: *Wasserkraft, Bewässerung, Umwelt - Planungs- und Bewertungsschwerpunkte der Wasserbewirtschaftung,* 2003, ISBN 3-933761-19-0

117 Hinkelmann, Reinhard: *Efficient Numerical Methods and Information-Processing Techniques in Environment Water,* 2003, ISBN 3-933761-20-4

118 Samaniego-Eguiguren, Luis Eduardo: *Hydrological Consequences of Land Use / Land Cover and Climatic Changes in Mesoscale Catchments*, 2003, ISBN 3-933761-21-2

119 Neunhäuserer, Lina: *Diskretisierungsansätze zur Modellierung von Strömungs- und Transportprozessen in geklüftet-porösen Medien*, 2003, ISBN 3-933761-22-0

120 Paul, Maren: *Simulation of Two-Phase Flow in Heterogeneous Poros Media with Adaptive Methods*, 2003, ISBN 3-933761-23-9

121 Ehret, Uwe: *Rainfall and Flood Nowcasting in Small Catchments using Weather Radar*, 2003, ISBN 3-933761-24-7

122 Haag, Ingo: *Der Sauerstoffhaushalt staugeregelter Flüsse am Beispiel des Neckars - Analysen, Experimente, Simulationen -,* 2003, ISBN 3-933761-25-5

123 Appt, Jochen: *Analysis of Basin-Scale Internal Waves in Upper Lake Constance,* 2003, ISBN 3-933761-26-3

124 Hrsg.: Schrenk, Volker; Batereau, Katrin; Barczewski, Baldur; Weber, Karolin und Koschitzky, Hans-Peter: *Symposium Ressource Fläche und VEGAS - Statuskolloquium 2003, 30. September und 1. Oktober 2003,* 2003, ISBN 3-933761-27-1

125 Omar Khalil Ouda: *Optimisation of Agricultural Water Use: A Decision Support System for the Gaza Strip,* 2003, ISBN 3-933761-28-0

126 Batereau, Katrin: *Sensorbasierte Bodenluftmessung zur Vor-Ort-Erkundung von Schadensherden im Untergrund*, 2004, ISBN 3-933761-29-8

127 Witt, Oliver: *Erosionsstabilität von Gewässersedimenten mit Auswirkung auf den Stofftransport bei Hochwasser am Beispiel ausgewählter Stauhaltungen des Oberrheins*, 2004, ISBN 3-933761-30-1

128 Jakobs, Hartmut: *Simulation nicht-isothermer Gas-Wasser-Prozesse in komplexen Kluft-Matrix-Systemen*, 2004, ISBN 3-933761-31-X

129 Li, Chen-Chien: *Deterministisch-stochastisches Berechnungskonzept zur Beurteilung der Auswirkungen erosiver Hochwasserereignisse in Flussstauhaltungen,* 2004, ISBN 3-933761-32-8

130 Reichenberger, Volker; Helmig, Rainer; Jakobs, Hartmut; Bastian, Peter; Niessner, Jennifer: *Complex Gas-Water Processes in Discrete Fracture-Matrix Systems: Upscaling, Mass-Conservative Discretization and Efficient Multilevel Solution,* 2004, ISBN 3-933761-33-6

131 Hrsg.: Barczewski, Baldur; Koschitzky, Hans-Peter; Weber, Karolin; Wege, Ralf: *VEGAS - Statuskolloquium 2004,* Tagungsband zur Veranstaltung am 05. Oktober 2004 an der Universität Stuttgart, Campus Stuttgart-Vaihingen, 2004, ISBN 3-933761-34-4

132 Asie, Kemal Jabir: *Finite Volume Models for Multiphase Multicomponent Flow through Porous Media*. 2005, ISBN 3-933761-35-2

133 Jacoub, George: *Development of a 2-D Numerical Module for Particulate Contaminant Transport in Flood Retention Reservoirs and Impounded Rivers,* 2004, ISBN 3-933761-36-0

134 Nowak, Wolfgang: *Geostatistical Methods for the Identification of Flow and Transport Parameters in the Subsurface,* 2005, ISBN 3-933761-37-9

135 Süß, Mia: *Analysis of the influence of structures and boundaries on flow and transport processes in fractured porous media*, 2005, ISBN 3-933761-38-7

136 Jose, Surabhin Chackiath: *Experimental Investigations on Longitudinal Dispersive Mixing in Heterogeneous Aquifers,* 2005, ISBN: 3-933761-39-5

137 Filiz, Fulya: *Linking Large-Scale Meteorological Conditions to Floods in Mesoscale Catchments,* 2005, ISBN 3-933761-40-9

138 Qin, Minghao: *Wirklichkeitsnahe und recheneffiziente Ermittlung von Temperatur und Spannungen bei großen RCC-Staumauern*, 2005, ISBN 3-933761-41-7

139 Kobayashi, Kenichiro: *Optimization Methods for Multiphase Systems in the Subsurface - Application to Methane Migration in Coal Mining Areas*, 2005, ISBN 3-933761-42-5

140 Rahman, Md. Arifur: *Experimental Investigations on Transverse Dispersive Mixing in Heterogeneous Porous Media,* 2005, ISBN 3-933761-43-3

141 Schrenk, Volker: *Ökobilanzen zur Bewertung von Altlastensanierungsmaßnahmen,* 2005, ISBN 3-933761-44-1

142 Hundecha, Hirpa Yeshewatesfa: *Regionalization of Parameters of a Conceptual Rainfall-Runoff Model*, 2005, ISBN: 3-933761-45-X

143 Wege, Ralf: *Untersuchungs- und Überwachungsmethoden für die Beurteilung natürlicher Selbstreinigungsprozesse im Grundwasser,* 2005, ISBN 3-933761-46-8

144 Breiting, Thomas: *Techniken und Methoden der Hydroinformatik - Modellierung von komplexen Hydrosystemen im Untergrund*, 2006, 3-933761-47-6

145 Hrsg.: Braun, Jürgen; Koschitzky, Hans-Peter; Müller, Martin: *Ressource Untergrund: 10 Jahre VEGAS: Forschung und Technologieentwicklung zum Schutz von Grundwasser und Boden,* Tagungsband zur Veranstaltung am 28. und 29. September 2005 an der Universität Stuttgart, Campus Stuttgart-Vaihingen, 2005, ISBN 3-933761-48-4

146 Rojanschi, Vlad: *Abflusskonzentration in mesoskaligen Einzugsgebieten unter Berücksichtigung des Sickerraumes,* 2006, ISBN 3-933761-49-2

147 Winkler, Nina Simone: *Optimierung der Steuerung von Hochwasserrückhaltebecken-systemen,* 2006, ISBN 3-933761-50-6

148 Wolf, Jens: *Räumlich differenzierte Modellierung der Grundwasserströmung alluvialer Aquifere für mesoskalige Einzugsgebiete*, 2006, ISBN: 3-933761-51-4

149 Kohler, Beate: *Externe Effekte der Laufwasserkraftnutzung*, 2006, ISBN 3-933761-52-2

150 Hrsg.: Braun, Jürgen; Koschitzky, Hans-Peter; Stuhrmann, Matthias: *VEGAS-Statuskolloquium 2006,* Tagungsband zur Veranstaltung am 28. September 2006 an der Universität Stuttgart, Campus Stuttgart-Vaihingen, 2006, ISBN 3-933761-53-0

151 Niessner, Jennifer: *Multi-Scale Modeling of Multi-Phase - Multi-Component Processes in Heterogeneous Porous Media*, 2006, ISBN 3-933761-54-9

152 Fischer, Markus: *Beanspruchung eingeerdeter Rohrleitungen infolge Austrocknung bindiger Böden,* 2006, ISBN 3-933761-55-7

153 Schneck, Alexander: *Optimierung der Grundwasserbewirtschaftung unter Berücksichtigung der Belange der Wasserversorgung, der Landwirtschaft und des Naturschutzes*, 2006, ISBN 3-933761-56-5

154 Das, Tapash: *The Impact of Spatial Variability of Precipitation on the Predictive Uncertainty of Hydrological Models,* 2006, ISBN 3-933761-57-3

155 Bielinski, Andreas: *Numerical Simulation of CO_2 sequestration in geological formations*, 2007, ISBN 3-933761-58-1

156 Mödinger, Jens: *Entwicklung eines Bewertungs- und Entscheidungsunterstützungssystems für eine nachhaltige regionale Grundwasserbewirtschaftung*, 2006, ISBN 3-933761-60-3

157 Manthey, Sabine: *Two-phase flow processes with dynamic effects in porous media - parameter estimation and simulation,* 2007, ISBN 3-933761-61-1

158 Pozos Estrada, Oscar: *Investigation on the Effects of Entrained Air in Pipelines,* 2007, ISBN 3-933761-62-X

159 Ochs, Steffen Oliver: *Steam injection into saturated porous media – process analysis including experimental and numerical investigations*, 2007, ISBN 3-933761-63-8

160 Marx, Andreas: *Einsatz gekoppelter Modelle und Wetterradar zur Abschätzung von Niederschlagsintensitäten und zur Abflussvorhersage, 2007,* ISBN 3-933761-64-6

161 Hartmann, Gabriele Maria: *Investigation of Evapotranspiration Concepts in Hydrological Modelling for Climate Change Impact Assessment*, 2007, ISBN 3-933761-65-4

162 Kebede Gurmessa, Tesfaye: *Numerical Investigation on Flow and Transport Characteristics to Improve Long-Term Simulation of Reservoir Sedimentation*, 2007, ISBN 3-933761-66-2

163 Trifković, Aleksandar: *Multi-objective and Risk-based Modelling Methodology for Planning, Design and Operation of Water Supply Systems*, 2007, ISBN 3-933761-67-0

164 Götzinger, Jens: *Distributed Conceptual Hydrological Modelling - Simulation of Climate, Land Use Change Impact and Uncertainty Analysis*, 2007, ISBN 3-933761-68-9

165 Hrsg.: Braun, Jürgen; Koschitzky, Hans-Peter; Stuhrmann, Matthias: *VEGAS – Kolloquium 2007,* Tagungsband zur Veranstaltung am 26. September 2007 an der Universität Stuttgart, Campus Stuttgart-Vaihingen, 2007, ISBN 3-933761-69-7

166 Freeman, Beau: *Modernization Criteria Assessment for Water Resources Planning; Klamath Irrigation Project, U.S.*, 2008, ISBN 3-933761-70-0

167 Dreher, Thomas: *Selektive Sedimentation von Feinstschwebstoffen in Wechselwirkung mit wandnahen turbulenten Strömungsbedingungen*, 2008, ISBN 3-933761-71-9

168 Yang, Wei: *Discrete-Continuous Downscaling Model for Generating Daily Precipitation Time Series*, 2008, ISBN 3-933761-72-7

169 Kopecki, Ianina: *Calculational Approach to FST-Hemispheres for Multiparametrical Benthos Habitat Modelling,* 2008*,* ISBN 3-933761-73-5

170 Brommundt, Jürgen: *Stochastische Generierung räumlich zusammenhängender Niederschlagszeitreihen*, 2008, ISBN 3-933761-74-3

171 Papafotiou, *Alexandros: Numerical Investigations of the Role of Hysteresis in Heterogeneous Two-Phase Flow Systems*, 2008, ISBN 3-933761-75-1

172 He, Yi: *Application of a Non-Parametric Classification Scheme to Catchment Hydrology*, 2008, ISBN 978-3-933761-76-7

173 Wagner, Sven: *Water Balance in a Poorly Gauged Basin in West Africa Using Atmospheric Modelling and Remote Sensing Information*, 2008, ISBN 978-3-933761-77-4

174 Hrsg.: Braun, Jürgen; Koschitzky, Hans-Peter; Stuhrmann, Matthias; Schrenk, Volker: *VEGAS-Kolloquium 2008 Ressource Fläche III*, Tagungsband zur Veranstaltung am 01. Oktober 2008 an der Universität Stuttgart, Campus Stuttgart-Vaihingen, 2008, ISBN 978-3-933761-78-1

175 Patil, Sachin: *Regionalization of an Event Based Nash Cascade Model for Flood Predictions in Ungauged Basins*, 2008, ISBN 978-3-933761-79-8

176 Assteerawatt, Anongnart: *Flow and Transport Modelling of Fractured Aquifers based on a Geostatistical Approach,* 2008, ISBN 978-3-933761-80-4

177 Karnahl, Joachim Alexander: *2D numerische Modellierung von multifraktionalem Schwebstoff- und Schadstofftransport in Flüssen*, 2008, ISBN 978-3-933761-81-1

178 Hiester, Uwe: *Technologieentwicklung zur In-situ-Sanierung der ungesättigten Bodenzone mit festen Wärmequellen,* 2009, ISBN 978-3-933761-82-8

179 Laux, Patrick: *Statistical Modeling of Precipitation for Agricultural Planning in the Volta Basin of West Africa,* 2009, ISBN 978-3-933761-83-5

180 Ehsan, Saqib: *Evaluation of Life Safety Risks Related to Severe Flooding,* 2009, ISBN 978-3-933761-84-2

181 Prohaska, Sandra: *Development and Application of a 1D Multi-Strip Fine Sediment Transport Model for Regulated Rivers,* 2009, ISBN 978-3-933761-85-9

182 Kopp, Andreas: *Evaluation of CO_2 Injection Processes in Geological Formations for Site Screening,* 2009, ISBN 978-3-933761-86-6

183 Ebigbo, Anozie: *Modelling of biofilm growth and its influence on CO_2 and water (two-phase) flow in porous media,* 2009, ISBN 978-3-933761-87-3

184 Freiboth, Sandra: *A phenomenological model for the numerical simulation of multiphase multicomponent processes considering structural alterations of porous media*, 2009, ISBN 978-3-933761-88-0

185 Zöllner, Frank: *Implementierung und Anwendung netzfreier Methoden im Konstruktiven Wasserbau und in der Hydromechanik*, 2009, ISBN 978-3-933761-89-7

186 Vasin, Milos: *Influence of the soil structure and property contrast on flow and transport in the unsaturated zone*, 2010, ISBN 978-3-933761-90-3

187 Li, Jing: *Application of Copulas as a New Geostatistical Tool*, 2010, ISBN 978-3-933761-91-0

188 AghaKouchak, Amir: *Simulation of Remotely Sensed Rainfall Fields Using Copulas*, 2010, ISBN 978-3-933761-92-7

189 Thapa, Pawan Kumar: *Physically-based spatially distributed rainfall runoff modelling for soil erosion estimation*, 2010, ISBN 978-3-933761-93-4

190 Wurms, Sven: *Numerische Modellierung der Sedimentationsprozesse in Retentionsanlagen zur Steuerung von Stoffströmen bei extremen Hochwasserabflussereignissen*, 2011, ISBN 978-3-933761-94-1

191 Merkel, Uwe: *Unsicherheitsanalyse hydraulischer Einwirkungen auf Hochwasserschutzdeiche und Steigerung der Leistungsfähigkeit durch adaptive Strömungsmodellierung*, 2011, ISBN 978-3-933761-95-8

192 Fritz, Jochen: *A Decoupled Model for Compositional Non-Isothermal Multiphase Flow in Porous Media and Multiphysics Approaches for Two-Phase Flow*, 2010, ISBN 978-3-933761-96-5

193 Weber, Karolin (Hrsg.): *12. Treffen junger WissenschaftlerInnen an Wasserbauinstituten*, 2010, ISBN 978-3-933761-97-2

194 Bliefernicht, Jan-Geert: *Probability Forecasts of Daily Areal Precipitation for Small River Basins,* 2011, ISBN 978-3-933761-98-9

195 Hrsg.: Koschitzky, Hans-Peter; Braun, Jürgen: *VEGAS-Kolloquium 2010 In-situ-Sanierung - Stand und Entwicklung Nano und ISCO -,* Tagungsband zur Veranstaltung am 07. Oktober 2010 an der Universität Stuttgart, Campus Stuttgart-Vaihingen*, 2010, ISBN 978-3-933761-99-6*

196 Gafurov, Abror: *Water Balance Modeling Using Remote Sensing Information - Focus on Central Asia,* 2010, ISBN 978-3-942036-00-9

197 Mackenberg, Sylvia: *Die Quellstärke in der Sickerwasserprognose: Möglichkeiten und Grenzen von Labor- und Freilanduntersuchungen,* 2010, ISBN 978-3-942036-01-6

198 Singh, Shailesh Kumar: *Robust Parameter Estimation in Gauged and Ungauged Basins,* 2010, ISBN 978-3-942036-02-3

199 Doğan, Mehmet Onur: *Coupling of porous media flow with pipe flow,* 2011, ISBN 978-3-942036-03-0

Die Mitteilungshefte ab der Nr. 134 (Jg. 2005) stehen als pdf-Datei über die Homepage des Instituts: www.iws.uni-stuttgart.de zur Verfügung.